BEHAVIOUR OF A TWO–CELL PRESTRESSED CONCRETE BOX GIRDER BRIDGE –ANALYTICAL STUDY–

by

AMAR KHALED

Department of Civil Engineering and Applied Mechanics
McGill University
Montreal, Canada

January 1988

A thesis submitted to the Faculty of Graduate Studies
and Research in partial fulfillment of the requirements
for the degree of Masters of Engineering

To my PARENTS

ABSTRACT

The work presented in this thesis is an extension of Ferdjani and Hadj-Arab's work on prestressed concrete box girder bridges. This thesis deals with the static and dynamic behaviour of a medium span, simply supported, two-cell prestressed concrete box girder bridge. The static analysis consisted of investigating the strength and deformational behaviour of the bridge under symmetric and eccentric truck loadings, while the dynamic analysis was aimed at examining the influence of cracking and inelasticity of concrete on the dynamic characteristics of the structure.

Tests were carried out on a $\frac{1}{7.00}$-scale, direct model of the bridge. The bridge was then analysed using the finite element method using NONLACS, a new nonlinear finite element program developed at Carleton Uneversity at Ottawa and the SAP IV program in a quasi-nonlinear form.

The flexural and torsional stiffnesses of the box girder bridge decreased considerably with an increase in the applied load due to the formation and propagation of cracks and inelasticity of concrete. It has been noticed that the natural frequency of vibration of the bridge decreased by only 23% when the bridge was severely damaged, while the damping coefficient increased by about 250%.

The results from the analytical study using the NONLACS nonlinear program showed excellent correlation with the experimental results over the entire loading range up to failure. The quasi-nonlinear analysis, in which the stiffness of the bridge girder was varied in stages by incorporating information about cracking patterns and crack widths from the experimental data, was able to predict with reasonable accuracy the general behaviour of the box girder bridge.

RESUME

Le travail présenté dans cette thèse est une extension du travail qui a été entrepris par Ferdjani et Hadj–Arab sur le comportement de ponts à poutre caisson en béton precontraint. Le contenue de cette thèse traite du comportement statique et dynamique d'un pont à double caissons en béton précontraint de portée moyenne et simplement appuié à ses éxtrémitées. L'analyse statique a porté sur l'étude de la résistance et des déformations du pont sous l'effet de charges symetriques et éccentrées de camions. L'analyse dynamique, quant à elle, a porté sur l'éxamen de l'effet des fissures et de l'inélasticitée du béton sur les characteristiques dynamiques de la structure.

Des tèsts de laboratoire ont été menés sur un modèle réduit à l'échelle de 1/7.00. Le modèle été ensuite analysé par la méthode des éléments finis. Pour ce faire, deux programmes ont été utilisés: NONLACS, un nouveau programme nonlineaire dévelopé à l'université de Carleton à Ottawa, ainsi que le programme SAP IV dans une forme quasi–nonlineaire.

Les rigidités de flexion et de torsion du modèle ont diminué considerablement du fait de la formation et de la propagation des fissures. Il a été obsèrvé que la fréquence propre de vibration du pont a subis une diminussion modérée de 23% alors que le coéfficient de viscosité a accusé une augmentation de prés de 250%.

Les résultats obtenus par NONLACS ont été très proches des résultats éxpérimentaux. Quant aux résultats obtenus par SAP IV, ils ont été dans l'ensemble comparables aux résultats éxpérimentaux.

ACKNOWLEDGMENTS

The work presented in this thesis was carried out under the direction of Professor M. S. Mirza, to whom the author wishes to express his sincere thanks for his knowledgeable and skillful guidance, his continued encouragement and his patience throughout this research, the course of this study and the writing of the thesis.

In addition the writer wishes to express his appreciation and gratitude to Dr. A. G. Razaqpur for his precious advice and guidance during the work at Carleton University as well as his graduate student Mr. M. Nofal, who spent a considerable amount of time running the program NONLACS to analyse the bridge response.

The financial assistance was provided by the Ministry of Higher Education and Scientific Research of Algeria which is gratefully acknowledged. The continuing assistance of the Natural Sciences and Engineering Research Council of Canada, and the Department of Civil Engineering and Applied Mechanics, McGill University is also gratefully acknowledged.

Thanks are also due to K. Joucdar for his cooperation in this joint project. The assistance of Mr. B. Cockayne and Mr. R. Sheppard during the experimental phase is acknowledged with thanks.

The author wishes also to express his gratitude to the staff members and his fellow graduate students in the Civil Engineering Department at McGill University for providing helpful and constructive criticism.

TABLE OF CONTENTS

LIST OF FIGURES

LIST OF TABLES

LIST OF SYMBOLS

A_m	model cross–sectional area
A_p	prototype cross–sectional area
$(A_p)_m$	area of the model prestressing steel
$(A_p)_p$	area of the prototype prestressing steel
b	width of the model top slab
c	crack width
DL_p	dead weight of the prototype
DL_m	dead weight of the model
DL_m^r	required dead weight of the model
DL_m^a	additional dead weight for the model
d_p	depth of the prestressing steel
E_1, E_2	moduli of elasticity of an element along the principal axes
E_c	modulus of elasticity of concrete
E_p	modulus of elasticity of concrete in the direction perpendicular to the crack
E_s	modulus of elasticity of steel
E_s^*	strain–hardening modulus of steel
e	distance from the section centroid to the center of gravity of steel
f'_c	compressive strength of concrete
f_y	yield strength of steel
$(f_{pu})_m$	ultimate strength of the model prestressing steel
$(f_{pu})_p$	ultimate strength of the prototype prestressing steel
f_{ps}	stress in the prestressing steel
G	shear modulus of concrete
I	second moment of area of the model cross–section
l	span length of the model bridge
m	mass per unit length of the model
M_{DL}	bending moment due to dead load
M_{LL}	bending moment due to live load
M_u	ultimate bending moment
P_m	applied concentrated load on the model
P_p	applied concentrated load on the prototype
P_u	ultimate load

LIST OF SYMBOLS *(continued)*

P_i	initial prestressing force
P_f	final prestressing force
S_l	scale factor for length
S_t	section modulus for the top fibre
S_b	section modulus for the bottom fibre
α	angle between the crack direction in an element and the X–axis
v	amplitude of vibration
β	shear reduction factor
δ	displacement
δ_m	logarithmic decrement
ϵ	strain
ϕ	reduction factor
ν	Poisson's ratio
ρ	density of concrete
σ	stress
ω	undamped frequency of vibration
ω_D	damped frequency of vibration
ξ	damping ratio

CHAPTER 1
INTRODUCTION

1.1 Overview of Bridges

Bridges have always had an enormous impact upon society. Most of them combine a strong visual impression along with obvious benefits in the way of improved communications.

Bridges have occupied much of the working lives of many great engineers and researchers in the last century and a half. They concentrated on improving the structural safety and efficiency of bridges besides making them more pleasant aesthetically. In the early years, engineers were limited by the available materials with timber and masonry bridges being more popular until the 19^{th} century. With the beginning of the industrial revolution in Europe in the 19^{th} century and the increasing need for bridges to improve communications, new materials were developed. However, there was little data available for material properties and design, and the techniques of structural analysis were very limited. One of the tragic consequences of that was the collapse of the Tay Bridge during a storm in 1879, which led to a great deal of new thinking by engineers.

Towards the end of the 19^{th} century, the gradual transition from timber to steel was rapidly followed by a change from masonry to concrete. French and Swiss engineers were among the pioneers of concrete bridges. They developed economical reinforced concrete arch bridges of outstanding appearance. Another major contribution from

France was Freyssinet's development of prestressed concrete[1]. High strength materials permitted the introduction of prestressed concrete for bridges. The prestressing enables an optimum combination of high-strength steel with high-strength concrete by a process in which the steel reinforcement is tensioned against the concrete. This operation results in a self equilibrating system of internal stresses which improves the response of the concrete to external loads, ensuring a longer life for the structure.

With the introduction and expansion of prestressed concrete, great advancements have been achieved in the construction of concrete bridges in industrialized countries. While pretensioned beam bridges flourished in the United States because of available transportation and erection facilities, many continuous post-tensioned bridges were constructed in Europe. In addition to the traditional form, rigid-frame bridges have taken new shapes, in the form of inclined piers and Y-shaped piers rather than vertical supports.

More recently the box section has become very popular and is being used extensively for modern bridges. A box combines the advantages of lightness and stiffness in both bending and torsion. Reinforced concrete box girder bridges were first used in Europe some thirty years ago. Since then their popularity has increased to such an extent, that in 1965, approximately 60% of the total deck area of all bridges constructed was of this type of construction. The relative economy of the box girder bridge has contributed greatly to its popularity because of its relatively slender and pleasant appearance. It also provides space within the cells to carry utilities safely. Another important advantage of box sections is the relatively low depth-to-span ratio that can be achieved economically besides their excellent lateral load distribution characteristics. The introduction of prestressing in bridges enables engineers to build longer span box girder bridges with relatively thin webs and slab thicknesses. Box girder bridges were first designed using empirical formulas and specifications modified from those used for the T-beam concrete bridges. Since then significant effort in research has been made to study the strength and deformational behaviour of box girder bridges. The use of direct large scale models has led to the establishment of new criteria for the analysis of box section structures. However, much more effort is required to fully understand the behaviour of such a complex structure.

1.2 Previous Work

A box girder bridge is an extremely complex structure; researchers have focussed their efforts in trying to understand the behaviour of such structures to improve the design methods. Extensive research has been undertaken over the past two decades through experimental and analytical studies.

Scordelis[2] investigated the elastic response of simply supported box girder bridges. He developed a direct stiffness solution for box girder bridges using a folded plate harmonic analysis based on the elasticity method. The final goal of his investigation was the development of a general computer program, capable of determining displacements and internal forces in multi–celled, simply supported box girder bridges subjected to a variety of loading and boundary conditions.

Cordoba[3] and Tschanz[4] conducted an experimental–analytical study on a 1:3.76 direct model of a two–cell, precast pretensioned box girder bridge with cast–in–place deck. They examined the behaviour of this type of bridge with emphasis on load distribution characteristics. The bridge was analyzed using the finite element method and the findings were compared with results from the experimental study. The results of the two analysis showed good agreement. The behaviour of the bridge at service load and overload conditions and at the collapse stage was satisfactory. The transverse distribution of the concentrated load through the thin top slab was found adequate.

Leonhardt and Walther[5] tested two prestressed concrete, single cell, single span, box girders with side cantilevers and transverse diaphragms at midspan and supports. The first specimen was subjected to a concentric midspan loading until flexural failure was approached, and then the loading was made eccentric to induce torsion. The second girder was loaded with a more eccentric midspan load so that torsion dominated. The experimental deformation values in the uncracked girder agreed well with the values calculated using the elastic theory. They also observed that cracking caused a decrease in torsional rigidity. The diagonal compressive stresses in the side of the webs were noted to be a critical factor in the design of thin-walled structures, providing that the principal tensile stresses were adequately resisted by the reinforcement.

Scordelis, Bouwkamp, and Wasti[6] carried out an extensive investigation on the structural behaviour of a 1:2.82 large scale, two span, four cell, reinforced concrete box girder bridge model. They investigated the effect of the current AASHTO loadings on bridges of this type and the response of the bridge to actual scaled loads of AASHTO HS20-44 trucks placed in two or three lanes and of a proposed Class I overload construction vehicle placed in one lane only. They concluded that concrete box girder bridges have excellent load distribution properties. However, the current AASHTO empirical formula, which ignores the number of lanes on the bridge, underestimates the true values of the girder moments for three lane truck loading on the bridge.

Swamy[7] reported tests on the behaviour of prestressed concrete, single cell, box beams loaded in bending and torsion. The size and shape of the box section were varied and the effect of a nominal amount of torsional reinforcement was investigated. He found that bending moments have a beneficial effect on the torsional behaviour.

Soliman[8] studied the strength and deformational behaviour of an intermediate span of a continuous box girder bridge through tests on a 1:2.82 scale, direct model. He investigated the effect of concrete cracking on the flexural and torsional behaviour of this type of box girder bridge, and the effect of warping restraint on stress configuration along the length of the box girder. He also studied the effect of crack formation and propagation on shear transfer across the crack and on the element stiffness perpendicular to the crack direction. He introduced a quasi-nonlinear finite element analysis using the SAP IV program, in which the stiffness of the box girder was modified in stages by incorporating information about the cracking pattern and crack widths from experimental data.

Razaqpur and Mazikins[9] modified and implemented two large size general purpose finite element programs on a micro–computer. The first program was for linear analysis while the second one was for nonlinear analysis of reinforced and prestressed concrete structures. They verified the implementation and accuracy of the results by analyzing the Leonhardt–Walter box girder bridge[5], and comparing the results with the experimental data. The two analyses showed good agreement over the entire loading range.

Campbell and Batchelor[10] tested a 1:3.47–scale direct model of a two span continuous prestressed concrete trapezoidal bridge girder. The tests were conducted to assess the response of the girder to post–tensioning, to static loading in the elastic range, and to AASHTO loading up to failure. They observed that the mode of failure of the girder was flexural and that the ultimate load capacity was in excess of that required by AASHTO. The girder resisted an overload of $1.5DL + 2.5(LL + I)$ with only slight flexural cracking. As a result of the study, they concluded that the performance of the prototype girder under service load is satisfactory and can be predicted by elastic analysis, while the ultimate load capacity can be expected to be in excess of that specified.

Swann[11] conducted tests on a 1:16–scale prestressed micro–concrete model of a typical interior span of a three cell segmental box beam bridge. The precast segments were transversely stressed, jointed together with mortar and the resulting structure partially prestressed longitudinally before being placed onto its bearings. He investigated the distribution of prestressing forces through the cross section, the general behaviour of the structure under dead load and design live load and its ultimate strength. He found that the behaviour of the model was satisfactory in all of the tests in the elastic range and that the structure showed an adequate reserve of strength. However, the accuracy of determination of prestressing stresses was unsatisfactory. He also found that the variation in the modulus of elasticity was not serious. He noticed that the combination of bearing flexibility and high torsional stiffness of the superstructure can cause significant torsional stresses.

Spiller, Kromolicki and Danglidis[12] studied the lateral forces due to longitudinal prestressing of concrete box spine–beam bridges with inclined webs. They derived an acceptably accurate method of deriving the loss of prestress associated with duct curvature and unintentional variation from duct profile for beams with inclined webs and tendons profile.

Seible and Scordelis[13] developed a simple analytical model, using a three–dimensional grillage formulation, which can trace the complete nonlinear behaviour of reinforced concrete multi–cell box girder bridges under increasing static loads up to the ultimate load and collapse of the structure. The structure was modeled by longitudinal beam elements, transverse bending frames and torsional shear panels for the linear elastic model. For the nonlinear model, flexural and shear hinges were introduced in the proposed displacement model. The analytical model was verified using extensive experimental data on post–working load level and failure tests of large scale reinforced concrete box girder bridge models and excellent agreement was obtained.

West and McClure[14] conducted an experimental–analytical study on a full scale prestressed concrete segmental bridge at the Pennsylvania State University. The bridge was tested at service load levels and for overloads. A nonlinear analysis was performed using the SAP IV program. The nonlinearity of the materials was taken into account by modifying the material properties of the old and new cracked elements and updating the structure stiffness matrix at the end of each load step. The results of the finite element analysis compared reasonably well with the experimental results in the elastic and post–cracking range up to failure. They concluded that the general analytical approach, which is based upon the finite element method and used Kostovos and Newman's material model for concrete[15], provides a satisfactory means of analyzing the load–displacement response and strains in the bridge.

Unlike the static response, much less research work has been undertaken to study the dynamic response of box girder bridges. This is mainly due to the fact that concrete box girder bridges are quite stiff transversely. Also, no major accidents or problem encountered in this type of structure have been attributed to dynamic response. However, the increasing tendency to use slender bridge sections could result in considerable vibration problems due to the passage of heavy vehicles. A comprehensive review of vibration of bridges was undertaken by Huang[16]. Some of the experimental and analytical studies undertaken to study the dynamic response of highway bridges are presented here for completeness.

Mirza et al.[17] undertook an analytical–experimental program to study the dynamic response of a 1:10.45–scale composite concrete deck–steel box girder bridge for various configurations of a selected bracing system. The model was also used to study the nonlinear static response at higher load levels to establish a framework for the limit states design of composite concrete deck–steel box girder bridges. The analytical study was accomplished using the SAP IV program. The finite element analysis results agreed well in terms of the natural modes of vibration. Both analytical and experimental results showed that provision of bracing in different configurations did not have any significant influence on the composite bridge static and dynamic response.

Conrad and Sahin[18] developed a series of empirical equations for direct evaluation of the natural frequency of straight and curved box girders. A parametric study, conducted on a series of simple, two and three span continuous curved bridges, showed excellent correlation between the approximate and the exact natural frequency results.

Tabba[19] reported an experimental study on the free vibration response of one and two–cell curved box girder Plexiglas models. The aim of his study was to evaluate the simplifying assumptions made in the thin walled beam theory. He compared the experimental results with the analytical results and found reasonable agreement between the theoretical and experimental frequencies and modal shapes.

Hadj-Arab[20] and Ferdjani[21] completed an experimental–analytical study on a 1:7.1–scale direct model of a simply supported, single span, one cell, prestressed concrete box girder bridge. They investigated the strength and deformational behaviour of the structure in the elastic and inelastic ranges, and the dynamic characteristics of the structure at different levels of damage. The finite element analysis was conducted using two types of program, the SAP IV program[37] in a quasi–nonlinear form in which the elasticity matrix was modified in stages by incorporating information from the experimental data, and the FELARC program[9] which was used to trace the complete response of the model up to failure. They also investigated the response of a thin rectangular simply supported beam having a geometry identical to that of model box girder webs. This test was undertaken to develop the pretensioning technique for the model bridge and to evaluate the losses. After releasing the force applied by the jack, a loss of about 4% of the initial applied forces was noted; this value increased to about 15% after cutting the wires. The bridge model was able to resist an ultimate load equal to six times the Ontario Highway Bridge Design Code truck loading, showing the significant reserve of strength of the prestressed box girder bridge. The structural stiffness of the model decreased considerably with the formation and propagation of cracks. A decrease of the natural frequency was observed at high load levels. The experimental value of the damping ratio was found equal to 1.54% for the uncracked structure and 4.63% for the severely cracked structure. These values were within the limits given by Newmark and Hall[22]. The experimental results and the finite element analysis were in good agreement.

1.3 Scope of the Present Study

The present study is an extension of Hadj-Arab and Ferdjani's work on a simply supported, single span, one-cell, prestressed concrete box girder bridge[20,21] to a two–cell, simply supported prestressed concrete box girder bridge. It is aimed at investigating the static and dynamic behaviour of a two–cell, simply supported, prestressed concrete box girder bridge.

The objectives of the experimental–analytical program were:

- To determine the flexural and torsional stiffness of the model bridge.
- To study the effect of cracking of concrete at different levels of damage on the stiffness characteristics.
- To study the behaviour of the model bridge under working load conditions.
- To obtain information on the ultimate load, the reserve strength and the mode of failure of the bridge.
- To study the load distribution characteristics of the structure under truck loading.
- To study the effect of cracking and inelasticity of the concrete on the dynamic characteristics of the structure.

Both static and dynamic studies were performed on a 1:7.0–scale direct model bridge. The bridge was constructed and tested at the Structures Laboratory of McGill University. It was then analyzed by the finite element method using a nonlinear program (NONLACS) at Carleton University, and the SAP IV program[37] in a quasi–nonlinear form. The experimental results were correlated with the analytical results wherever possible and appropriate conclusions were drawn.

CHAPTER 2

THE BRIDGE MODEL

2.1 Introduction

Structural models have always played a significant role in structural engineering research and design. Since 1930, models have been used extensively to study the response of complex structures subjected to static and dynamic loads. The use of physical models to supplement analytical techniques continues to be an important part of research, development and design of complex structures. The generally lower cost of testing small and medium scale models makes it possible to perform more tests and to examine a large number of variable influencing the structural response which would not have been possible with the prototype for reasons of cost, space and time.

Various design codes, such as the National Building Code of Canada (NBCC)[23] and the Ontario Highway Bridge Design Code (OHBDC)[24] have derived some of their empirical formulas from tests on direct models. Scordelis[2] and other investigators have shown in their studies that such models can predict satisfactorily the modes of behaviour of the prototype at all load levels up to the ultimate load stage.

2.2 Preliminary Design

The "beam theory" was used for the preliminary design. This approach for determining the longitudinal stresses in a box girder consists of considering the entire cross section to act as a beam section and calculating the longitudinal stresses on the basis of the flexure formula from the elementary beam theory. The assumptions of this theory are:

- The longitudinal fiber strains and stresses have a planar distribution over the entire cross-section.
- All points on a given cross-section experience the same deflection and therefore, there is no transverse distortion of the cross section.
- The resultant of the external loads passes through the shear center.

A box girder is made up of relatively thin plates. Thus, the assumption that no transverse distortion occurs is not generally satisfied; also the effect of torsion must be considered, since in such structures the resultant load normally does not pass through the shear center. However, it has been established that the beam theory along with good engineering judgment is adequate for a preliminary design[25].

2.3 Dimensional Analysis

The use of scale models for solving difficult engineering problems is now a well-established technique[20]. The similitude requirements that relate the model to the prototype structure are determined using dimensional analysis. The physical quantities involved in this study and the dimensional measures required to describe them are summarized in Table 2.1.

Since static and dynamic response are to be investigated, the fundamental quantities are chosen as the length (L), the force (F) and the time (T). The different physical quantities are assembled to get a complete set of independent dimensionless

Table 2.1 Dimensions of the Governing Physical Quantities.

Description	Physical Quantity	Dimension
Length	l	L
Displacement	δ	L
Force	F	F
Stress	σ	FL^{-2}
Modulus of Elasticity	E	FL^{-2}
Time	t	T
Velocity	v	LT^{-1}
Acceleration	a	LT^{-2}
Gravitational Acceleration	g	LT^{-2}
Frequency	f	T^{-1}
Mass Density	ρ	$FL^{-4}T^{2}$
Strain	ϵ	—
Poisson's Ratio	ν	—

Table 2.2 Summary of Scale Factors.

Group	Physical Quantities	Scale Factor	Scale Factor ($S_E = 1$)
Loading	Force, F	$S_E\, S_l^2$	S_l^2
	Gravitational, g	1	1
	Acceleration, a	1	1
	Time, t	$S_l^{1/2}$	$S_l^{1/2}$
	Velocity, v	$S_l^{1/2}$	$S_l^{1/2}$
Geometry	Linear Dimention, l	S_l	S_l
	Displacement, δ	S_l	S_l
	Frequency, f	$S_l^{-1/2}$	$S_l^{-1/2}$
Material Propreties	Young's Modulus, E	S_E	1
	Mass Density, ρ	$S_E\, S_l^{-1}$	S_l^{-1}
	Stress, σ	S_E	1
	Strain, ϵ	1	1
	Poisson's Ratio, ν	1	1

products $(\pi_1, \pi_2, \ldots, \pi_n)$. According to Buckingham's *Pi* theorem, the mathematical formulation of any physical phenomenon is given by:

$$\pi_1 = \phi(\pi_2, \pi_3, \ldots, \pi_n) \tag{2.1}$$

Equation 2.1 can be written once for the prototype and once for the model. Dividing the prototype equation by the model equation, one obtains:

$$\frac{\pi_{1p}}{\pi_{1m}} = \frac{\phi(\pi_{2p}, \pi_{3p}, \ldots, \pi_{np})}{\phi(\pi_{2m}, \pi_{3m}, \ldots, \pi_{nm})} \tag{2.2}$$

where π_{1m} refers to π_1 in the model and π_{1p} refers to π_1 in the prototype, etc. For complete similarity (true model), all of the dimensionless products must be equal for both the model and the prototype:

i.e.

$$\begin{aligned} \pi_{2m} &= \pi_{2p} \\ \pi_{3m} &= \pi_{3p} \\ &\vdots \\ \pi_{nm} &= \pi_{np} \end{aligned} \tag{2.3}$$

Equation 2.2 may be written as follow:

$$\frac{\pi_{1p}}{\pi_{1m}} = \frac{\phi(\pi_{2p}, \pi_{3p}, \ldots, \pi_{np})}{\phi(\pi_{2m}, \pi_{3m}, \ldots, \pi_{nm})} = 1 \tag{2.4}$$

or

$$\pi_{1p} = \pi_{1m} \tag{2.5}$$

The formulation of scaling relations for any true modeling problem can be established by translating the π–terms into required scale factors. Table 2.2 summarizes the resulting scale factors.

2.4 Description of the Bridge

The prototype structure consists of a two–cell prestressed concrete box girder bridge, simply supported with a span of 25.00 m, a depth of 1.80 m and a width of 7.840 m including two 0.980 m cantilivered overhangs on both sides. The width of the bridge deck accommodates two highway traffic lanes. Figure 2.1 shows a typical cross section of the prototype bridge. The prestressing reinforcement consists of eighty–13mm diameter low relaxation strands with an ultimate strength of 1860 MPa (A_p = $99mm^2$).

A medium–scale direct model of the prototype bridge was constructed and tested in the laboratory. The main considerations taken into account in selecting the scale reduction factor for the length were:

- The available space in the Structures Laboratory of McGill University.
- The slab and web thicknesses of the model which permit accommodation of the D2 deformed wires and the prestressing wires without congestion.
- The requirements for loading devices for simulating loads accurately.
- The casting procedure.

Since it was not possible to obtain small size model strands, high tensile strength steel wires of 5 mm diameter ($(A_p)_m = 19.6mm^2$) were used as prestressing tendons. These wires have an ultimate tensile strength of 1550 MPa. As a compromise between all of above considerations, a length scale factor of 1:7.0 was selected. The model bridge was therefore 3531 mm long, 1120 mm wide and 257 mm deep (Fig. 2.2 and 2.3). The model prestressing reinforcement consisted of ten–5 mm diameter wires, six wires with a straight profile and four wires depressed by a single harping point at midspan. The area of the model reinforcement is given by:

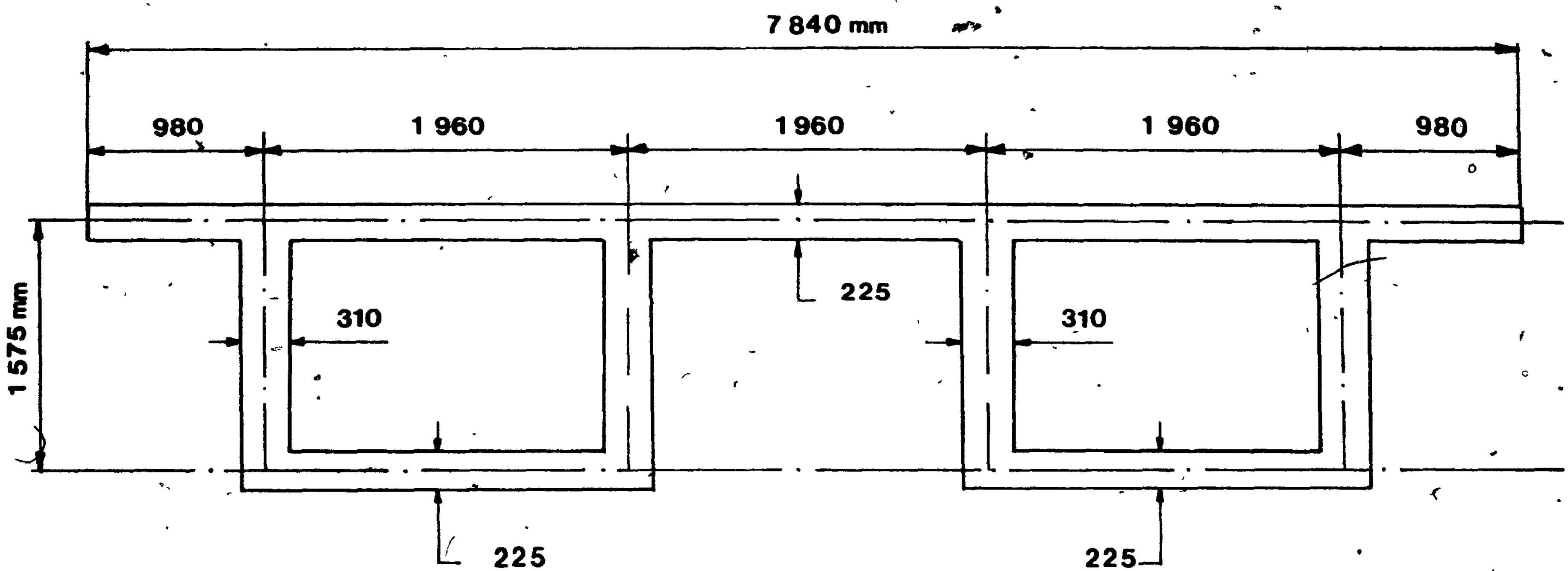

Figure 2.1   Prototype Cross–Section.

$$(A_p)_m = \frac{(A_p)_p (f_{pu})_p}{S_l^2 (f_{pu})_m} = \frac{(80 \times 99)(1860)}{(7^2)(1550)}$$
$$= 194 mm^2 \tag{2.6}$$

where $(A_p)_m$ *and* $(A_p)_p$ are the area of the model and the prototype prestressing steels, respectively.

$(f_{pu})_m$ *and* $(f_{pu})_p$ are the ultimate tensile strengths of the model and the prototype prestressing steels, respectively.

S_l is the scale factor for length.

$972 \times 356 \times 225 mm$ end blocks were provided at the supports to prevent distortions at these locations (Fig. 2.14).

2.5 Loads

2.5.1 Dead Loads

Since the problem involves studies of both the static and dynamic responses, the dead weight of the bridge plays an important role. The dimensionless product $\frac{\rho l}{E}$ must have the same value for the model and for the prototype. Thus:

$$(\frac{\rho l}{E})_{model} = (\frac{\rho l}{E})_{prototype} \tag{2.7}$$

or

$$\rho_m = \rho_p (\frac{l_p}{l_m})(\frac{E_m}{E_p}) \tag{2.8}$$

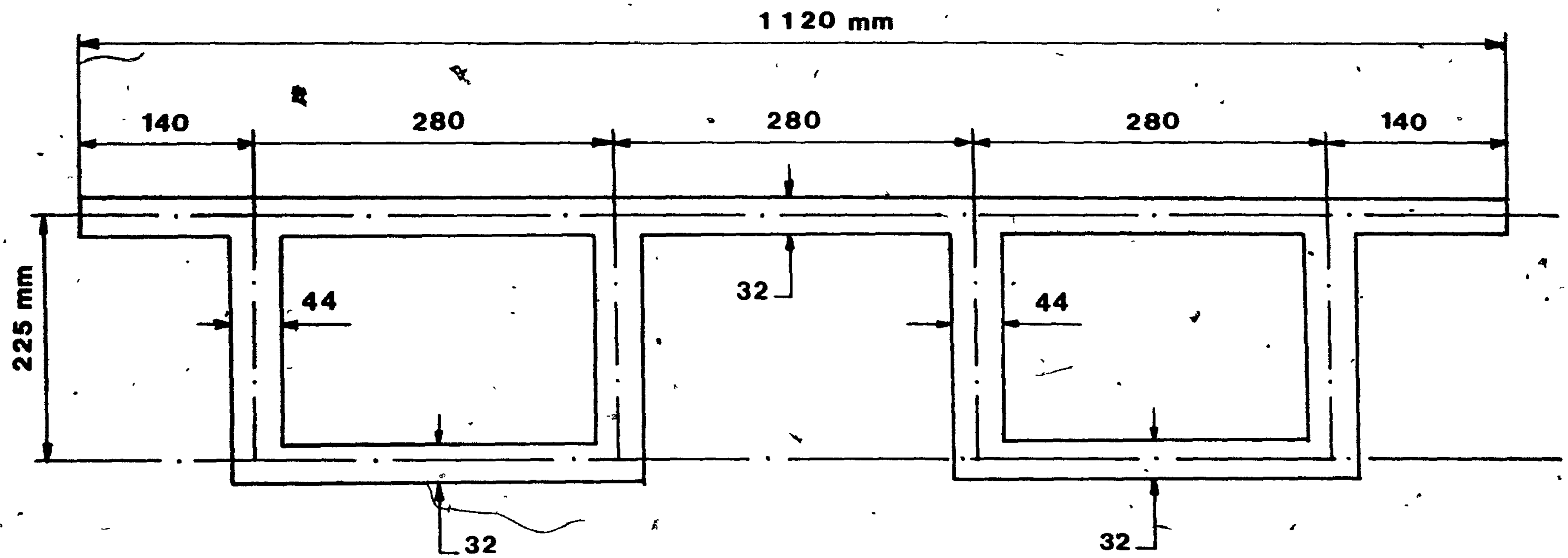

Figure 2.2 Model Cross-Section.

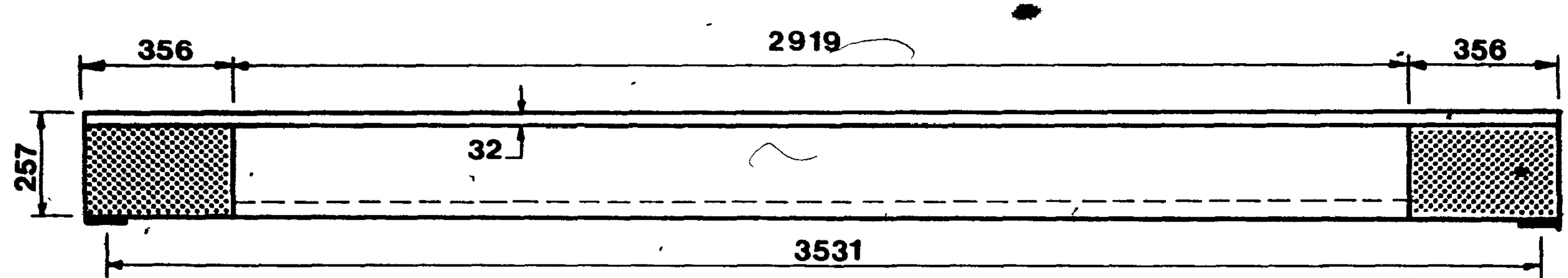

(a) ELEVATION

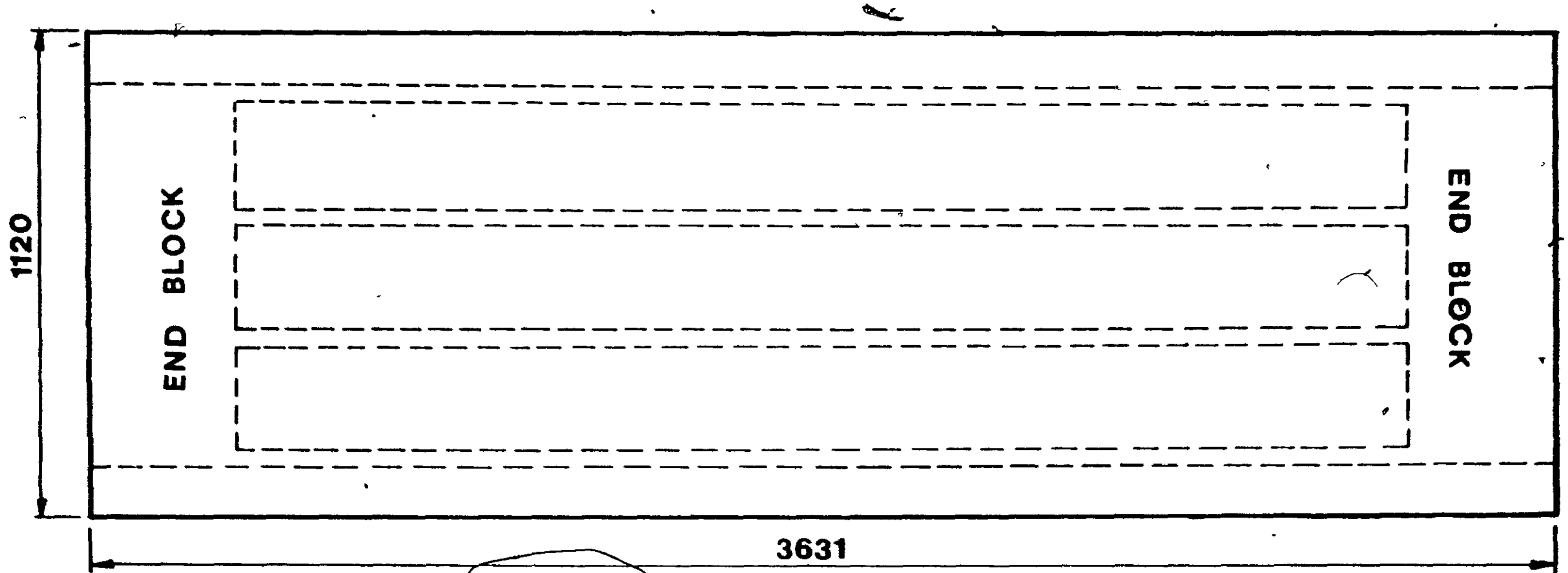

(b) PLAN

Figure 2.3 Overall Dimensions of the Model.

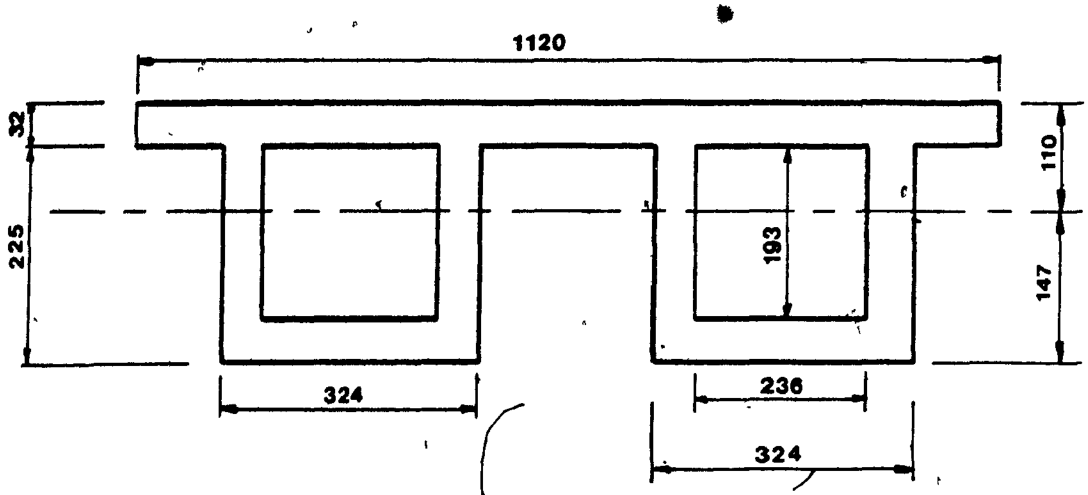

$A = 90{,}408 mm^2$ $\qquad y_t = 110mm$

$I = 793 \times 10^6 mm^4$ $\qquad S_b = 5.40 \times 10^6 mm^3$

$y_b = 147mm$ $\qquad S_t = 7.20 \times 10^6 mm^3$

Figure 2.4 Model Section Properties.

where ρ_m *and* ρ_p are the density of the model concrete and the density of the prototype concrete.

l_m and l_p are the length of the model and the length of the prototype.

E_m and E_p are the modulus of elasticity of the model concrete and the modulus of elasticity of the prototype concrete.

Since concrete is used for the model, therefore $E_m = E_p$, and Equation (2.8) becomes:

$$\rho_m = \rho_p\left(\frac{l_p}{l_m}\right) \tag{2.9}$$

The prototype bridge is simulated with a 1:7.0 scale microconcrete model with a density of $\rho_m = 2290 kg/m^3$. The dead load similitude requires that the density of the model material should be:

$$\rho_m^r = \rho_p \times S_l = 2403 \times 7.0$$
$$= 16,821 kg/m^3 \qquad (2.10)$$

where ρ_m^r is the required density of the model material.

In order then to satisfy Equation (2.9), additional dead weight was provided using steel billets uniformly dispersed within each box girder during construction and appropriate concrete blocks placed on top of the deck. The required dead load for the model is then:

$$DL_m^r = \rho_m^r g A_m = 16,821 \times 9.81 \times 90408$$
$$= 14.92 N/mm \qquad (2.11)$$

where ρ_m^r is the required density for the model.
g is the acceleration due to gravity.
A_m is the cross-sectional area of the model.
DL_m^r is the required dead load for the model.

The dead load of the constructed model is:

$$DL_m = \rho_m g A_m = 2290 \times 9.81 \times 90,408$$
$$= 2.03 N/mm \qquad (2.12)$$

The additional dead load required is:

$$DL_m^a = DL_m^r - DL_m = 14.92 - 2.03$$
$$= 12.89 N/mm \qquad (2.13)$$

where DL_m^a is the additonal dead load required for the model.

The maximum moment at midspan due to the dead load is:

$$M_{DL} = \frac{DL_m^r l_m^2}{8} = \frac{14.92 \times 3531^2}{8}$$
$$= 23,253 kN.mm \tag{2.14}$$

2.5.2 Live Loads

The preliminary design showed that the truck loading was more critical than the lane loading. Therefore the model was loaded by two scaled–down versions of the standard OHBDC truck (total load for each truck = 700 kN) as shown in Fig. 2.5. All linear dimensions were reduced by the length scale factor of 7.00. Similitude requires that the concentrated load be reduced by a factor of $1{:}S_l^2 = 1{:}49$ (Table 2.2) so that strains, deformations, and stresses in the model for each loading condition are representative of similar quantities in the prototype for the corresponding loading condition.

$$P_m = \frac{P_p}{S_l^2} \tag{2.15}$$

where P_m is the concentrated load on the model.
P_p is the concentrated load on the prototype.

Thus for the model, the total load for each scaled down truck was 14.28 kN. For practical reasons and simplicity, the first axle of the simulated OHBDC truck was eliminated.The total load for each scaled down truck then became 13.20 kN (Fig. 2.6).
It was estimated that this would influence bending stresses by not more than 6 percent. Figure 2.7 shows the position and direction of the trucks that give the maximum bending moment at midspan.

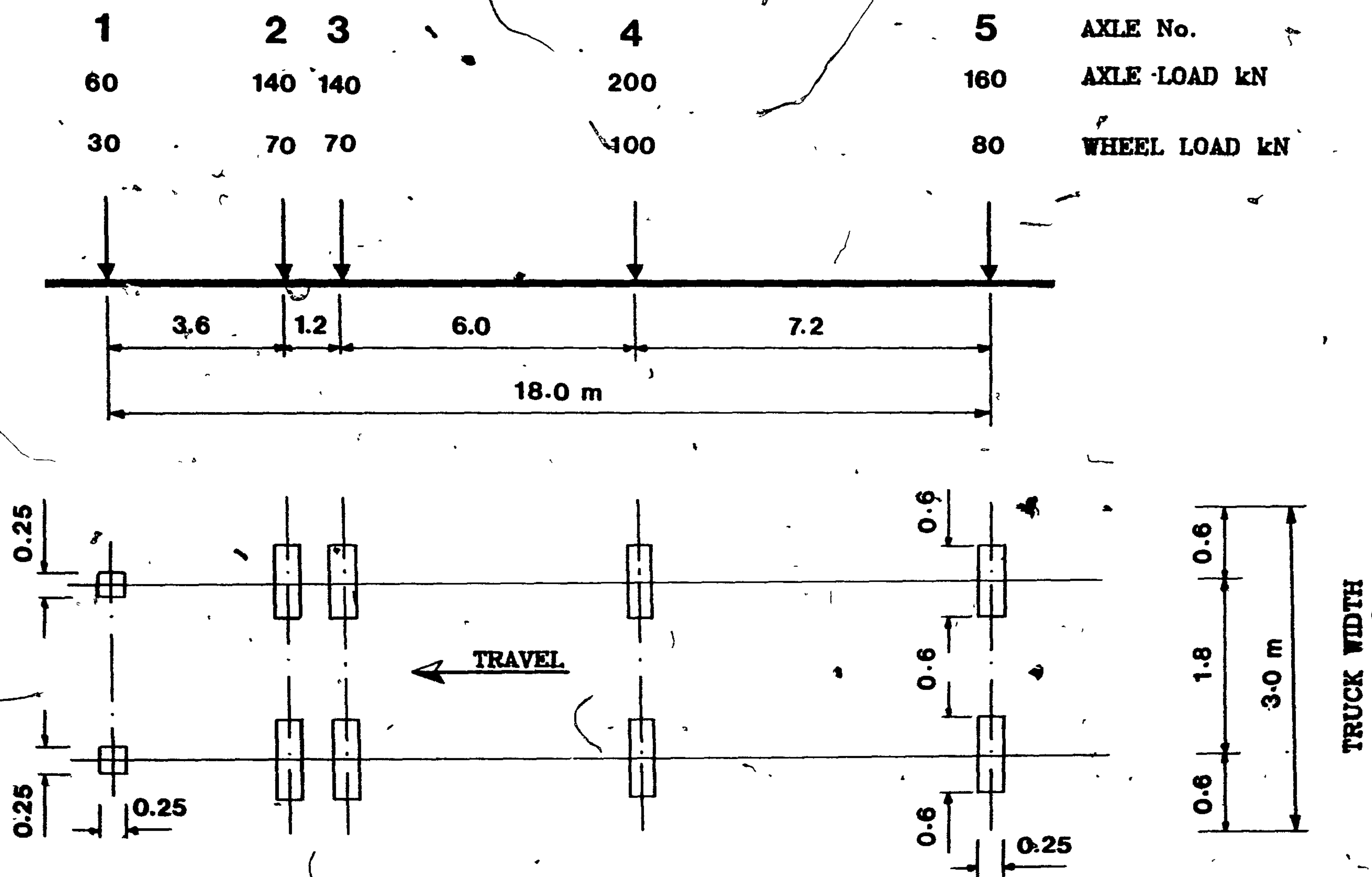

Figure 2.5 Standard OHBDC Truck.

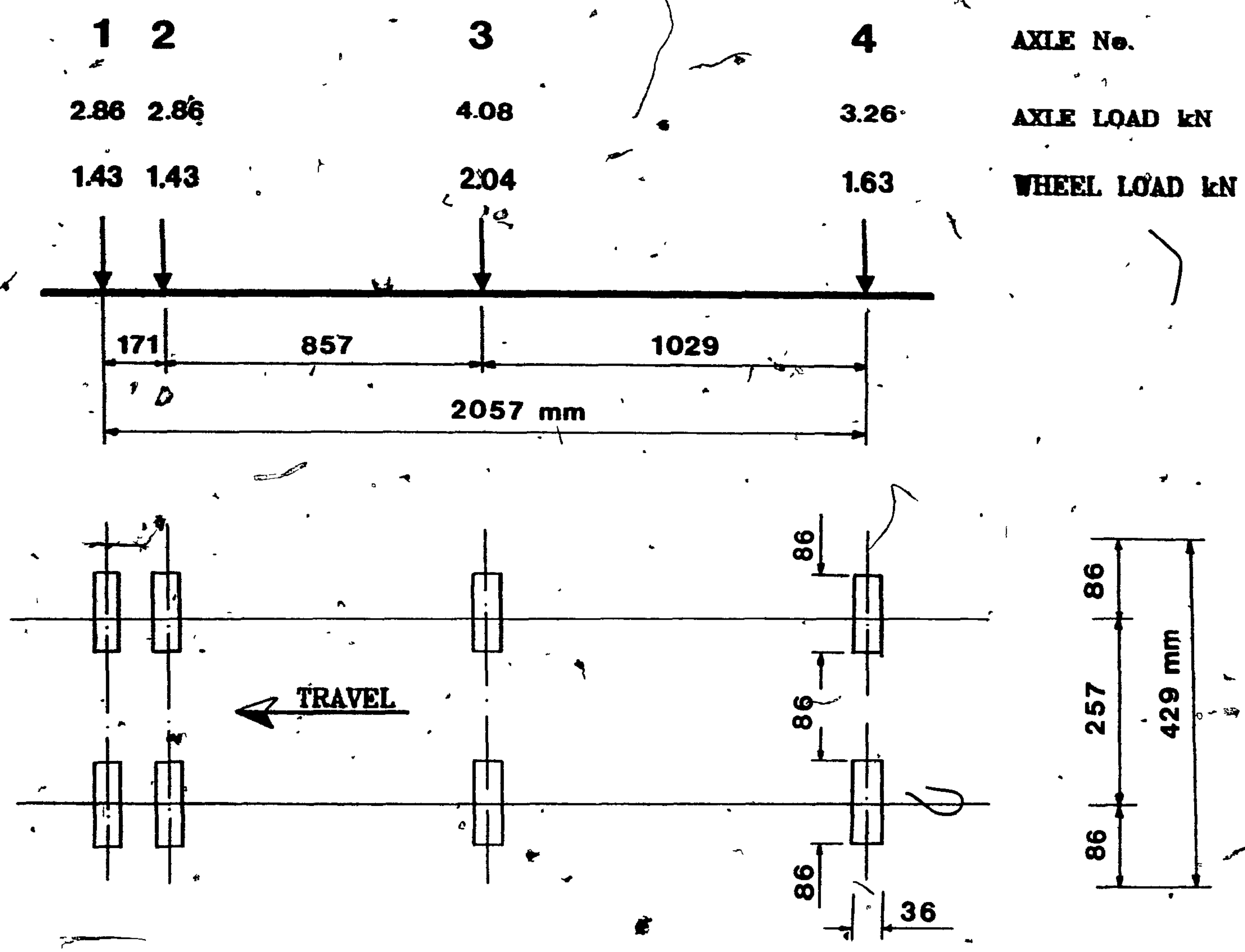

Figure 2.6 Simulated OHBDC Truck for the Model.

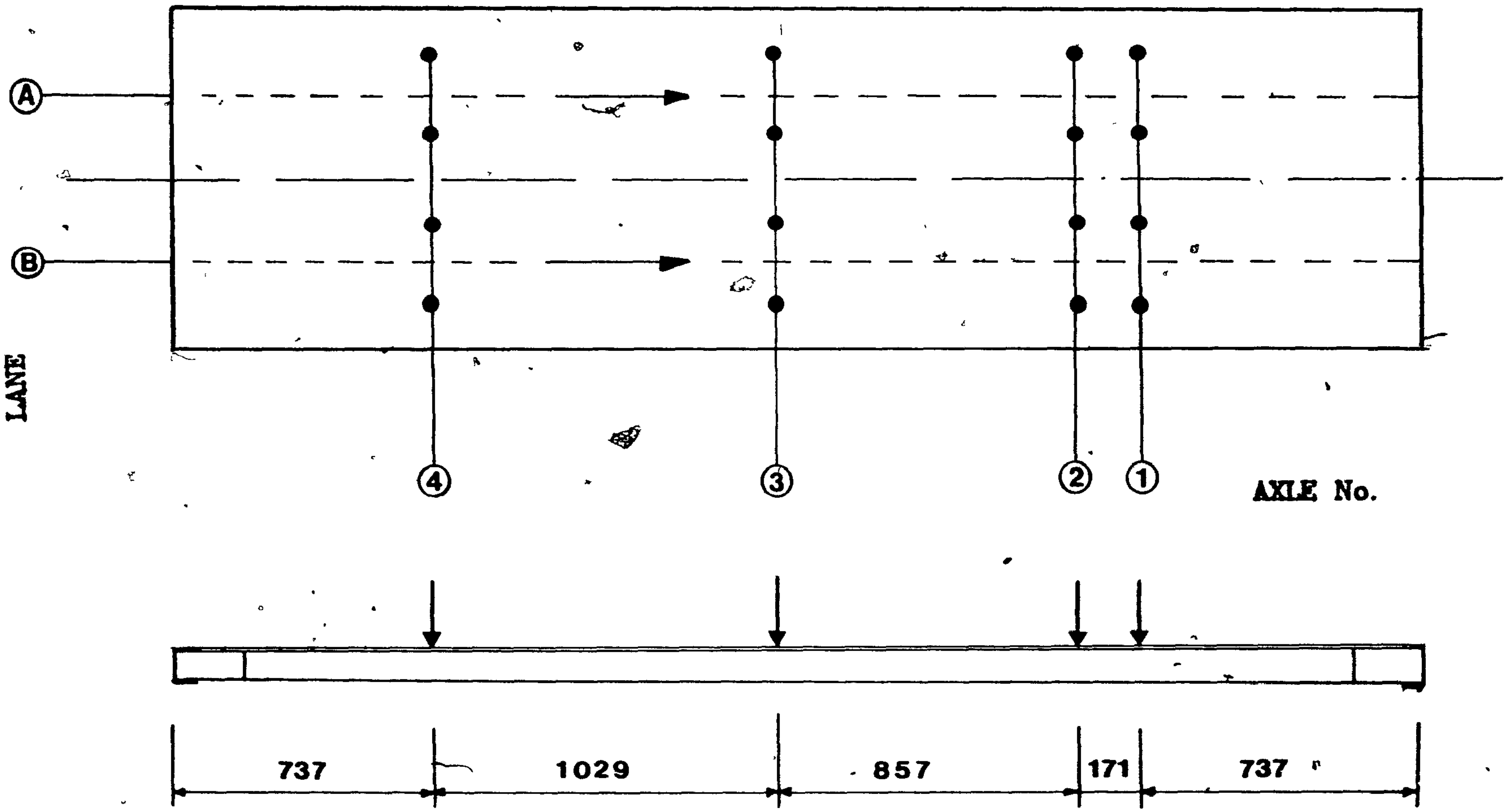

Figure 2.7 Position and Direction of the Trucks for Maximum Moment at Mid-span.

The maximum moment at midspan due to live load is:

$$M_{LL} = 14,442 kN.mm \tag{2.16}$$

Accounting for the impact factor of 0.4 given by the OHBDC[26] specifcations, the bending moment at midspan becomes:

$$M_{LL} = 20,219 kN.mm \tag{2.17}$$

2.5.3 Prestressing Forces

The wires were tensioned to 0.7 f_{pu} in the prestressing bed. The average total losses were estimated to be 10% of the initial force. The experimental results were close to this estimate. The prestressing bed used to apply these forces is described in Reference 42 along with the information concerning the prestress losses.

The final prestressing force P_f in each wire after all losses have occurred is then:

$$P_f = 0.9 \times 0.7 \times 19.6 \times 1550 = 19.20 kN \tag{2.18}$$

2.6 Stresses

2.6.1 Initial Stresses (after release)

The state of stresses due to prestressing and dead load is given by the following expressions:

(a) For the top fiber:

$$\sigma_t = -\frac{P_i}{A_m} + P_i \frac{e}{S_t} - \frac{M_{DL}}{S_t} \tag{2.19}$$

(b) For the bottom fiber:

$$\sigma_b = -\frac{P_i}{A_m} - P_i\frac{e}{S_b} + \frac{M_{DL}}{S_b} \tag{2.20}$$

The state of stresses at a distance of 50 wire diameters from the support, at 0.4 l from the support, and at midspan due to the dead load and the prestressing forces is shown in Fig. 2.8.

2.6.2 Final Stresses (after applying the live load)

With the full service loads, and with all of the prestressing losses having occurred, the state of stresses is given by the following expressions:

(a) For the top fiber:

$$\sigma_t = -\frac{P_f}{A_m} + P_f\frac{e}{S_t} - \frac{M}{S_t} \tag{2.21}$$

(b) For the bottom fiber:

$$\sigma_b = -\frac{P_f}{A_m} - P_f\frac{e}{S_b} + \frac{M}{S_b} \tag{2.22}$$

The state of stresses at a distance of 50 wire diameters from the support, at 0.4 l from the support, and at midspan after applying the live loads is shown in Fig. 2.9.

2.7 Bridge Details

The bridge was designed in accordance with the specifications of the Ontario Highway Bridge Design Code[26] for an ultimate bending moment of:

$$M_u = \phi A_p d_p f_{ps}\left[1 - 0.6\frac{A_p f_{ps}}{bd_p f'_c}\right] = 60,716kN.mm \tag{2.23}$$

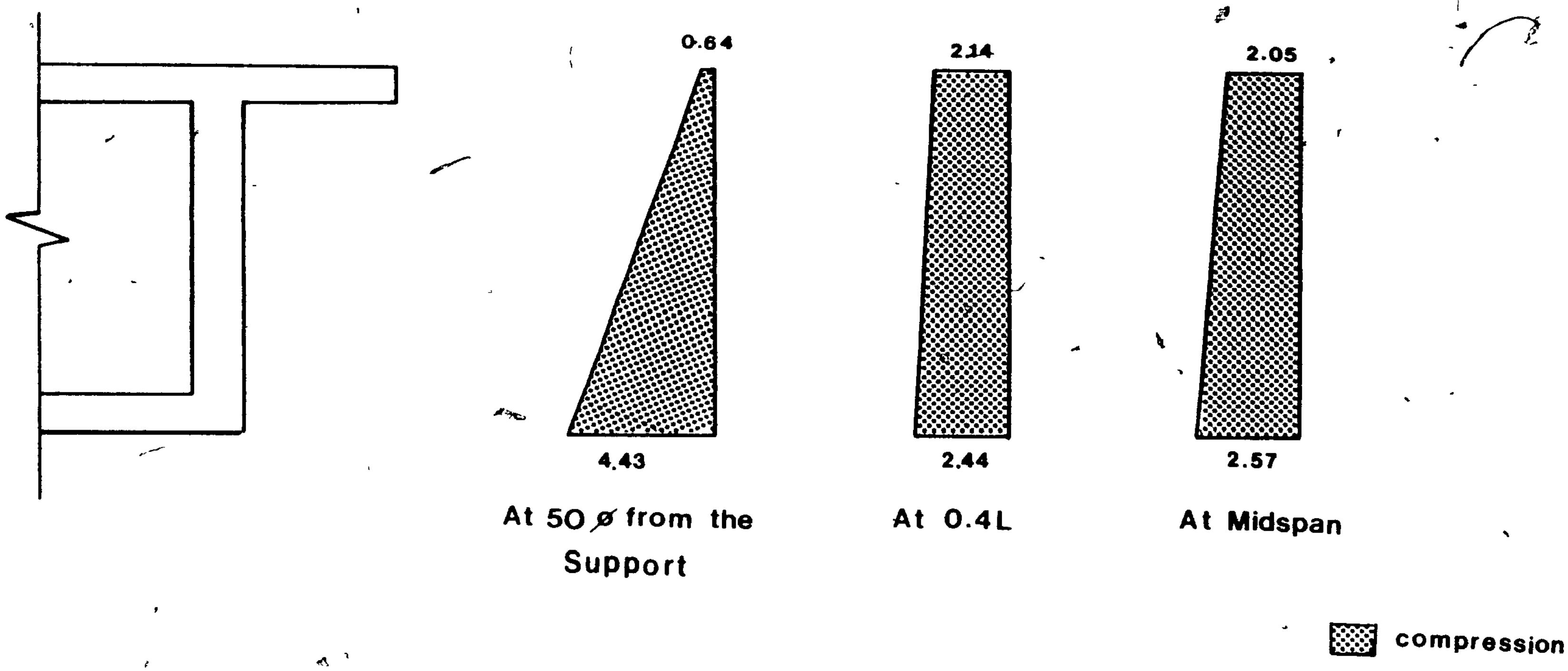

Figure 2.8 State of Stresses at Transfer.

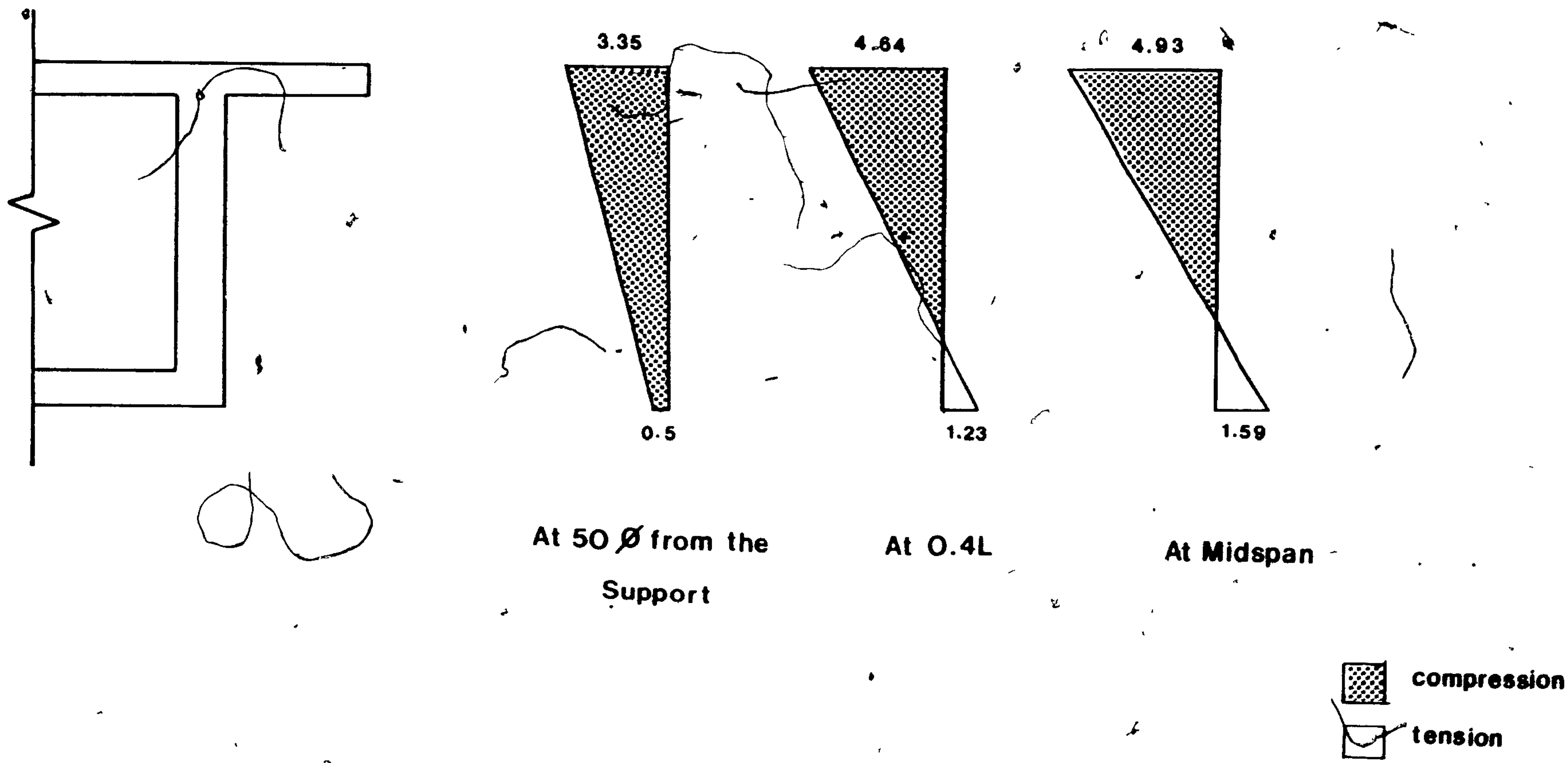

Figure 2.9 Final Stresses.

This ultimate moment is produced by an ultimate load $P_u = 43kN$ equivalent to 3.22 times the simulated OHBDC truck. The girders were checked for flexural and shear stresses at midspan, at 0.4 l from the supports and at the ends. The top slab was checked for bending stresses under concentrated loads. The reinforcement details of the model are shown in Figures 2.10 through 2.14.

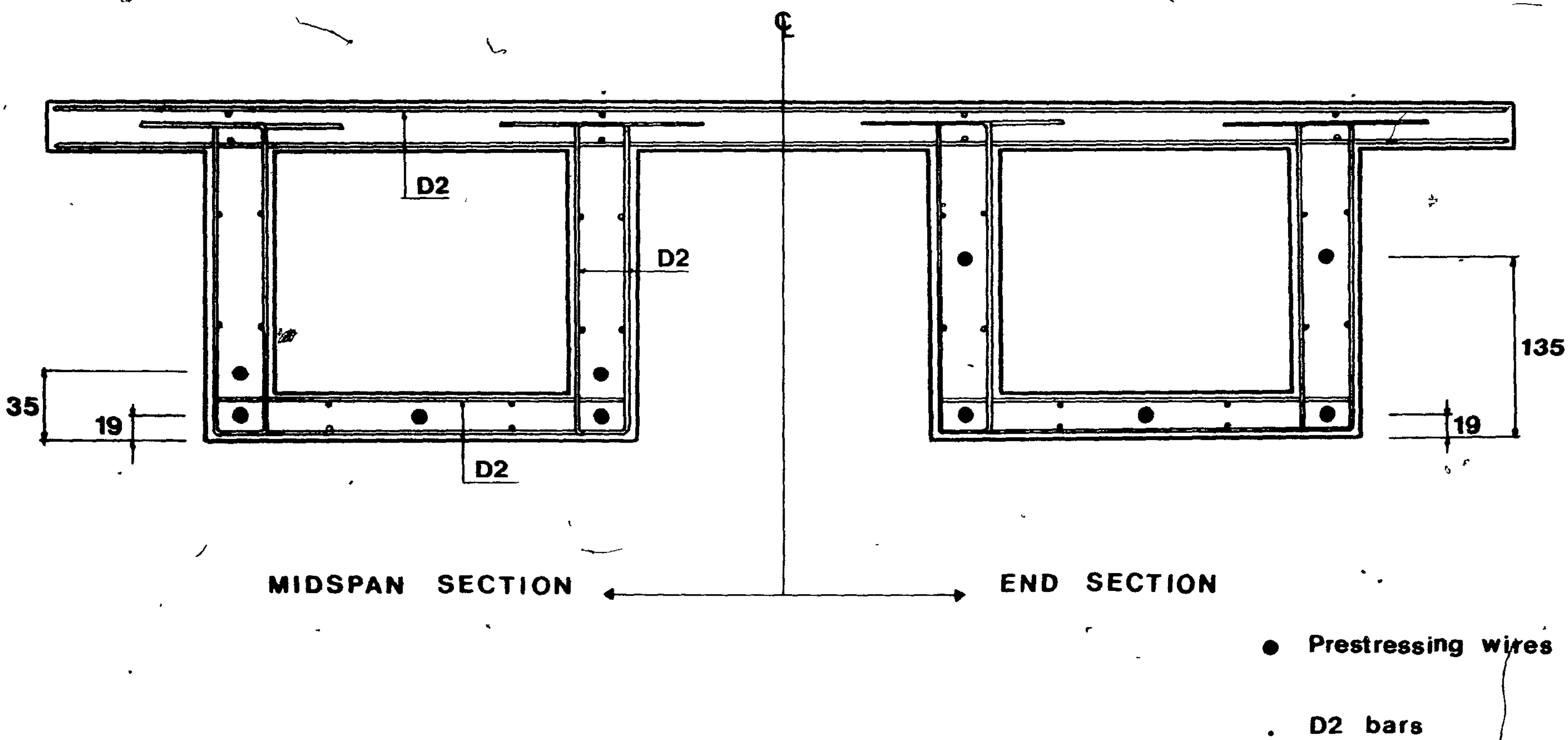

Figure 2.10 Model Cross–Section Details.

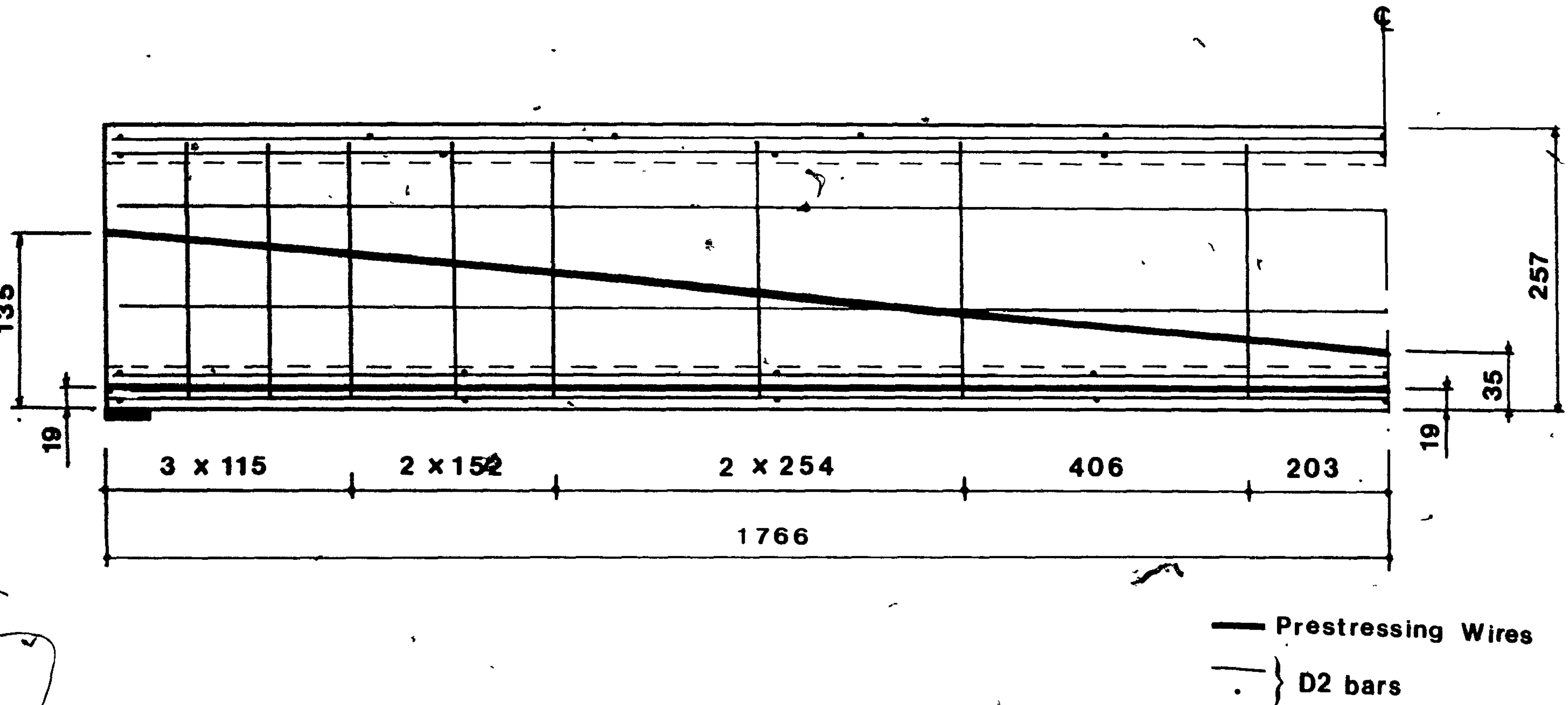

Figure 2.11 Web Details.

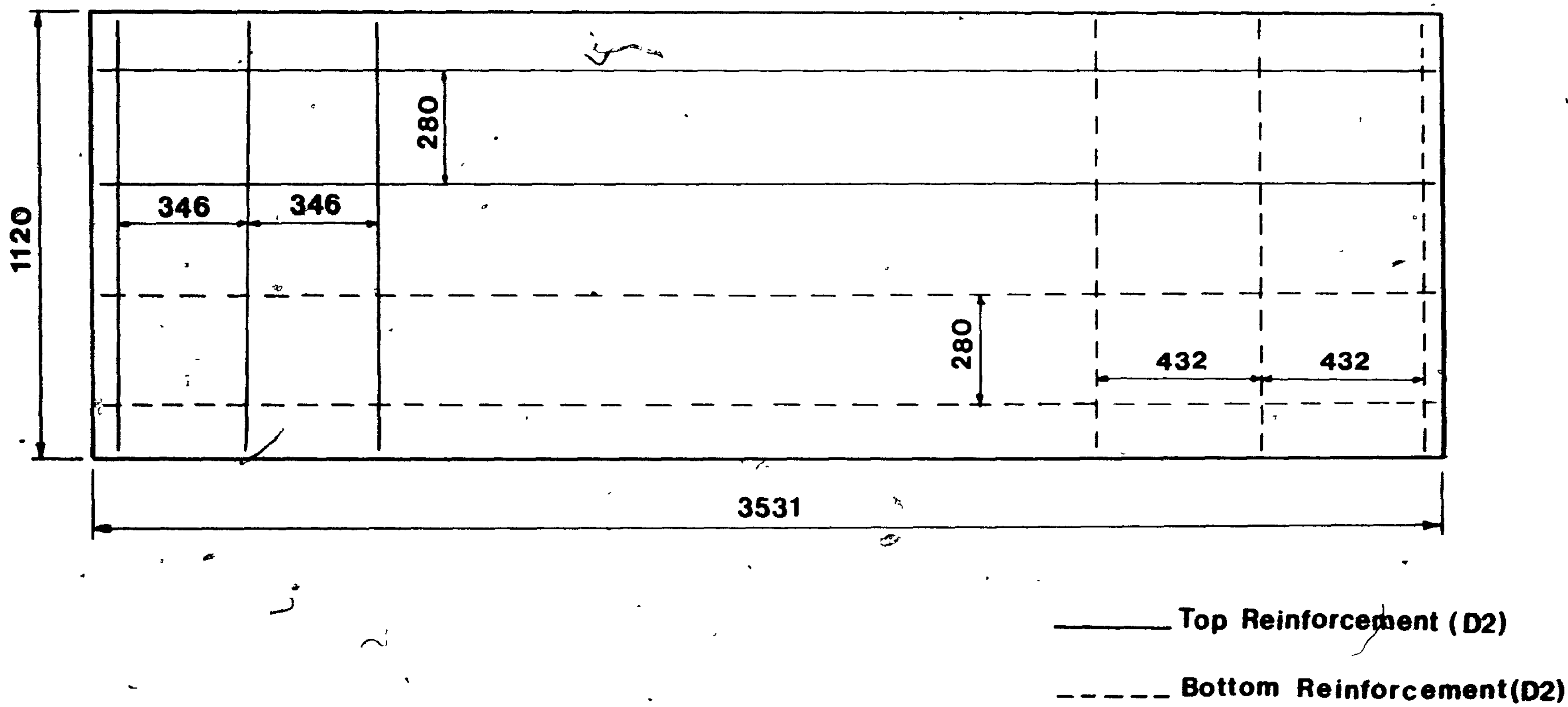

Figure 2.12 Top Slab Details.

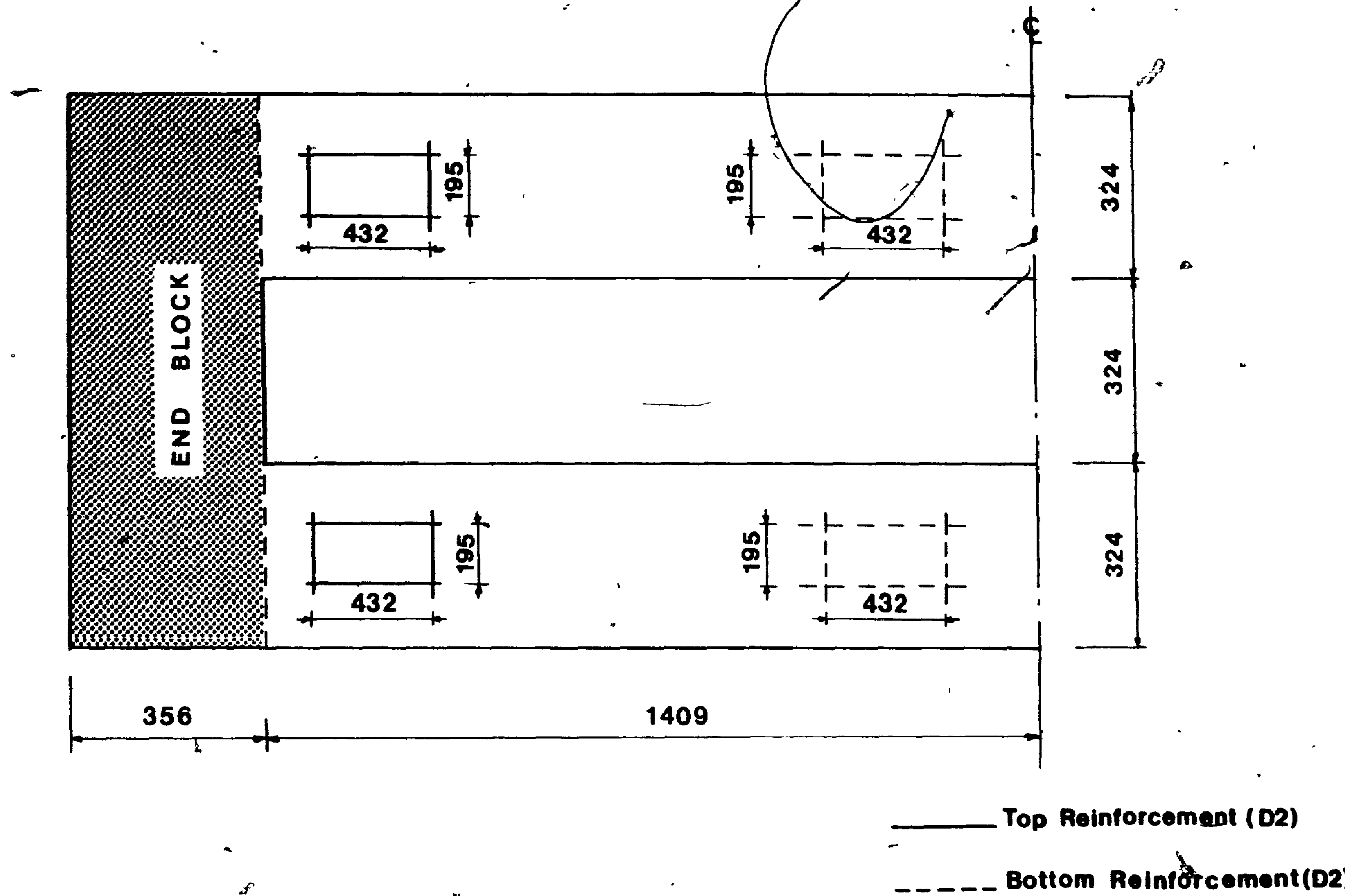

Figure 2.13 Bottom Slab Details.

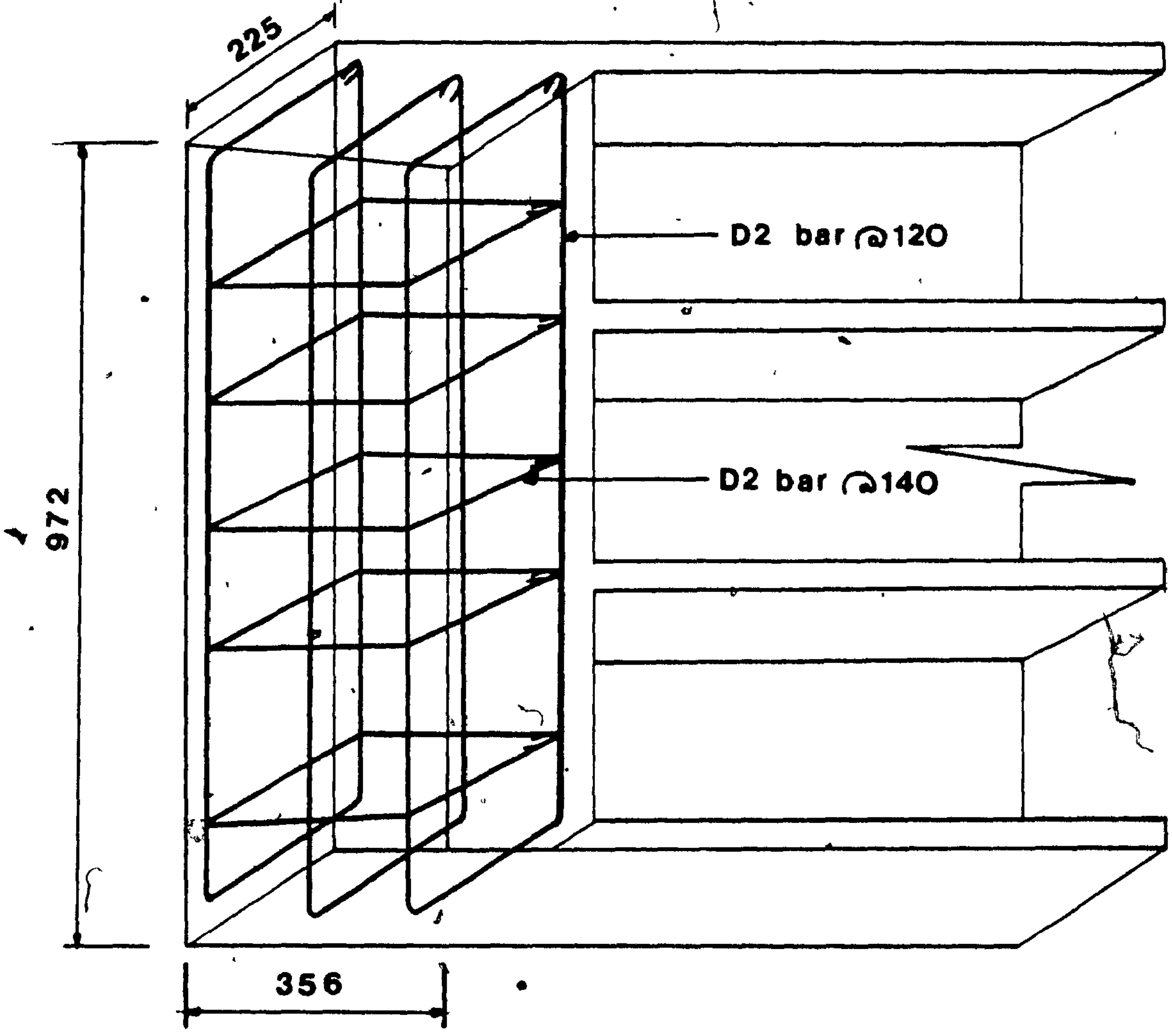

Figure 2.14 End Block Details.

CHAPTER 3

EXPERIMENTAL PROGRAM

3.1 Intoduction

A brief description of the experimental work conducted on a $\frac{1}{7.00}$–scale, two–cell, prestressed concrete box girder bridge model is presented in this chapter. A more detailed description is presented in Reference 42.

The $\frac{1}{7.00}$–scale direct model of the prototype bridge was tested in the Structures Laboratory of McGill University. The overall plan dimensions of the model were 1120 mm by 3531 mm. The model was subjected alternately to dynamic and static loadings.

3.2 Material Properties

Since the model was intended to provide information on the behaviour of the prototype bridge beyond the elastic range, it was necessary to pay special attention to simulation of the material properties. The model material used must simulate as closely as possible the basic characteristics of the prototype concrete and the reinforcement[29]. However, because of the limited knowledge of the bond mechanism it is difficult to satisfy the bond requirements. It is enough to ensure that there is sufficient bond resistance so that bond failure does not occur[26,27]. This can be achieved by providing sufficient embedment length to develop the yield strength of the bars. For this purpose, pull–out tests were conducted on the prestressing wires. These tests are described in Reference 42.

3.2.1 Concrete

A concrete mix, 0.55 : 1.0 : 2.75 (Water : Cement : Aggregate) ratio by weight was used. It was designed for a strength of 34 MPa at an age of 28 days. Type III–High Early Strength Portland Cement was used for the concrete mix. The model concrete aggregates were chosen in the following proportions by weight:

(1.59mm - 3.18mm) Limestone Aggregate	15%
# 10 Crushed Silica Sand	15%
# 16 Crushed Silica Sand	15%
# 24 Crushed Silica Sand	25%
# 40 Crushed Silica Sand	20%
# 70 Crushed Silica Sand	10%

Several concrete cylinders ($50 \times 100mm$) were cast with the model concrete mix during the casting of the bridge model. These cylinders were tested in uniaxial compression and in indirect tension at an age of 28 days. From the results obtained, an evaluation was made of the compressive strength f'_c, the tensile strength f_t, and the modulus of elasticity E_c of the concrete. Tables 3.1 and 3.2 show the results and variations. A typical stress–strain curve for the concrete is presented in Fig. 3.1.

Table 3.1 Compressive Strength of the Concrete.

Element	Number of Cylinders*	Age (days)	f'_c (MPa)	Standard Deviation(MPa)	Coef. of Variation(%)	E_c (MPa)
Bottom Slab	5	28	34.10	1.20	2.90	28500
and Webs	8	42**	37.00	1.10	2.90	28700
Top Slab	5	28	34.20	1.25	3.20	28600
	8	42**	36.90	1.18	2.60	29000

Table 3.2 Tensile Strength of the Concrete.

Element	Number of Cylinders*	Age (days)	f_t (MPa)	Standard Deviation(MPa)	Coef. of Variation(%)	E_c (MPa)
Bottom Slab	5	28	2.15	0.10	3.60	28500
and Webs	8	42**	2.30	0.10	3.10	28700
Top Slab	5	28	2.65	0.10	3.60	28600
	8	42**	2.80	0.08	2.90	29000

* The size of cylinders was 50x100 mm

** Corresponding to the day of testing

3.2.2 Reinforcement

3.2.2.1 Prestressing Wire

High tensile strength steel wires of 5 mm diameter with a cross-sectional area of $19.6 mm^2$ were used as prestressing tendons. The wires were supplied with indentations for good bond resistance. These wires have a 0.2% offset yield point of 1360 MPa and an ultimate tensile strength of 1550 MPa (indicated by the supplier). This value of the tensile strength was verified by testing six samples in tension. The average value of the ultimate tensile strength obtained was the same as the one supplied by the manufacturer (1550 MPa). A typical stress-strain curve for the prestressing wire is shown in Fig. 3.2.

3.2.2.2 Normal Reinforcement

The normal reinforcement consisted of D2 bar meshes. After testing some samples in tension, it was noted that their yield strength was too high (600 MPa) and that the steel was not ductile. In order then to lower the yield strength and to render the steel more ductile, it was necessary to heat-treat the D2 bars[28]. The D2 bars were heat-treated at a temperature of 600° C for a period of 2 hours. The yield strength decreased to 300 MPa and the steel became ductile. The effect of the heat-treatment on the normal reinforcement is shown in Fig. 3.3.

3.3 Construction of the Model

The procedure used to construct the model was maintained as close as possible to the one used in the field on a prototype bridge.

A prestressing bed was first fabricated. Subsequently, the formwork for the bottom slab, the girder webs and the end blocks was prepared. The reinforcement was then instrumented and installed. After prestressing the wires, the bottom slabs, the webs and the end blocks were cast and cured, vertical shear connectors being provided on the

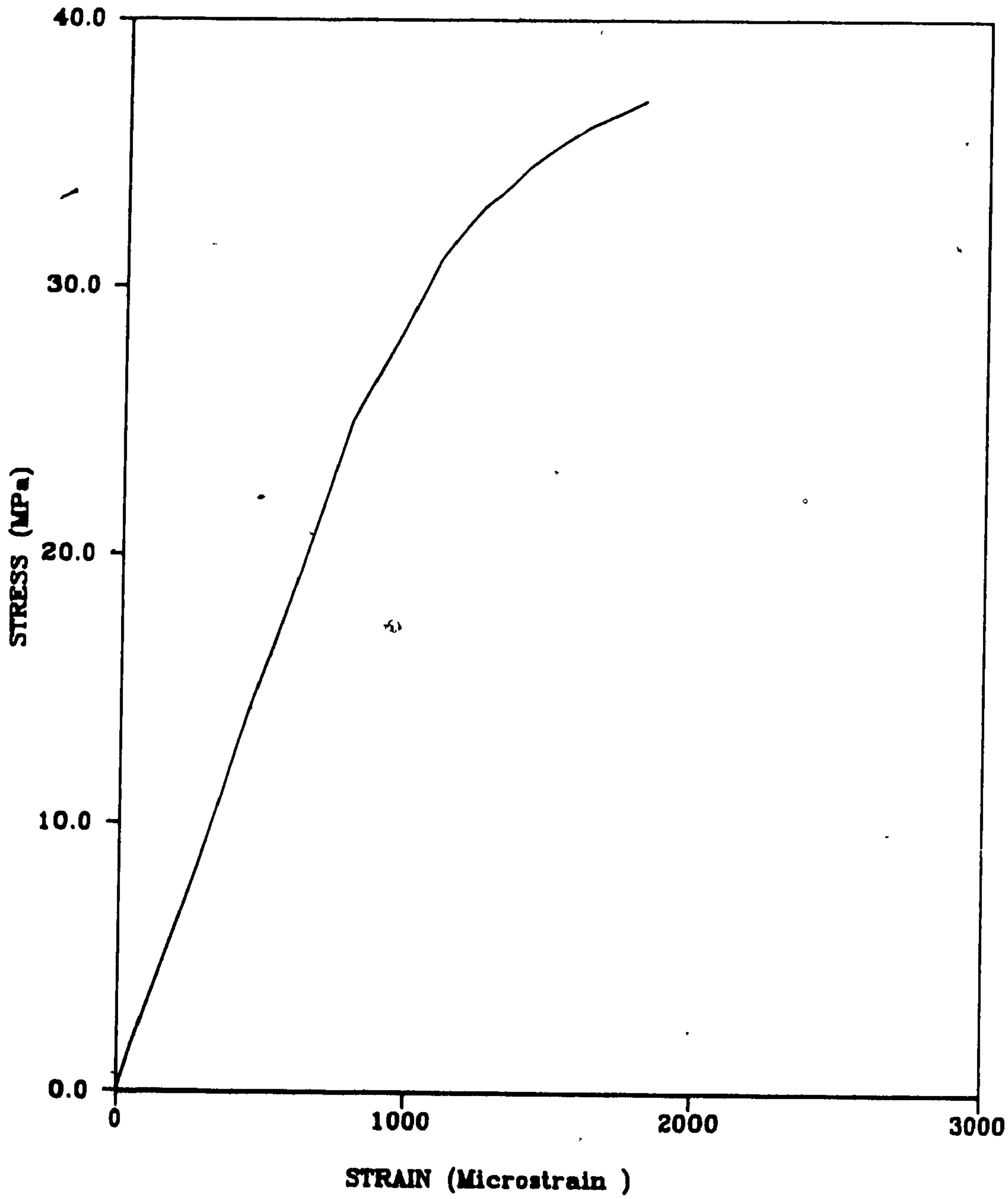

Figure 3.1 Typical Stress–Strain Curve for Concrete.

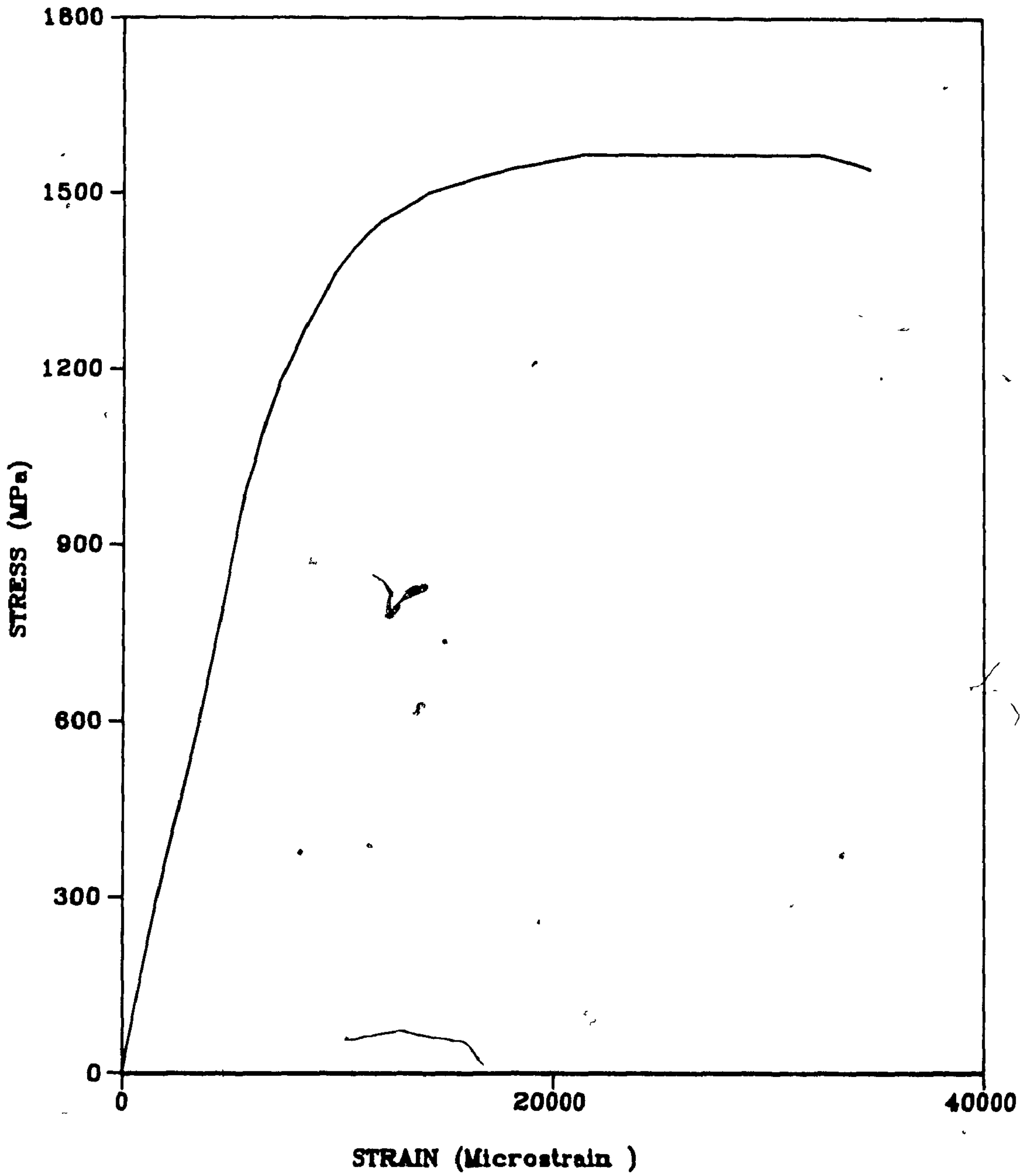

Figure 3.2 Typical Stress–Strain Curve for 5mm Diameter Prestressing Wire.

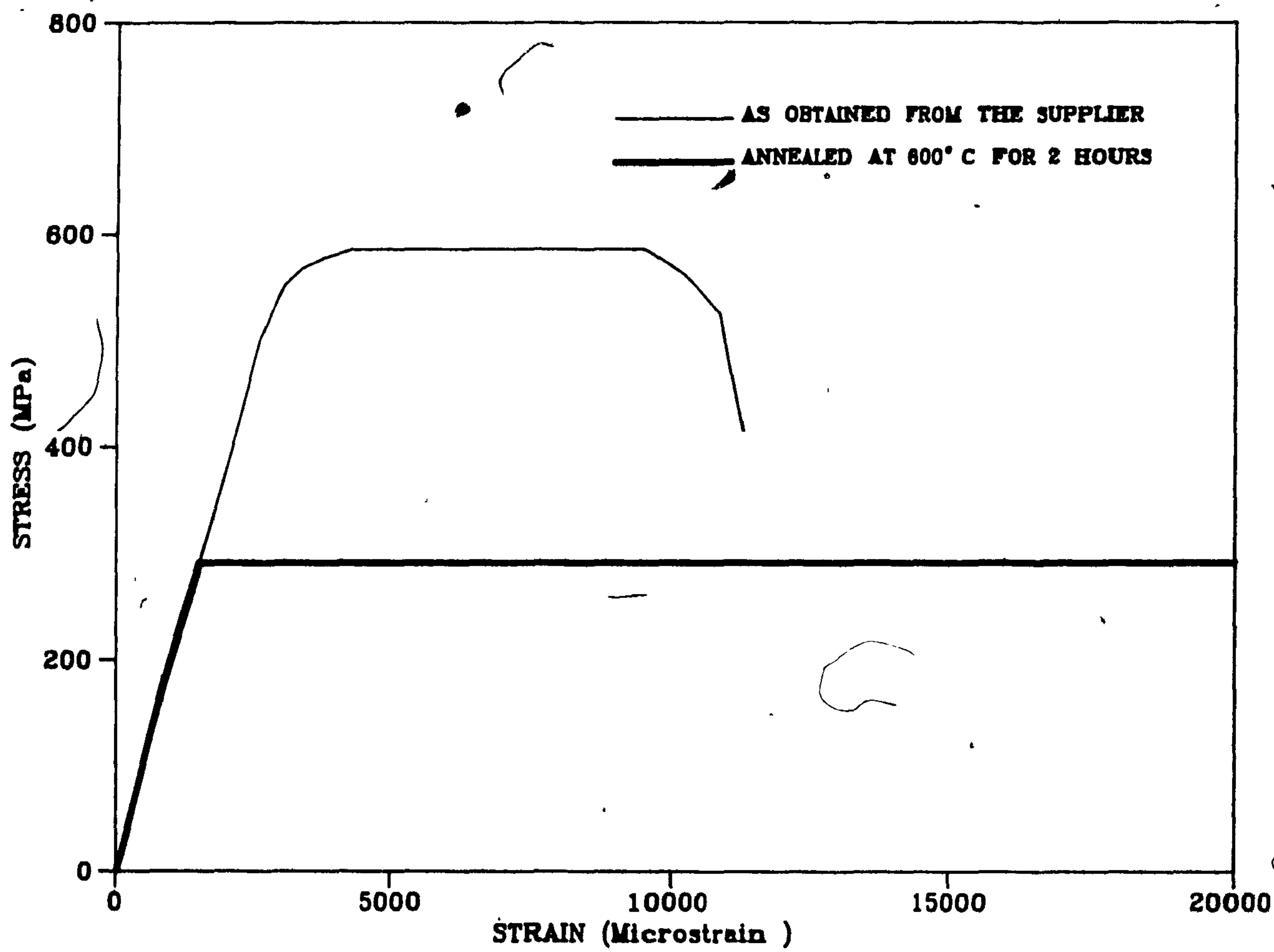

Figure 3.3 Stress–Strain Curve for D2 Steel Wire.

upper surface. At this stage, extra-dead weight in form of steel billets was placed in the cells. The deck was then reinforced, cast and cured. To satisfy the required model-prototype weight ratio of 1:7.0, it was necessary to add concrete blocks on top of the concrete deck. These blocks were placed uniformly on the total area of the deck. At the end, the prestressing wires were cut at the ends one by one and symmetrically to avoid any significant eccentric loading. Losses after release were measured and recorded. At this stage, the prestressing bed was removed. Surfaces at chosen locations were finished for the placement of the strain gauges and the dial gauges.

3.4 Instrumentation

3.4.1 General

The data to be recorded during the model investigation were strains in the concrete and the prestressing steel, deflections, crack locations and pattern and the crack widths. Electrical resistance strain gauges, mechanical dial gauges, and LVDT's were used as measuring devices. The data were obtained by a data acquisition system, which recorded the readings continuously, as well as by visual observation. The strains were acquired with an OPTILOG Data Acquisition and Control System connected to an IBM personal computer and a printer.

3.4.2 Loads

The prestressing forces during the construction and the applied live loads during the testing phase were measured using three load cells. The prestressing force was applied through a hydraulic jack and measured directly using a 10-kip calibrated hollow load cell. In the static tests, the applied live loads were monitored using two 10-kip calibrated load cells placed on top of the loading arm. The three load cells were connected to the data acquisition system.

3.4.3 Strains

Linear electrical resistance (SR–4) strain gauges and rosettes were used as strain measuring devices. They were applied at selected locations in the center of the webs, top slab and bottom slabs for reading the strains at the extreme fibers of the concrete. Electrical strain gauges were also placed on the prestressing reinforcement. The strain gauges were connected to the data acquisition system.

3.4.4 Deflection

To measure the deflection of the external surface points, six sets of mechanical dial gauges were placed at midspan and at quarterspans.

In the dynamic tests, the time–dependent deflections were obtained using linear voltage differential transformers (LVDT's) placed at midspan and at the quarterspan sections and connected to a Minc Digital computer.

3.4.5 Crack Locations, Patterns and Widths

Crack locations and patterns were acquired by visual observation and recorded in a note book. The crack widths were measured using a crack width gauge consisting of a ruler with crack widths marked on it.

3.5 Loading System

3.5.1 Static Tests

To apply the live load to the model bridge, an articulated loading system simulating the OHBDC truck was designed. The truck loading device consisted of hollow square steel sections, connected by loose pins to prevent their movements (Fig. 3.4). The live load was transmitted from the strong floor to the rubber pads (86 × 36 *mm*), which simulated the truck wheel contact areas, through a stiff built–up section beam by pulling on the two hydraulic jacks. Details of the loading system are shown in Fig. 3.4. More details can be found in Reference 42.

3.5.2 Dynamic Tests

To excite the bridge in its first natural mode of vibration, a concentrated mass weighing 250 kg was suspended at midspan under the bridge by a thin wire. The wire was then cut by a pair of sharp scissors forcing the bridge to vibrate for a few seconds. During this time interval, the vibrations of the bridge were recorded by the MINC digital computer. A more detailed description is given in Reference 42.

3.6 Test Procedures

The complete test was divided into seven phases, consisting of the following operations. All of the tests were static tests except for one dynamic test in each phase as mentioned.

- Phase 0 :
  - a. Dynamic test of the uncracked bridge (within the elastic range).
- Phase 1 :
  - a. Symmetrical two truck loads.
  - b. Eccentric one truck load.
  - c. Dynamic test.
- Phase 2 :
  - a. Symmetrical four truck loads.
  - b. Eccentric one truck load.
  - c. Dynamic test.
- Phase 3 :
  - a. Symmetrical six truck loads.
  - b. Eccentric one truck load.

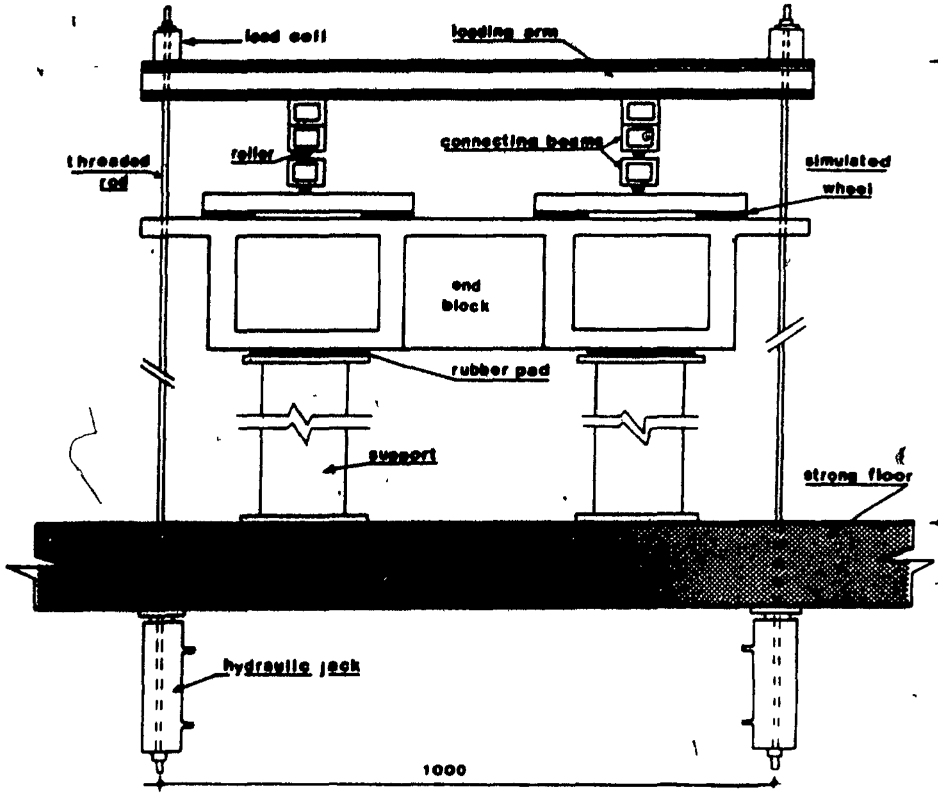

(a) Symmetrical Loading

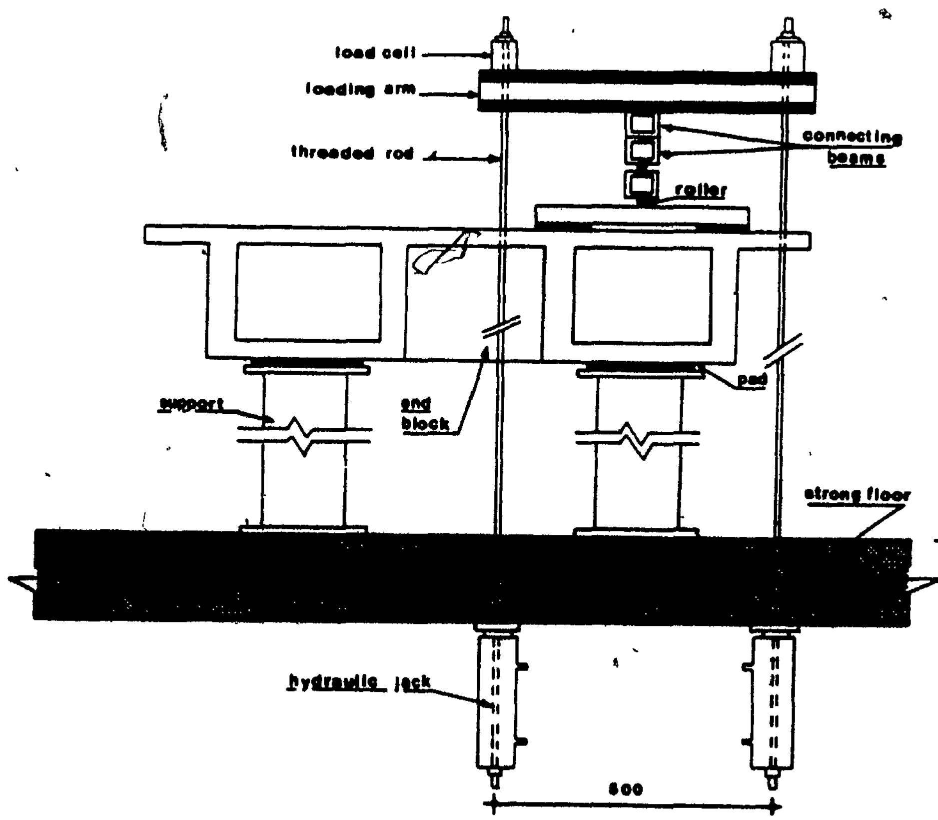

(b) Eccentric Loading

Figure 3.4 **Details of the Loading System.**

c. Dynamic test.

- Phase 4 :

  a. Symmetrical eight truck loads.

  b. Eccentric one truck load.

  c. Dynamic test.

- Phase 5 :

  a. Symmetrical ten truck loads.

  b. Eccentric one truck load.

  c. Dynamic test.

- Phase 6 :

  a. Ultimate load test.

Figure 3.5 Model in the Instrumentation Stage (Dynamic Test).

Figure 3.6 **Model in the Instrumentation Stage (Static Test).**

CHAPTER 4

FINITE ELEMENT ANALYSIS

4.1 Introduction

Studies of the response of reinforced and prestressed concrete box girder bridges to applied loads have received considerable attention. The complexity of the type of structural actions that occurs in a box section, such as distortion, warping and shear lag, make the prediction of its response difficult and not accurate using the classical methods of analysis.

Early box-beam designs employed wall thicknesses large enough to render these effects negligible so that the "simple beam" theory and "St. Venant" torsion theory were adequate analytical tools within the elastic range. However, with the present tendency to more slender sections to reduce the self-weight and the prestressing forces required[25], distortional and warping effects need to be considered. Also, as the structure is loaded beyond the elastic limit, cracks appear and propagate causing significant changes in its static and dynamic properties.

Recent developments in high speed computers and the finite element approach for the analysis of such complex structures makes it possible to overcome these difficulties. The finite element method is an approximate method, therefore it is important to select the finite elements so as to accurately represent the behaviour of the structure[30,31].

The finite element method requires solutions to a large number of equations for structures with the complexity of the box section and therefore, it is time consuming and expensive. However, by making a judicious choice of the finite elements and an appropriate mesh, consistent with the level of accuracy required, and taking advantage of symmetry, if any, the CPU time and the computer memory requirements can be reduced considerably. This can result in considerable savings.

In this study, two finite element programs were used for analysis purposes. The NONLACS[43], a nonlinear program developed by Razaqpur and Nofal at Carleton University in Ottawa and the well-known SAP IV program[37] in a quasi-nonlinear form.

4.2 Nonlinear Analysis Using NONLACS

4.2.1 General

The NONLACS program (NONLinear Analysis of Concrete and Steel Structures) was developed by Razaqpur and Nofal[43]. The origin of the program goes to the program FELARC (Finite Element Layered Analysis of Reinforced Concrete) developed by Ghoneim and Ghali[32] at the University of Calgary and modified by Razaqpur and Mazikins[9] at Carleton University and other similar programs developed at the University of Illinois and at the University of California at Berkley.

NONLACS is, however, much more general than its predecessers. It can analyze any concrete (plain, reinforced or prestressed), steel or composite concrete-steel structure. Five basic types of elements are available in the NONLACS element library: a two node bar element with three degrees of freedom per node, a shear connector element, a higher order four node plane quadrilateral element with vertex rotation[44], a four node quadrilateral plate bending element with three degrees of freedom per node and a four node quadrilateral facet shell element. This last element is obtained by

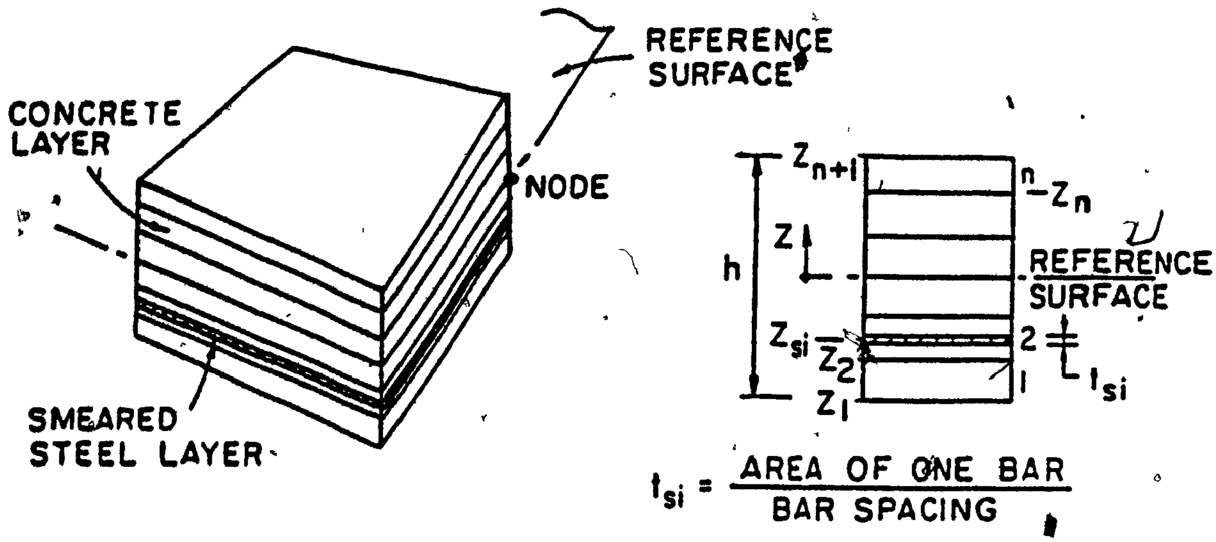

Figure 4.1 Concrete and Steel Layered System[32].

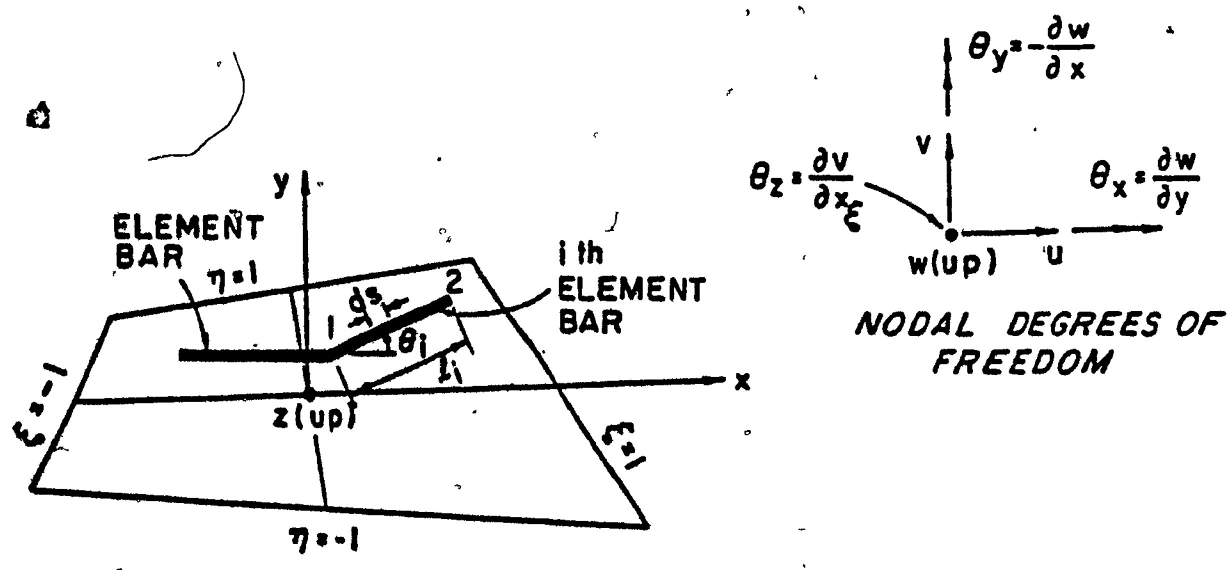

Figure 4.2 The Quadrilateral Facet Shell Element and the Fully Bonded Bar[32].

combining the plane quadrilateral element with the plate bending quadrilateral element (Fig. 4.1 and 4.2).

4.2.2 Description of the Program

The NONLACS program can trace the complete nonlinear response up to failure of reinforced, prestressed concrete, steel and composite concrete–steel structures made up of an assemblage of thin shell elements such as box girders, shear walls, shells, folded plates, etc. The efficiency of the finite elements used in the idealization of the reinforcement makes possible the analysis of such complicated structures with a small number of elements. Therefore, the effort in the preparation of data, the computation and the effort in the interpretation of the results are minimized.

Each finite element is divided into a number of concrete or steel layers. The steel layer may represent the reinforcement smeared into a layer or an actual steel plate as in the case of composite structures (Fig. 4.1). Each layer is treated as an orthotropic material and can assume any state: elastic, yielded, cracked, or crushed depending on the stress level reached and the type of material involved. Element stiffness is obtained by summing the stiffness contribution of the various layers. As stated, uniformly distributed reinforcement is idealized by a smeared steel layer (Fig. 4.1). Heavy reinforcing bars or prestressed bonded tendons are modeled as fully bonded truss elements (Fig. 4.2) along with their stiffness contributions. Shear connectors in composite structures are modelled by specialized elements.

NONLACS uses the incremental–iterative tangent stiffness technique of nonlinear analysis. The nonlinear stress–strain relationships of concrete and steel are considered by applying the load in increments and performing a series of iterations. The program can handle monotonic or cycling loading. It can also deal with time–dependent effects such as creep and shrinkage. The concrete material modelling in this program is the same as in program FELARC[32], but otherwise the program is quite different.

4.2.3 Material Modeling

4.2.3.1 Concrete

In the NONLACS program, the stress–strain relationship for concrete subjected to uniaxial compressive stress (Fig. 4.3.a) is a combination of the two models due to Saenz[34] (1964) and Smith and Young[35] (1955). Concrete under a biaxial state of stress is idealized as an orthotropic material. In the uncracked state, the axes of orthotropy are oriented along the principal axis. Under the biaxial stress state, the incremental constitutive relationship for concrete is:

$$\{\Delta\sigma\} = [D(\sigma_1, \sigma_2)]\,\{\Delta\varepsilon\} \tag{4.1}$$

where [D], a function of the principal stress values σ_1 and σ_2, is the elasticity matrix of the orthotropic material given by:

$$[D] = \frac{1}{1-\nu^2}\begin{bmatrix} E_1 & \nu\sqrt{E_1 E_2} & 0 \\ \nu\sqrt{E_1 E_2} & E_2 & 0 \\ 0 & 0 & (1-\nu^2)G \end{bmatrix} \tag{4.2}$$

where ν is the Poisson's ratio and G is the shear modulus given by:

$$G = \frac{1}{4(1-\nu^2)}\left(E_1 + E_2 - 2\nu\sqrt{E_1 E_2}\right) \tag{4.3}$$

The values of E_1 and E_2 represent the uniaxial tangent moduli and are calculated from the stress–strain curve using the "Equivalent Strain" concept described in Reference 32. When the principal tensile stress in an element exceeds the uniaxial tensile strength (predefined in the input), cracks are assumed to form along the plane perpendicular to the maximum principal tensile stress direction. The cracks are then smeared into the element and the elasticity matrix, [D], is modified appropriately.

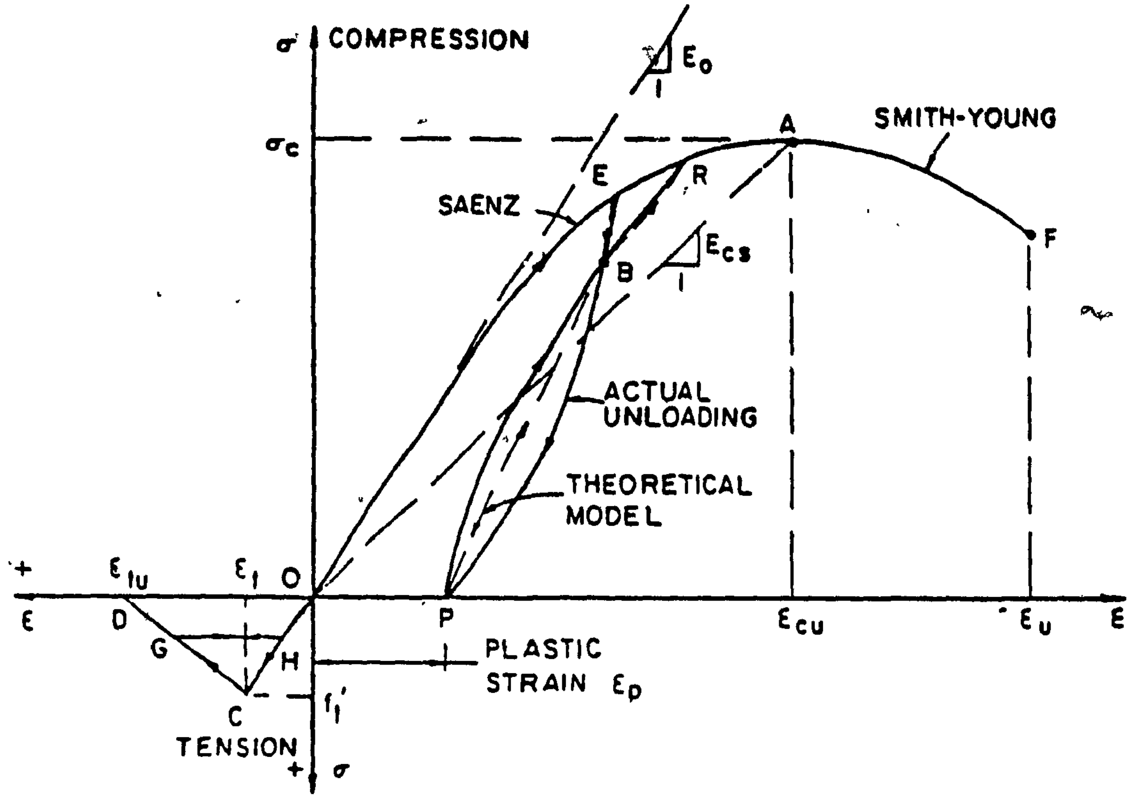

(a) Concrete

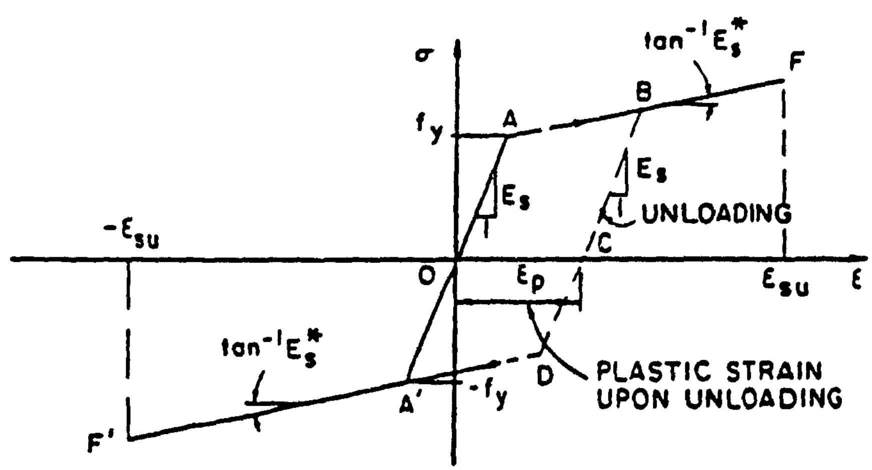

(b) Reinforcement and Prestressing Steel

Figure 4.3 Stress–Strain Relationships[32].

4.2.3.2 Steel Reinforcement

The reinforcing and the prestressing steels are modeled as bilinear strain–hardening materials (Fig. 4.3.b). The model is defined by four parameters: the yield strength f_y, the elastic modulus E_s, the strain-hardening modulus E_s^* and the ultimate strain ϵ_{su}.

4.2.4 Analysis Procedure

As mentioned earlier, the program uses the incremental–iterative tangent stiffness technique of nonlinear analysis. The load is applied in increments. Iterations are applied after each load increment to reduce the unbalanced forces to a small value. Each iteration proceeds as follows:

(i) Calculation of the displacement using the tangent stiffness evaluated at the end of the previous load increment.

(ii) Calculation of the stresses and strains in the concrete and the steel.

(iii) Adding the calculated stresses and strains in (ii) to the previously obtained total stresses and strains to obtain the current approximate total stresses and strains.

(iv) Calculating the true stresses corresponding to the current strains, using the non-linear constitutive relations.

(v) Calculating the unbalanced forces and the equivalent nodal forces.

This ends the iteration. At the beginning of the following iteration, the unbalanced nodal forces are applied and the procedure is repeated until convergence is obtained (i.e. unbalanced forces or displacements become very small), or until the maximum allowable number of iterations (specified as input data) is reached. When the values of the displacements or the unbalanced forces become very large, a failure mechanism is assumed to have occurred and the solution is stopped indicating that the ultimate load has been reached.

4.2.5 Analysis of the Bridge Model

The NONLACS program was used in this study to determine the nonlinear response of the prestressed concrete box girder bridge model, subjected to a monotonic truck loading varying from zero to a load consisting of eleven truck loads. Only one half of the bridge was modeled because of the symmetry of geometry and loading in the longitudinal direction of the bridge. The bridge was divided into 160 quadrilateral facet shell elements which resulted in a total of 168 nodes (Fig. 4.4). The input data required to run the program is outlined below.

(a) Nodal point data. Each node is defined by its boundary conditions and constraints and by its coordinates in the global system.

(b) Material properties data. Material properties of concrete are input in terms of its compressive and tensile strengths, strain at maximum compressive stress, ultimate compressive strain, cracking strain in tension, modulus of elasticity, density and Poisson's ratio (Table 4.1). Prestressing steel and normal reinforcement are defined by their yield strengths, ultimate strains, moduli of elasticity and strain hardening moduli (Table 4.2).

(c) Element data. Each element is defined by the four corner nodes and its thickness. Reinforcement and prestressing steel in the element are defined by their local coordinates, their cross–sectional area and the initial prestressing stress for the prestressing steel.

(d) External nodal force data. The number of load steps, the number of iterations per load step, the loaded nodes, the external loads along with their directions terminate the input data sequence.

The results of the NONLACS computer program include the total external nodal forces, the unbalanced nodal forces, the joint displacements, the stresses and strains, including the principal stresses and the principal directions, at nine locations of the

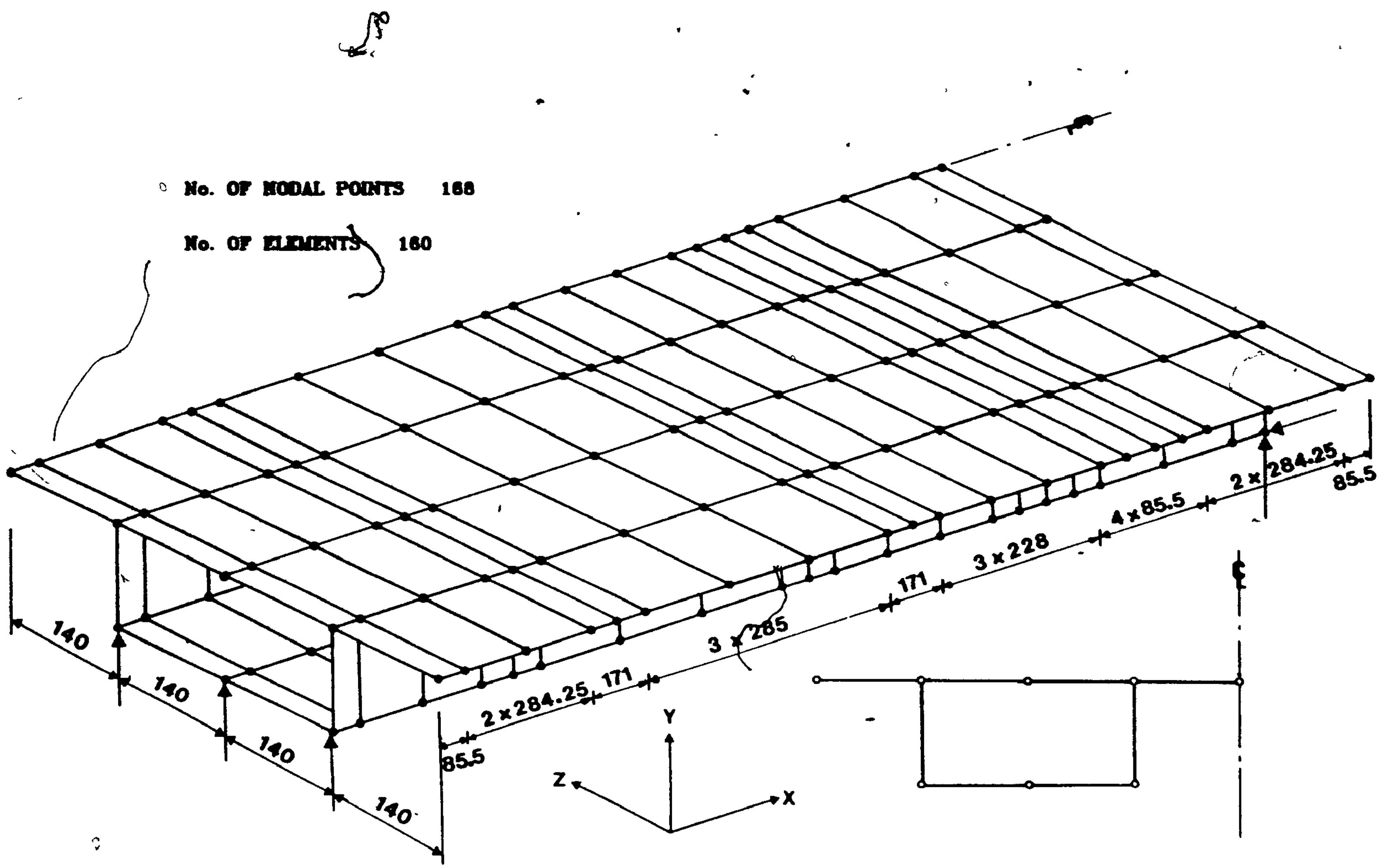

Figure 4.4 Finite Element Idealization of the Model (NONLACS Program).

Table 4.1 Material Properties of Concrete.

Compressive Strength (MPa)	37
Tensile Strength (MPa)	2.25
Compressive Strain at Maximum Compressive Stress	0.0018
Maximum Compressive Strain	0.0045
Cracking Strain in Tension	0.0002
Modulus of Elasticity (MPa)	28663
Density (kg/m^3)	2290
Poisson's Ratio	0.18

Table 4.2 Material Properties of Reinforcement.

		Prestressing Wire	D2 Bar
Diameter	(mm)	5	4
Cross-Sectional Area	(mm^2)	19.6	12.90
Yield Strength	(MPa)	1550	298
Ultimate Strain		0.035	0.018
Modulus of Elasticity	(MPa)	175000	200000
Strain-Hardening Modulus E_s^*		0.21	—

concrete layers and the bar stresses and strains. An example of the application of the NONLACS program is shown in the Appendix.

4.3 Quasi–Nonlinear Analysis

The quasi–nonlinear finite element analysis used in the present study was introduced by Soliman[8]. Ferdjani[21] investigated the nonlinear behaviour of a one–cell box girder bridge using this technique and showed that such an analysis could be a useful inexpensive tool for predicting, with reasonable accuracy, the behaviour of box girder bridges. The quasi–nonlinear analysis could be conducted using any linear finite element program. This has the advantage of being inexpensive in terms of cost and not being time consuming.

SAP is an acronym for Structural Analysis Program, which is a general purpose finite element program developed by Wilson[33] at the University of California at Berkely. It was first published as SAP I in September 1970 and has since been revised. The SAP IV version[37], first released in June 1973 and revised in April 1974, was used in this study. The nonlinearity introduced by the cracks is taken into account by making appropriate changes in the parameters that affect the stiffness of the structure at each loading stage. These parameters, such as crack locations, crack widths and concrete strains, were obtained from the experimental data from the tests conducted on the bridge model.

4.3.1 Material Modeling

In this study, attention was focussed on two major points which are peculiar to the analysis. These are modeling of the concrete cracking and modeling of the steel reinforcement.

4.3.1.1 Modeling of Concrete Cracking

In the finite element analysis of concrete structures, two different approaches have been employed for crack modeling: the discrete–cracking model and the smeared–cracking model[38].

a. The Discrete–Cracking Model was introduced by Ngo and Scordelis[31]. Any cracking that takes place in the concrete can be represented by separating the concrete elements on either side of the crack and by introduction of additional nodal points along the two sides of the crack (Fig. 4.5). For problems involving a few dominant cracks, this model offers a realistic representation. One obvious disadvantage in such an approach is that continued propagation of the cracks with increasing loads implies continued redefinition of the finite element mesh. This has the effect of increasing the computational effort considerably to solve the equilibrium equations, especially when high load levels are reached.

b. The Smeared–Cracking Model in which the cracks are smeared in a continuous fashion (Fig. 4.6), is probably the best choice and is generally used in most structural engineering applications. Due to its simplicity, the smeared– cracking model is used in this quasi–nonlinear analysis.

The application of this approach to the quasi–nonlinear analysis consists of making appropriate changes in the elasticity matrix of the cracked elements by examining the crack pattern obtained experimentally after each loading step. For the uncracked isotropic linear elastic element, the elasticity matrix [D] is given by:

$$[D] = \begin{bmatrix} \frac{E_c}{(1-\nu^2)} & \frac{\nu E_c}{(1-\nu^2)} & 0 \\ \frac{\nu E_c}{(1-\nu^2)} & \frac{E_c}{(1-\nu^2)} & 0 \\ 0 & 0 & G \end{bmatrix} \tag{4.4}$$

where E_c is the modulus of elasticity of the concrete, ν is the Poisson's ratio and G the shear modulus of elasticity of the concrete given by:

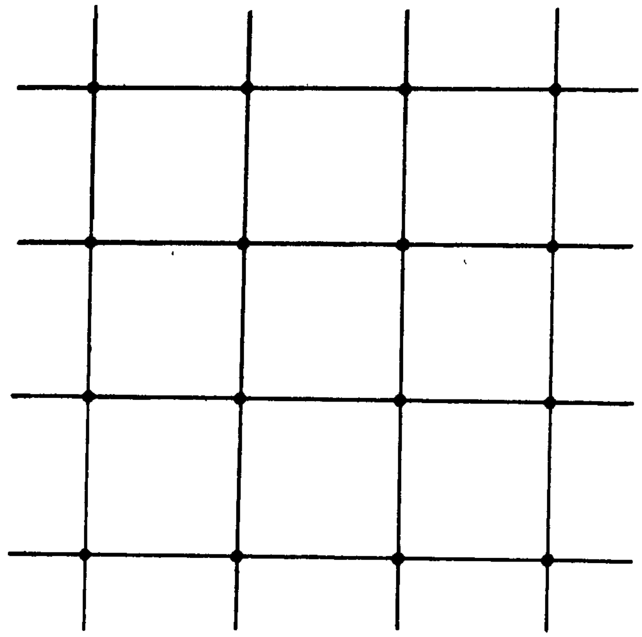

(a) Before Cracking

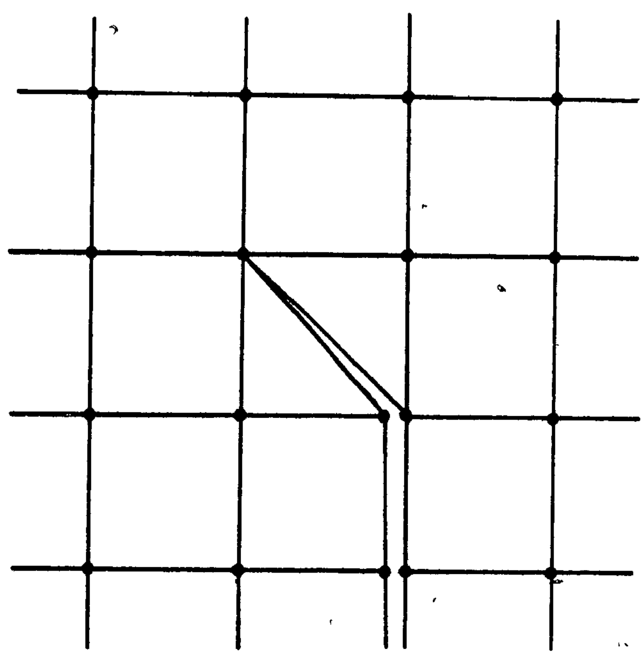

(b) After Cracking

Figure 4.5 Discrete Crack Representation.

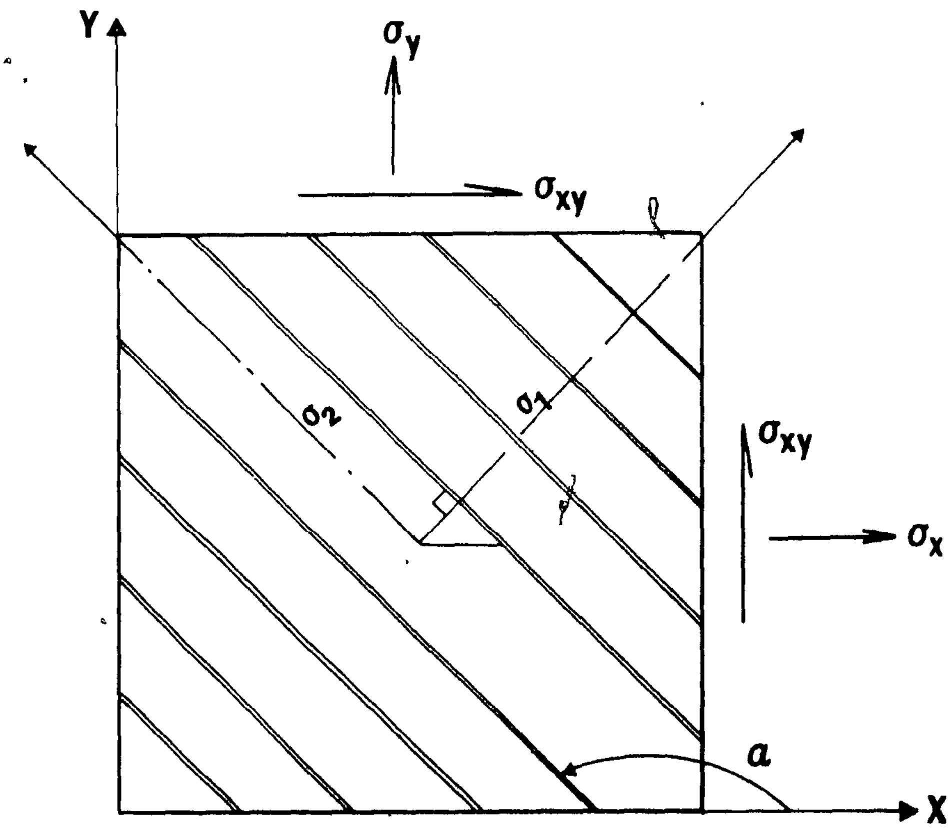

Figure 4.6 Smeared–Cracking Model[36].

$$G = \frac{E_c}{2(1+\nu)} \tag{4.5}$$

After cracking has occurred, the cracked concrete becomes an orthotropic material[38]. The Poisson effect is neglected (i.e. $\nu = 0$) and the modulus of elasticity, E_p, of the concrete perpondicular to the direction of the crack and the shear force transferred across the crack are varied depending on the stress level and the crack width.

While many researchers have recommended a zero value for the modulus of elasticity E_p of the concrete in the direction normal to the crack, Berg[39] has proposed the use of the following equation to evaluate E_p:

$$E_p = 0.4 \left(\frac{0.0001}{\epsilon}\right)^2 E_c \tag{4.6}$$

where ϵ is the concrete strain at the cracking level.

Also, the cracks in the concrete cause an immediate reduction in the shear stiffness. A reduced shear modulus βG is then assumed on the cracked plane. Many researchers have proposed values and expressions for the reduction factor β. Constant values of β were first proposed to account for aggregate interlock and dowel action that might be present. Studies by Houde and Mirza[40] on aggregate interlock at cracks have shown that the shear transfer across the crack is basically a function of the crack width and diminishes as the crack widens. They suggested the following equation which gives the variation of the reduced shear modulus βG with respect to the inverse of the crack width $\frac{1}{c}$ (Fig. 4.7).

$$\beta G = G - \frac{G^3}{E_c\left(\frac{1}{c}\right)^2 + G^2} \tag{4.7}$$

with β being the reduction factor.

Hanna[41] suggested the following expression to represent the shear reduction factor:

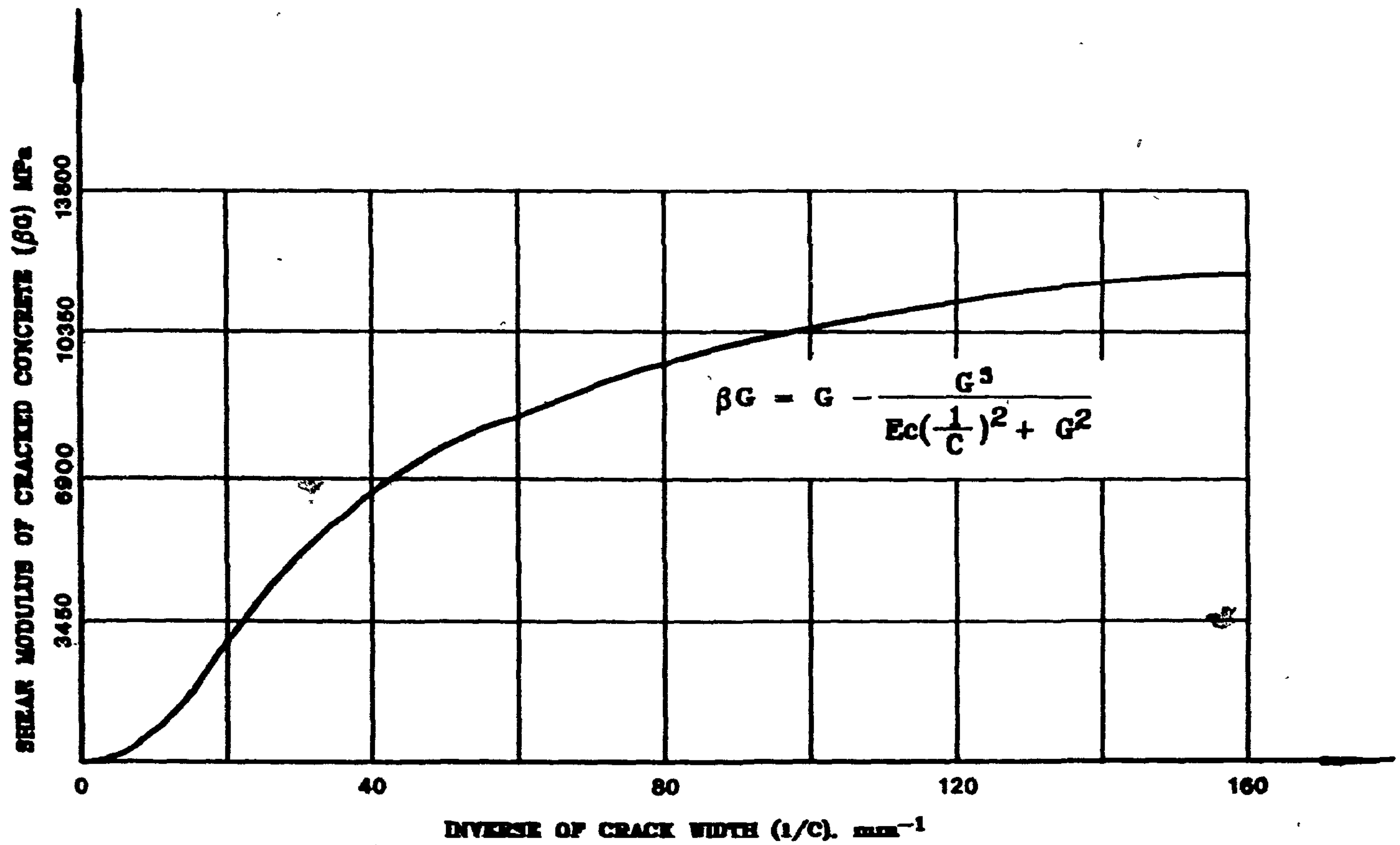

Figure 4.7 Influence of the Crack Width on the Shear Modulus of the Concrete[40].

$$\beta = e^{-140000\epsilon_p^2} \tag{4.8}$$

where ϵ_p is the strain perpondicular to the crack.

To account for the contribution of the dowel action mechanism at higher load level, Hanna suggested that the value of β should not be less than 0.7. As a final expression for the shear reduction factor he proposed:

$$\begin{aligned} &\beta = e^{-140000\epsilon_p^2} \\ &\beta \geq 0.7 \end{aligned} \tag{4.9}$$

The tangent elasticity matrix $[D_t]$ in the cracked direction becomes:

$$[D_t] = \begin{bmatrix} E_p & 0 & 0 \\ 0 & E_c & 0 \\ 0 & 0 & \beta G \end{bmatrix} \tag{4.10}$$

For stiffness calculations, the tangent elasticity matrix, $[D_t]$, is transformed into global coordinates by using the well-known transformation rules for stress and strain tensors:

$$[D] = [T]^T [D_t][T] \tag{4.11}$$

where [T] is the transformation matrix relating the global directions to the crack directions and $[T]^T$ is the transpose of [T]:

$$[T] = \begin{bmatrix} \cos^2\alpha & \sin^2\alpha & \sin\alpha\cos\alpha \\ \sin^2\alpha & \cos^2\alpha & -\sin\alpha\cos\alpha \\ -2\sin\alpha\cos\alpha & 2\sin\alpha\cos\alpha & \cos^2\alpha - \sin^2\alpha \end{bmatrix} \tag{4.12}$$

where α is the angle between the direction of the crack and the X-axis (Fig. 4.8).

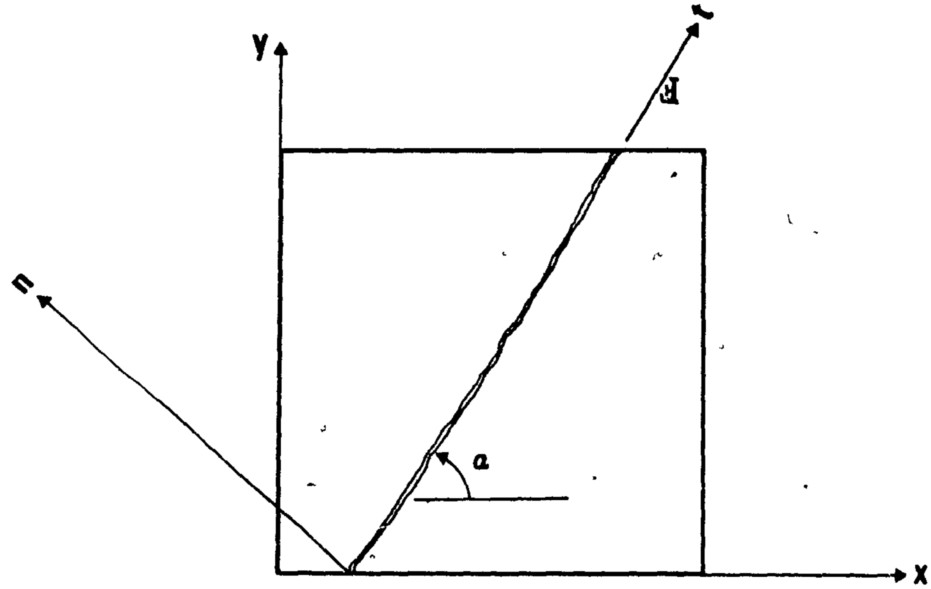

Figure 4.8 Cracked Element.

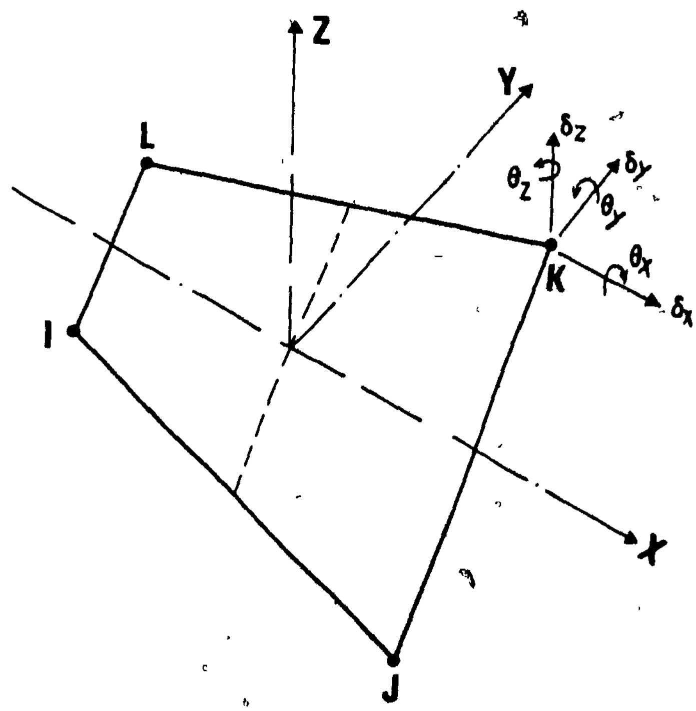

Figure 4.9 Thin Shell Element[37].

4.3.1.2 Modeling of Steel

One–dimensional members prossessing only axial stiffness were used to idealize each of the the prestressing wires. This approach was found appropriate and feasible in treating this case because of the small number of prestressing wires involved.

4.3.2 Finite Element Mesh

The SAP IV program has a number of different structural elements that can be used in analysis. The quasi–nonlinear finite element analysis in the present study was conducted using the thin-shell element[37]. It is a quadrilateral element of arbitrary geometry formed from four compatible triangles. The element has twenty-four degrees of freedom, i.e., six degrees of freedom per node in the global coordinate system (Fig. 4.9). In the analysis of the flat plates, the stiffness associated with the rotation normal to the shell surface is not defined; therefore it is not included in the analysis. The three dimensional truss element was used for the idealization of the ten prestressing wires. The layout of the finite element idealizations used in this analysis is shown in Figures 4.10 through 4.12.

For the symmetrical load case, one half of the bridge was modeled. The mesh consisted of 240 thin shell elements and 100 truss elements with a total of 252 nodes. For the eccentric load case, the full bridge was modeled. The mesh consisted of 480 thin shell elements and 200 truss elements with a total of 483 nodes. The same meshes were used for both static and dynamic analyses.

4.3.3 Analysis Procedures

The results of this finite element computer program include rotations and displacements at each nodal point, truss member stresses and forces and membrane and bending stresses at the element centroids. In the dynamic analysis, the results include the circular frequancies, the natural frequancies, the periods of vibration and the nodal displacements and rotations.

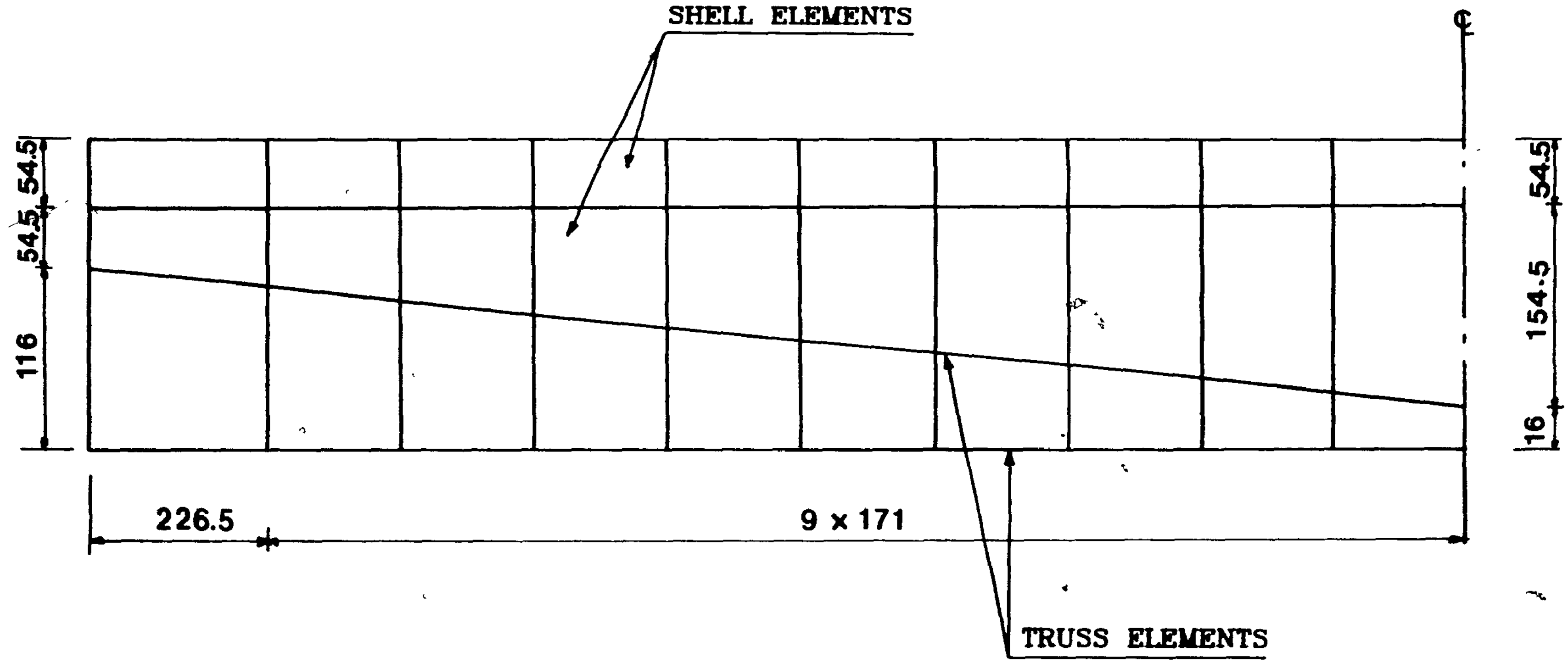

Figure 4.10 Web Idealization (SAP IV Program).

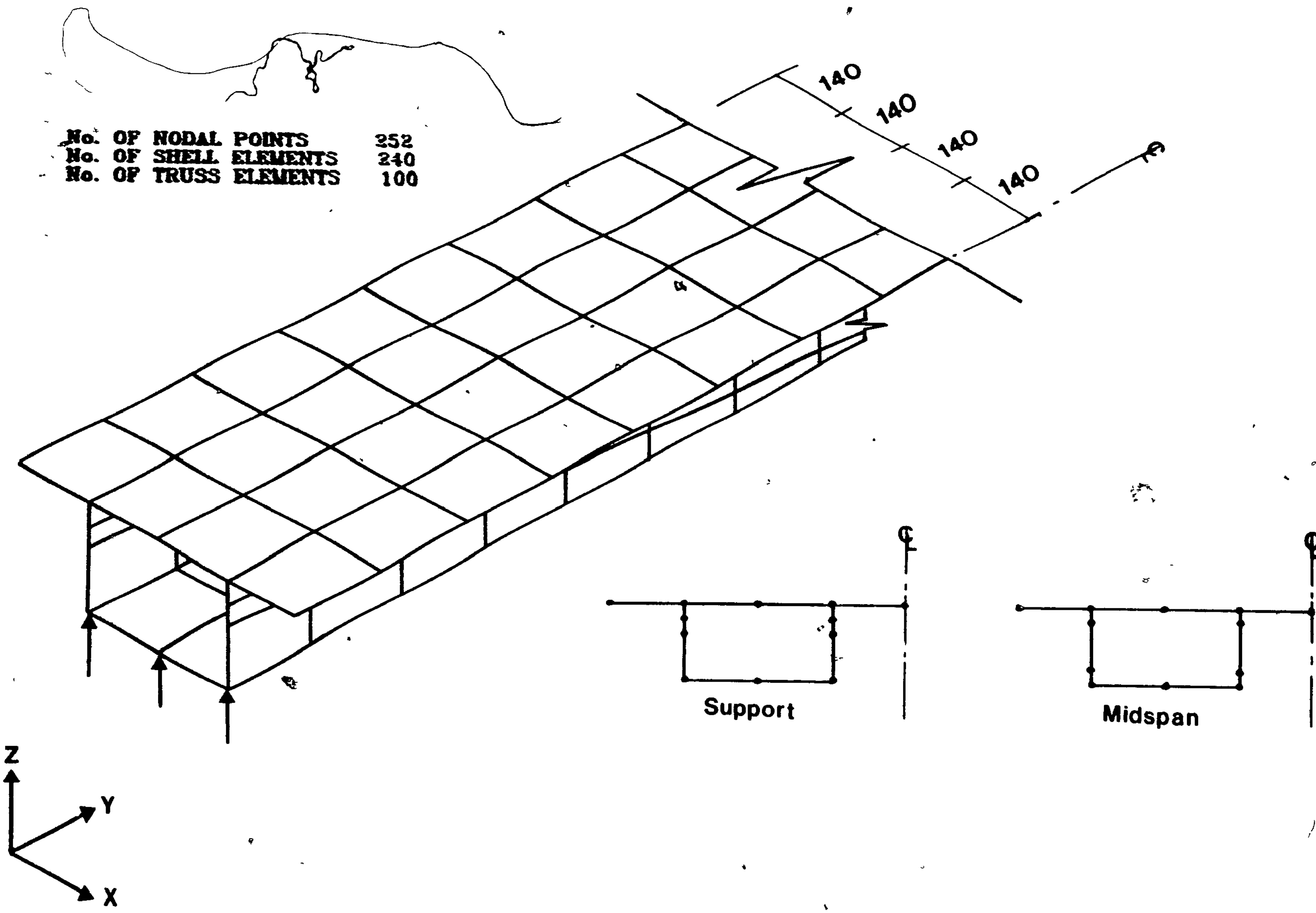

Figure 4.11 Finite Element Idealization for the Symmetrical Loading Case (SAP IV Program).

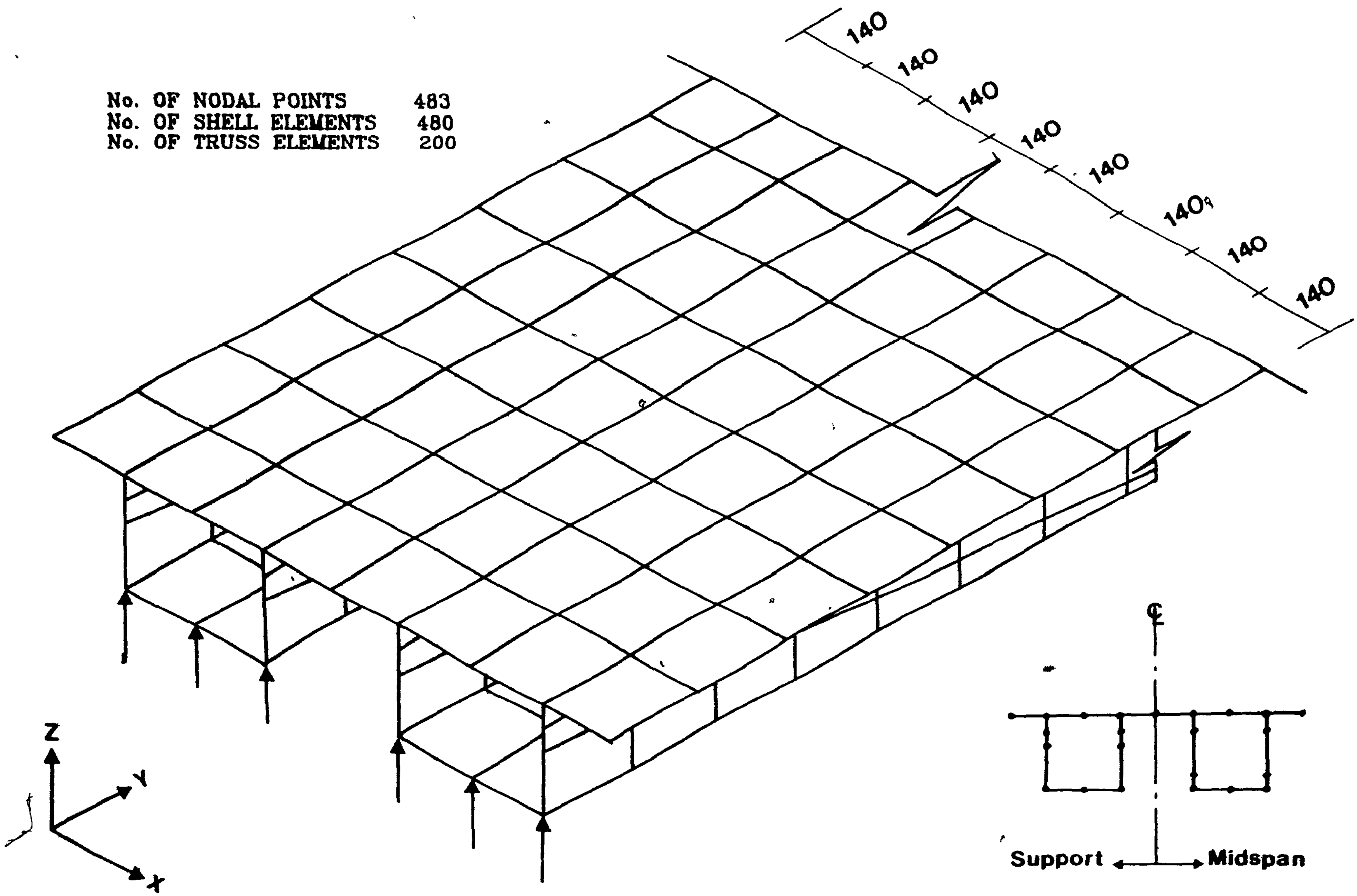

Figure 4.12 Finite Element Idealization for the Eccentric Loading Case (SAP IV Program).

The finite element analysis was conducted for the self weight of the bridge model, the extra dead load used to simulate the dead weight of the prototype and the prestressing forces, in addition to the following loading conditions:

4.3.3.1 Linear Analysis

(a) Two symmetric trucks.

(b) One eccentric truck.

(c) Free vibration analysis.

4.3.3.2 Quasi-Nonlinear Analysis

(a) Static Analysis. The quasi-nolinear analysis was performed for five loading cases (4, 6, 8, 10 and 11 truck loads). For each loading case, the elasticity matrix was modified to account for the nonlinearity introduced by the cracks. The value of E_p was calculated using equation (4.6) and the value of E_s was modified depending on the experimental strain values. The modified shear modulus of concrete, βG, was calculated using equation (4.7), depending on the approximate crack width in each element. After each analysis for the symmetrical truck loading case, an eccentric truck load was applied using the same procedure. Table 4.3 shows the values of the reduction factor and the reduced shear modulus values used for the different experimental crack widths.

Table 4.3 Values of the Reduction Factor β and the Reduced Shear Modulus βG used in the Static Analysis.

Crack width (mm)	β	βG(MPa)
0.03	0.7	8019
0.05	0.3	3306
0.10	0.08	972
0.25	0.02	243
0.30	0.012	150
0.80	0.004	49

(b) Dynamic Analysis. After each analysis for static loads, a free vibration analysis was performed. Again, the elasticity matrix was modified in stages by introducing new values of E_p, E_s and β in the elasticity matrix. However, in the experimental work, the cracks closed and the concrete strains diminished every time the bridge was unloaded for the performence of a dynamic test. For this reason, the values of E_p, E_s and β were modified depending on the experimental strain values and the crack widths after releasing the static loads. Table 4.4 shows the values of the reduction factor β and the reduced shear modulus βG for the different crack widths noted in the experiment.

Table 4.4 Values of the Reduction Factor β and the Reduced Shear Modulus βG used in the Dynamic Analysis.

Crack width (mm)	β	βG(MPa)
0.017	0.9	10931
0.020	0.8	9716
0.025	0.7	8019
0.030	0.6	7287
0.033	0.5	6073

CHAPTER 5

RESULTS AND DISCUSSION

5.1 Introduction

This chapter presents the results obtained from the finite element analyses and their comparison with the experimental findings. The effect of the dead load and the prestressing force, when acting alone, is described in Section 5.2. The behaviour of the model under symmetric and eccentric loads simulating the OHBDC truck is presented in Section 5.3, while the propagation of the cracks and the ultimate load test results are presented in Section 5.4. Finally, the dynamic analysis results are discussed in Section 5.5.

For each load case, the deflections, the stresses in the concrete and the strains in the prestressing wires obtained from the finite element analyses were compared with the corresponding experimental values. The experimental stress values in the concrete were obtained by converting the strain readings from the electrical resistance strain gauges to stresses using the stress-strain curve for concrete (Fig. 3.1). The natural frequencies of vibration of the structure at different levels of damage are presented and compared with the experimental findings as well as to the values obtained from the simple beam analysis.

Figure 5.1 shows details of the instrumentation used to monitor the deflections and strains in the concrete.

5.2 Dead Load and Prestressing Force

After removing the formwork, the model was instrumented so that the deflections and the strains at midspan could be recorded just after cutting the wires.

5.2.1 Deflections

Just after transfer, when only the self weight of the model and the prestressing force were acting, an upward deflection of 0.80 *mm* was observed at midspan. This was due to the force that the wires exerted upon the structure. The deflected shapes of the structure at this stage obtained from both NONLACS and SAP IV analyses are shown in Fig. 5.2. The upward deflections at midspan obtained from NONLACS and SAP IV were 0.82 *mm* and 0.75 *mm* respectively. The three analyses yielded similar results with the largest difference being 6% at midspan.

5.2.2 Stresses

The state of stresses at midspan just after transfer is shown in Fig. 5.3. It can be seen that the entire section was in compression. Again, the finite element results and the test results showed good agreement.

5.3 Simulated OHBDC Truck Load

5.3.1 General

To study the response of the bridge to truck loads, two models simulating the OHBDC truck were constructed[42]. The trucks were located so as to produce the maximum bending moment at midspan. To be able to evaluate the torsional rigidity and the dynamic characteristics of the bridge at each level of damage, the load was

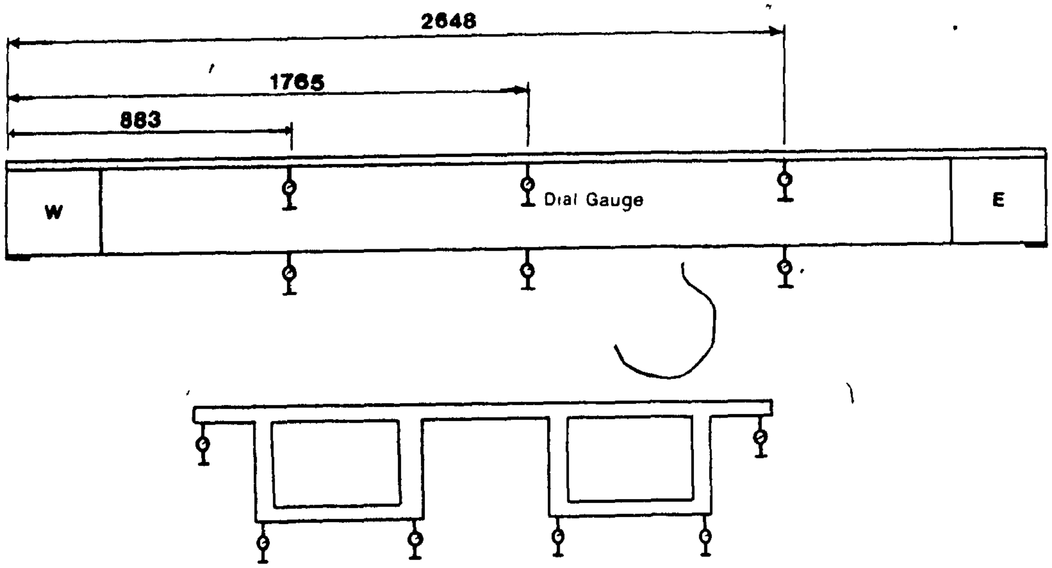

(a) Mechanical Dial Gauges

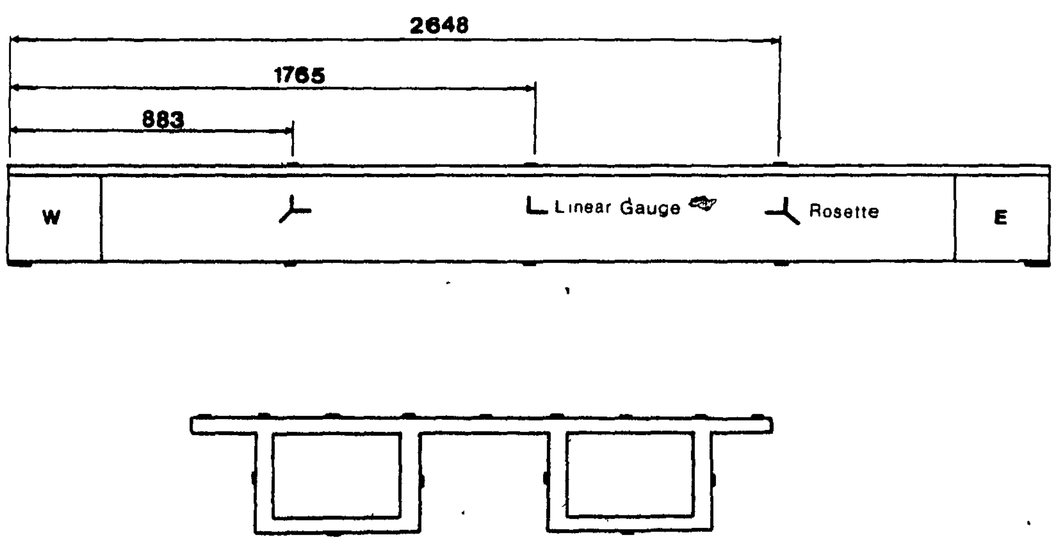

(b) Concrete Strain Gauges

Figure 5.1 Instrumentation Details.

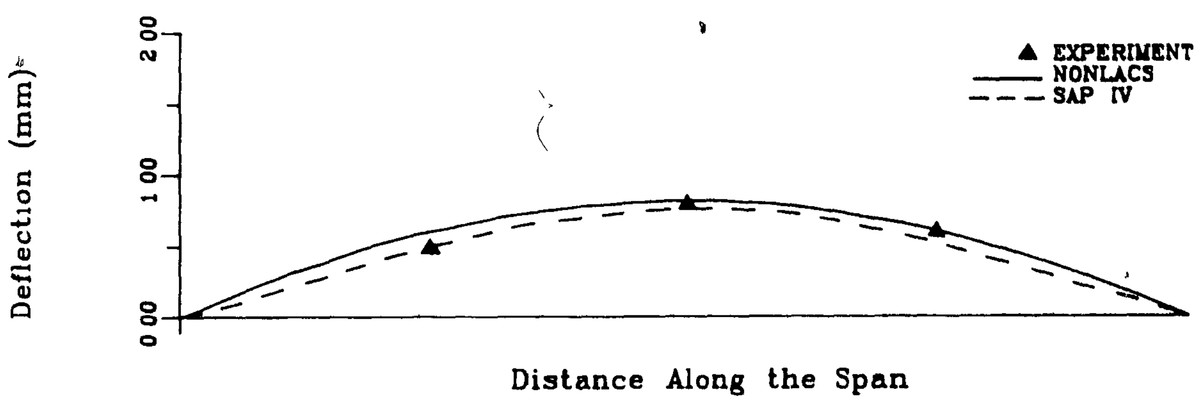

Figure 5.2 Deflected Shape at Prestress Transfer.

applied in five stages (2, 4, 6, 8 and 10 trucks). In each stage, the load was increased monotonically from zero to the load corresponding to that stage (26.40 kN, 52.80 kN, 79.20 kN, 105.60 kN and 132 kN). The total load was then released and one truck was removed. A total force of 13.20 kN equivalent to one simulated OHBDC truck was applied to induce torsion. After recording the readings, the load was released and the truck was removed. The dynamic test was then performed. The experimental procedure can be summarized as follow:

Day one:

1. Symmetrical load from 0.00 to 26.40 kN (2 trucks).
2. Eccentric load from 0.00 to 13.20 kN (one truck).
3. Dynamic test.

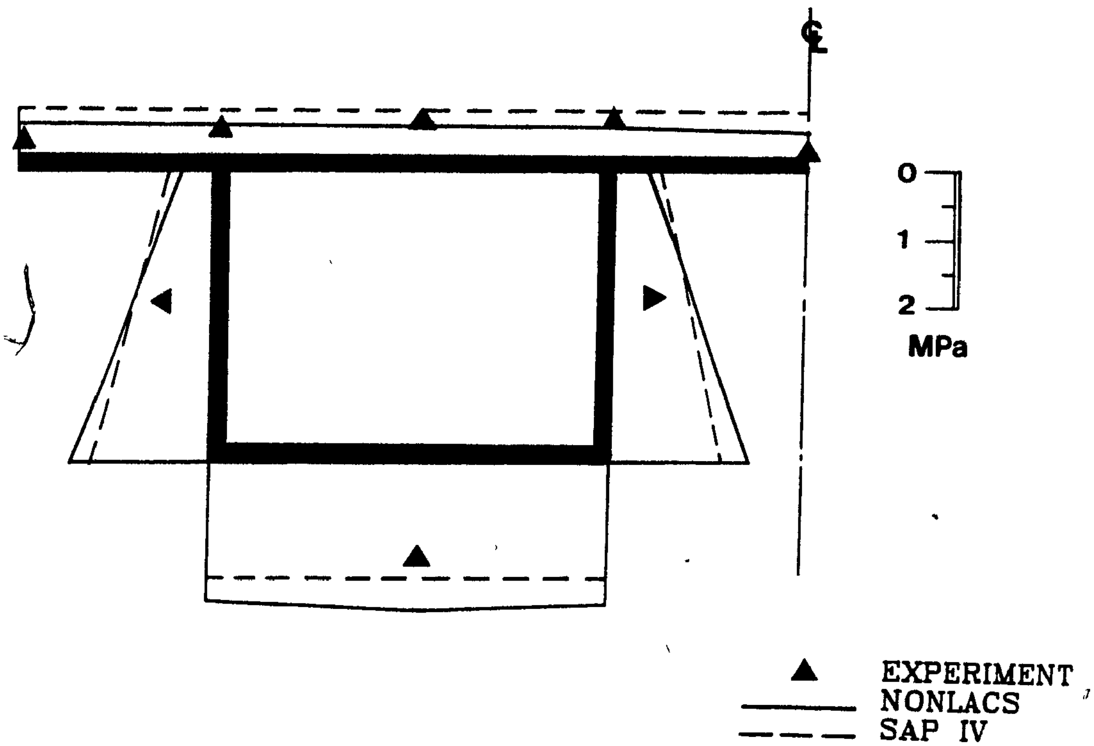

Figure 5.3 State of Stresses at Prestress Transfer.

Day two:

1. Symmetrical load from 0.00 to 52.80 kN (4 trucks).
2. Eccentric load from 0.00 to 13.20 kN (one truck).
3. Dynamic test.

Day three:

1. Symmetrical load from 0.00 to 79.20 kN (6 trucks).
2. Eccentric load from 0.00 to 13.20 kN (one truck).
3. Dynamic test.

Day four:

1. Symmetrical load from 0.00 to 105.60 kN (8 trucks).
2. Eccentric load from 0.00 to 13.20 kN (one truck).

3. Dynamic test.

Day five:

1. Symmetrical load from 0.00 to 132 kN (10 trucks).
2. Eccentric load from 0.00 to 13.20 kN (one truck).
3. Dynamic test.

Day six:

1. Ultimate load test.

The experimental program was completed in six days (i.e. one load stage per day).

The nonlinear finite element analysis using NONLACS program was performed at Carleton University in Ottawa. The loading sequence used in the NONLACS analysis was different from the one used in the experiment. In the NONLACS analysis the load was increased monotonically from 0.00 to 139 kN in 20 load steps. It should be noted that the same loading sequence as used in the experimental program could have been used, since NONLACS can handle repeated loading as well as monotonic loading. But because of time constraints, it was decided to load the model monotonically. The NONLACS finite element analysis was expected to give stiffer results compared with the experimental data due to the stiffness degradation caused by the loading and unloading in the experiment. However, because of the small number of repeated loadings (five), the stiffness degradation was not large enough to influence the general behaviour of the bridge so that a comparative study could be done.

The SAP IV quasi–nonlinear analysis consisted of making appropriate changes in the elasticity matrix to account for the nonlinearity introduced by the cracks at each load level, as explained in the previous chapter.

5.3.2 Deflections

5.3.2.1 Symmetrical Truck Loading

The vertical deflections at midspan and at quarterspans were observed experimentally by using mechanical dial gauges. After readings of the initial experimental deflections were made, all dial gauge readings were set to zero. Therefore, to obtain the total deflections from the NONLACS and the SAP IV analyses at any load, the initial deflections obtained in load Step 1 (due to the dead weight and the prestressing force) were subtracted from the deflections obtained in the following steps. This was necessary so that the deflections in all three analyses were measured from the same origin (i.e. zero). The analytical and experimental vertical deflections at midspan of the model under truck loading are shown in Fig. 5.4.

The figure shows reasonable agreement between the NONLACS finite element analysis and the experimental deflections with the NONLACS model showing slightly higher stiffness than the real structure. This was expected since the two models were loaded differently (Section 5.3.1). However, the two analyses yielded similar results up to a load of 52.80 kN (4 trucks). At this load level the deflection obtained by NONLACS was 1.50 *mm* while the experimental deflection was 2.10 *mm*, which represented a difference of about 35%. Beyond this load level, the difference between the two analyses varied between 25% and 30%. This shows that the program NONLACS predicted the general shape of the load deflection curve with reasonable accuracy. Near the ultimate load, the analytical deflection obtained from NONLACS was 11 *mm* and the experimental deflection was 15 *mm* which represent a difference of about 27%.

As shown in Fig. 5.4, the SAP IV quasi-nonlinear analysis yielded accurate results in the linear range and the beginning of the nonlinear range. At a load of 79.20 kN (6 trucks) the vertical deflection obtaind by SAP IV was 8% higher than the experimental vertical deflection. When cracks propagated and the response of the structure

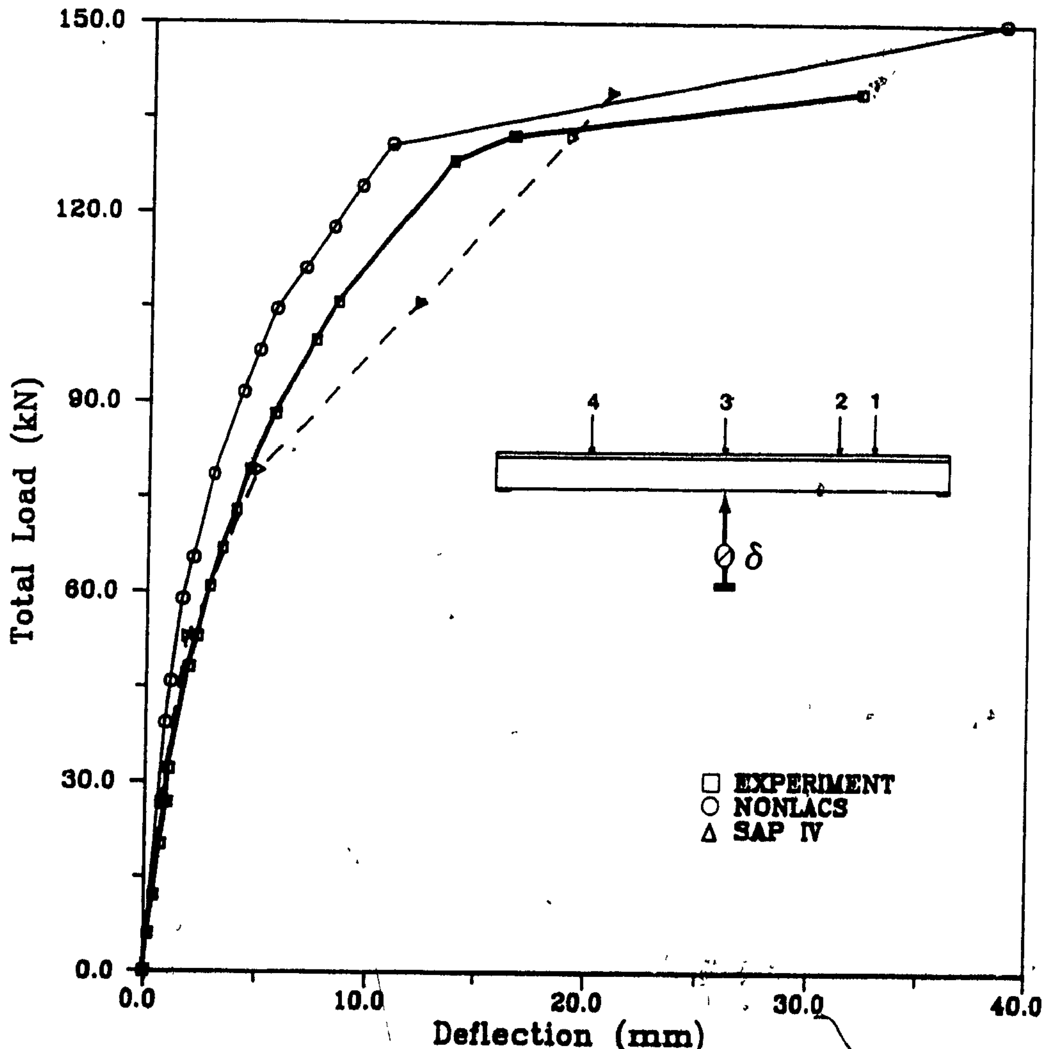

Figure 5.4 Load–Midspan Deflection Under Truck Loading.

became nonlinear, this difference increased significantly to about 30% near the ultimate load. It could be noticed by examining the load-deflection curve that SAP IV continued to show a higher stiffness while the stiffness of the bridge measured experimentally decreased considerably. Many factors (crack width, strains in concrete, etc.) could have affected the relative agreement of the two analyses especially in the nonlinear range. It was noticed after having performed several runs of the SAP IV quasi–nonlinear program, that the vertical deflections were very sensitive to the crack width variable. It is acknowledged that, without a very sophisticated crack measuring device, crack widths are very difficult to measure accurately. This was one of the main reasons for the deviation in the deflection between the results of the SAP IV quasi–nonlinear analysis and the test results.

The deflected shape of the bridge and the distribution of the vertical deflection across the midspan and quarterspan sections at different load levels are depicted in Figures 5.5 through 5.14. The deflection is distributed uniformly across the width of the bridge. Table 5.1 summarizes the values of the vertical deflection while Fig. 5.15 and Table 5.2 give the variation of the flexural stiffness of the bridge at the different loading stages. These values represent the tangent stiffness of the various load–deflection curves.

Table 5.1 Vertical Deflection at Midspan.

	Deflection (mm)		
Number of Trucks	Experiment	NONLACS	SAP IV
2	0.80	0.71	0.76
4	2.11	1.49	1.70
6	4.52	2.89	4.89
8	8.35	5.91	12.01
10	14.97	10.78	18.97

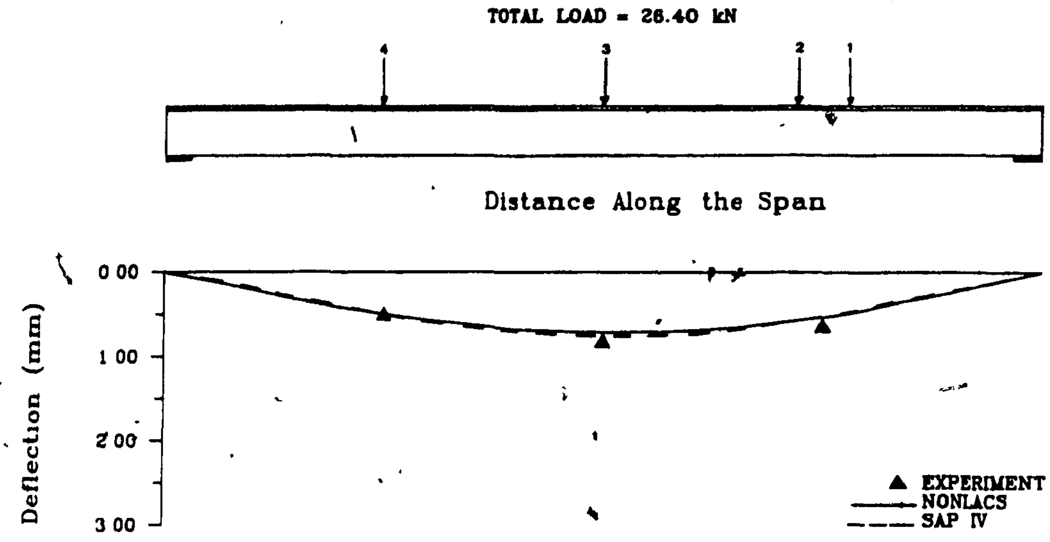

Figure 5.5 Deflected Shape Under Two Truck Loads.

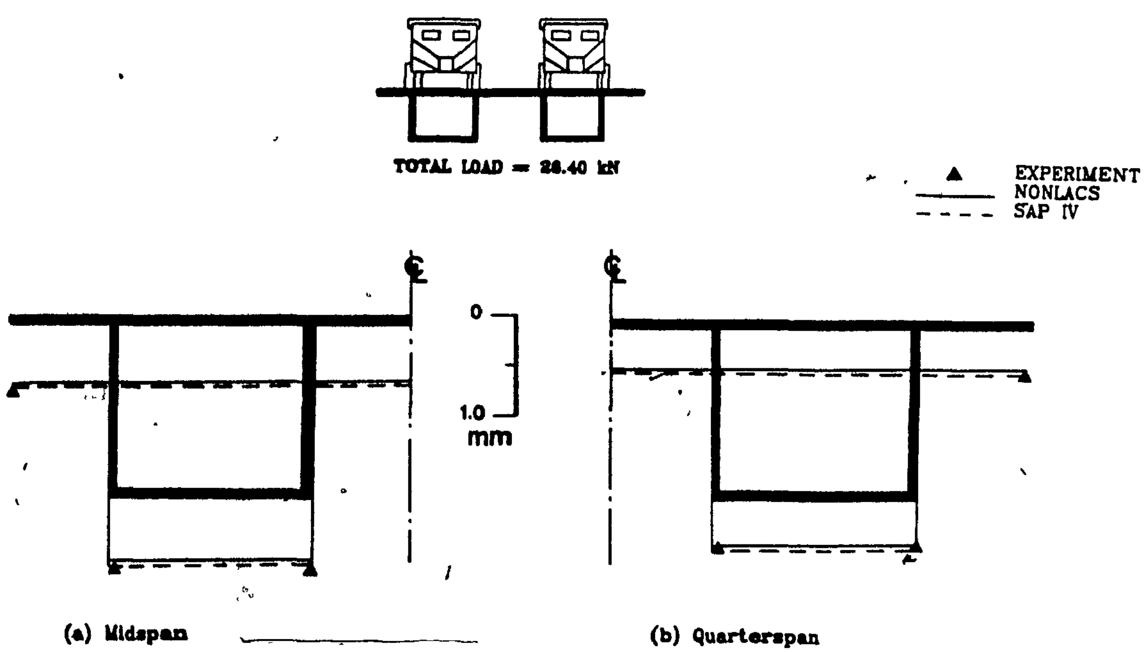

Figure 5.6 Deflection Under Two Truck Loads.

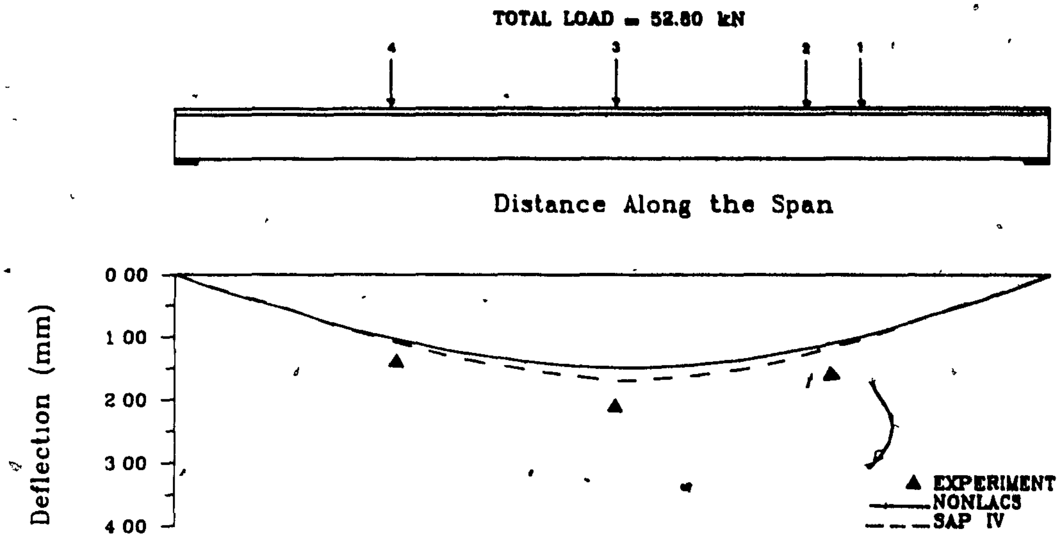

Figure 5.7 Deflected Shape Under Four Truck Loads.

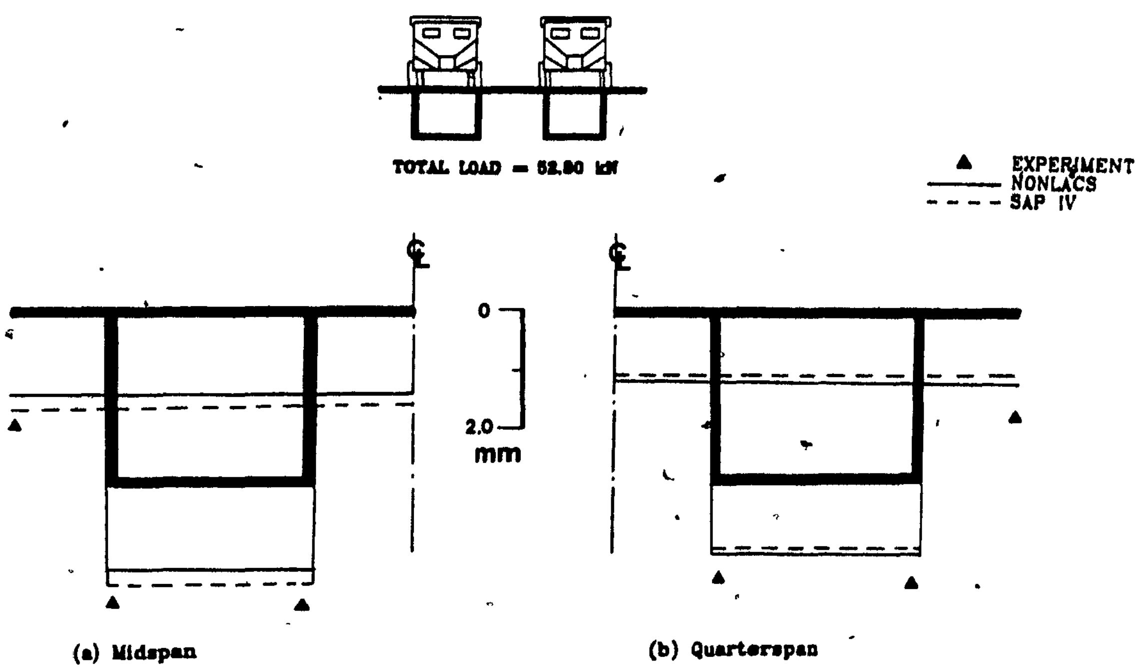

Figure 5.8 Deflection Under Four Truck Loads.

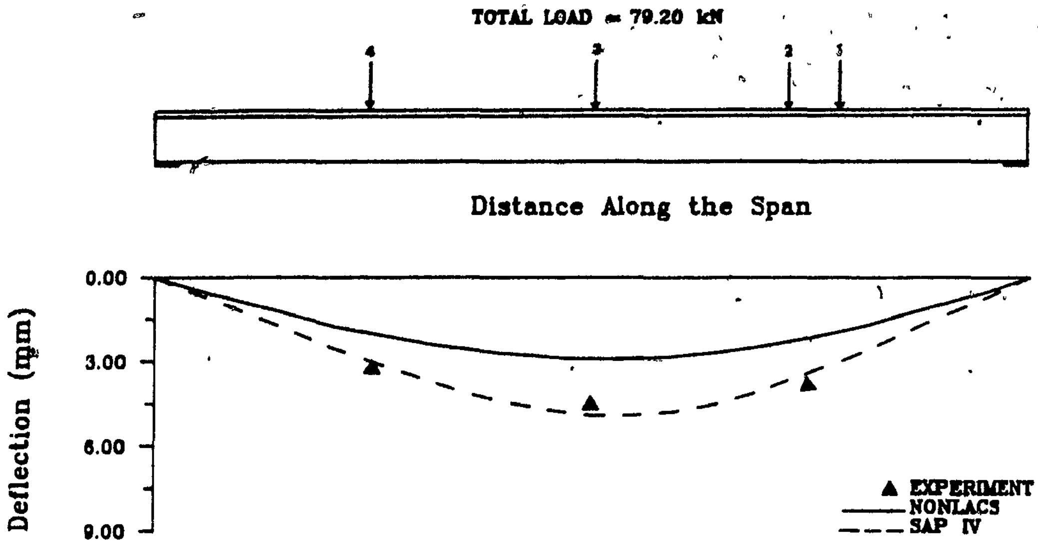

Figure 5.9 Deflected Shape Under Six Truck Loads.

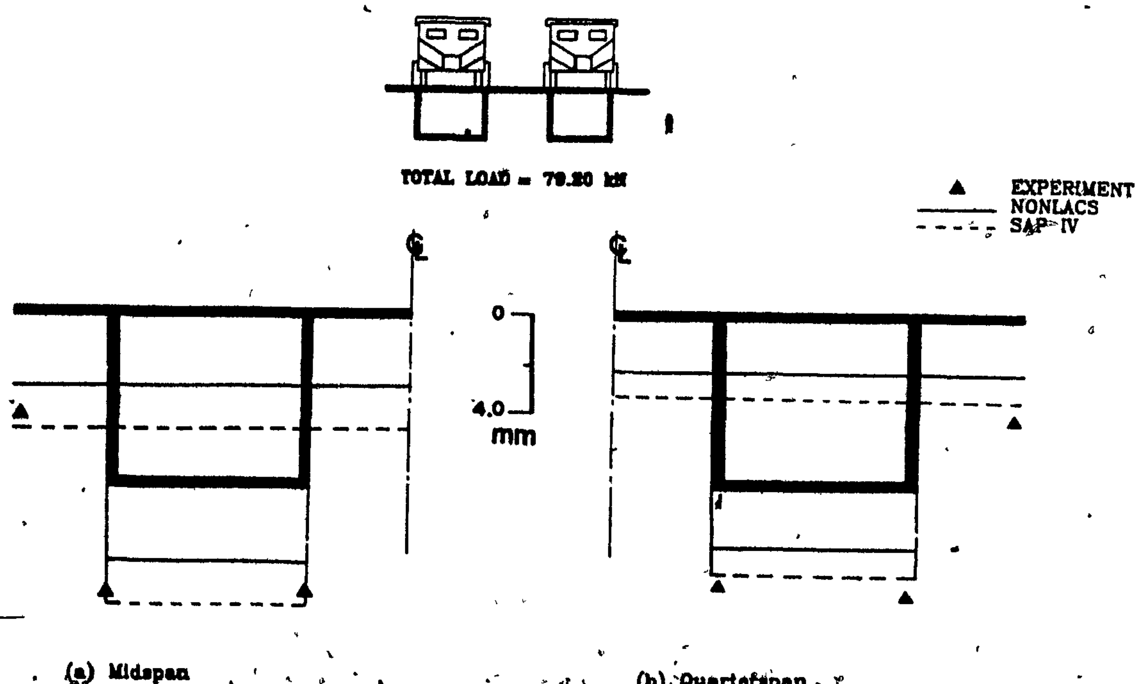

Figure 5.10 Deflection Under Six Truck Loads.

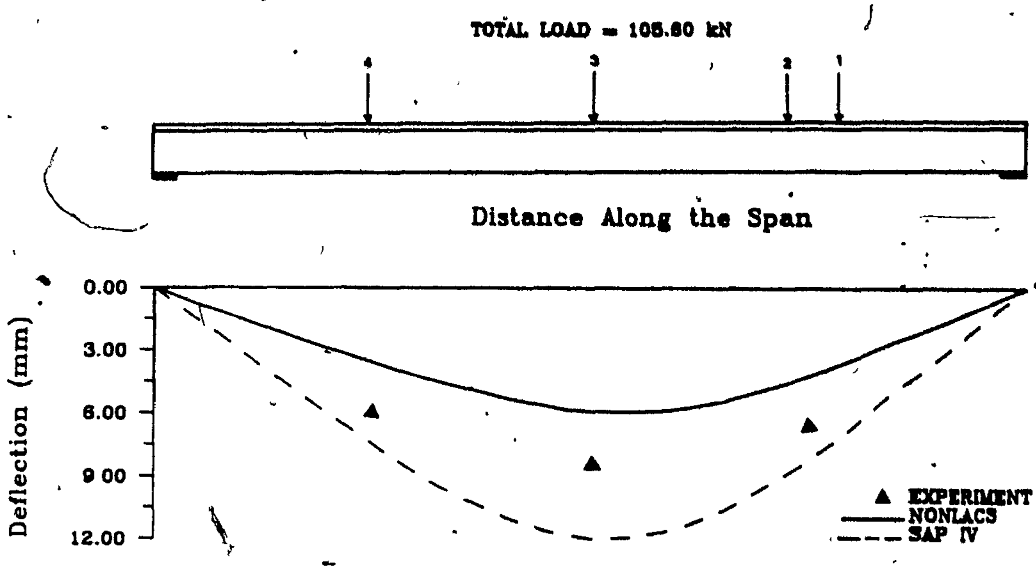

Figure 5.11 Deflected Shape Under Eight Truck Loads.

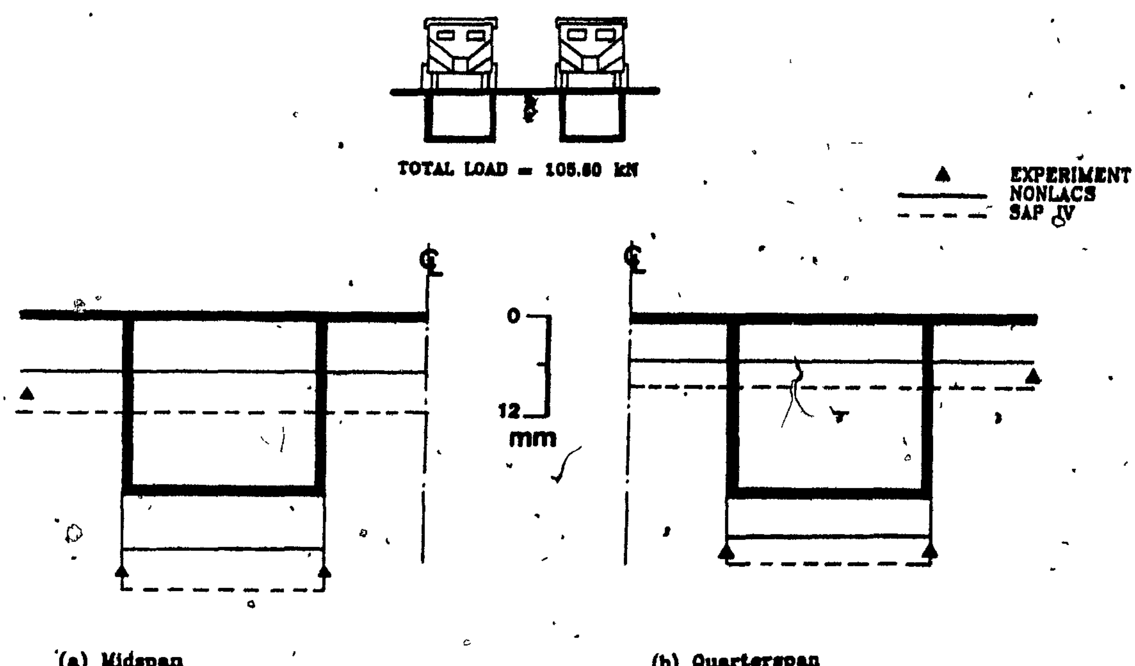

Figure 5.12 Deflection Under Eight Truck Loads.

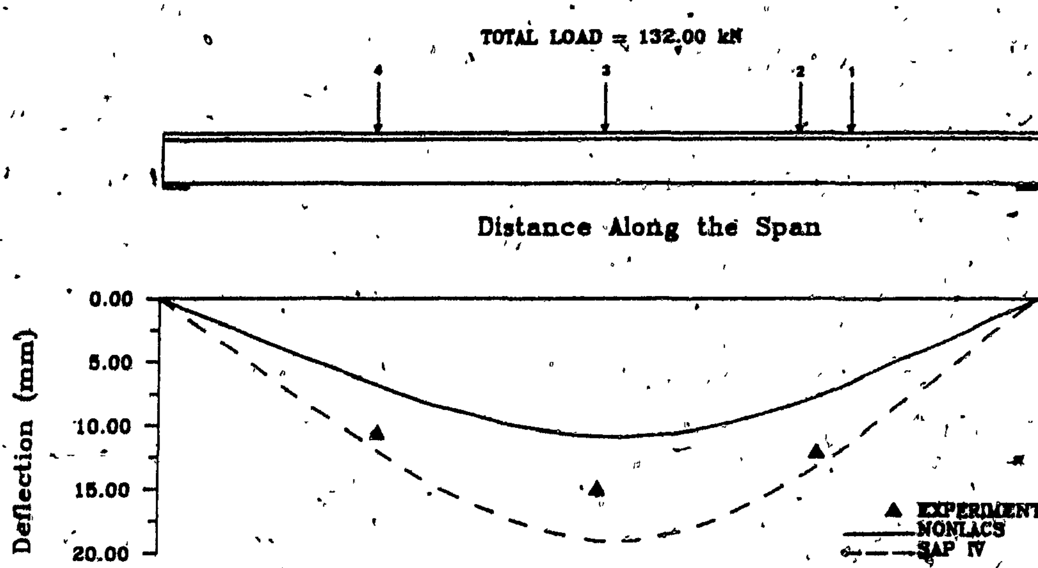

Figure 5.13 Deflected Shape Under Ten Truck Loads.

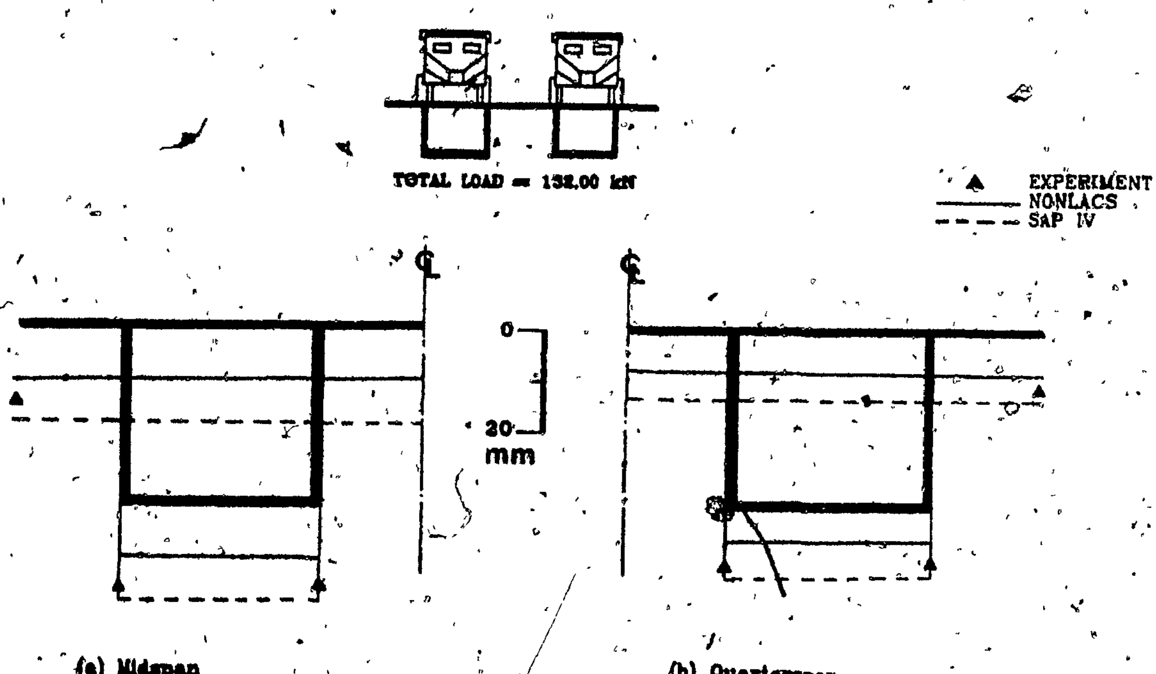

Figure 5.14 Deflection Under Ten Truck Loads.

As a summary, the three analyses showed that the bridge behaved linearly up to a total load equal to 4 truck loads and gave similar results. The stiffness of the bridge decreased to a much lower value than the initial value. In the nonlinear range, SAP IV overestimates the vertical deflection while the NONLACS program underestimates it. However, the difference between the two finite element results and the test results did not exceed 35% at any load level.

Table 5.2 Variation of the Flexural Stiffness.

	Flexural Stiffness (kN/mm)		
Total Load (kN)	Experimental	NONLACS	SAP IV
0	33.90	37.20	34.80
26.40	20.20	33.90	28.10
52.80	15.20	18.90	8.30
79.20	8.40	8.80	3.60
105.60	4.30	5.42	3.70

5.3.2.2 Eccentric Truck Loading

To evaluate the torsional stiffness of the model at different levels of damage, the bridge was loaded eccentrically, after each symmetrical static loading. The load was increased from zero to 13.20 kN (equivalent to one truck load), and the vertical deflections were measured. The angle of twist was calculated using the measured and the computed deflection values. The computed deflections were obtained using the SAP IV quasi–nonlinear program.

The torque–midspan twist curves at different levels of damage are shown in Figures 5.16 through 5.20. The variation of the torsional stiffness is plotted in Fig. 5.21 and the values are presented in Table 5.3. The difference between the experimental and the computed torsional stiffness ranged from 22% to 32%. It can be seen that SAP IV overestimates the torsional stiffness of the bridge. In the uncracked state, the torsional stiffness of the bridge structure was noted to be 20,555 $kN.m/rad$ (Fig. 5.16). After

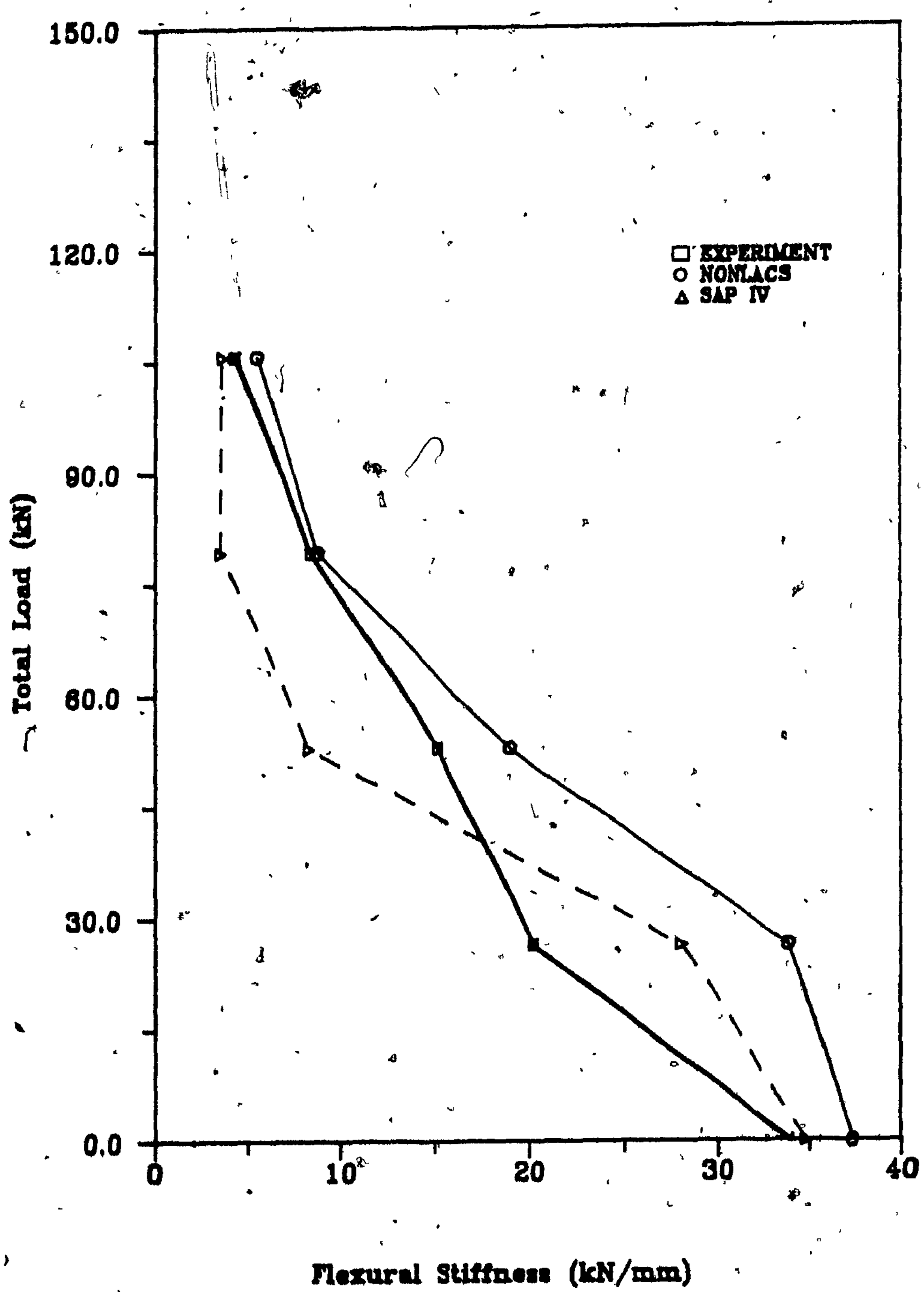

Figure 5.15 Variation of Flexural Stiffness with Load level.

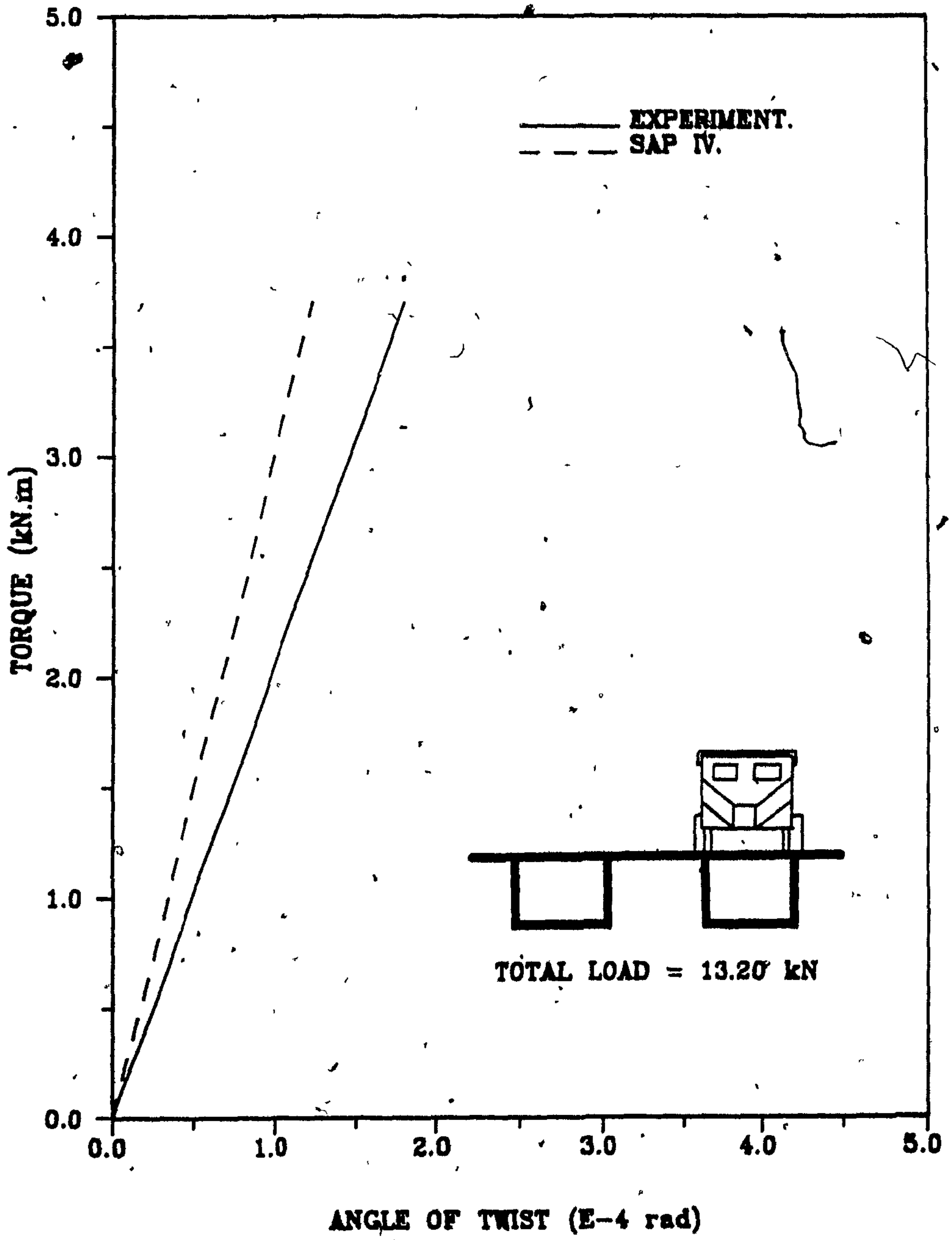

Figure 5.16 Torque–Midspan Twist Under Eccentric Truck Load (Uncracked Bridge).

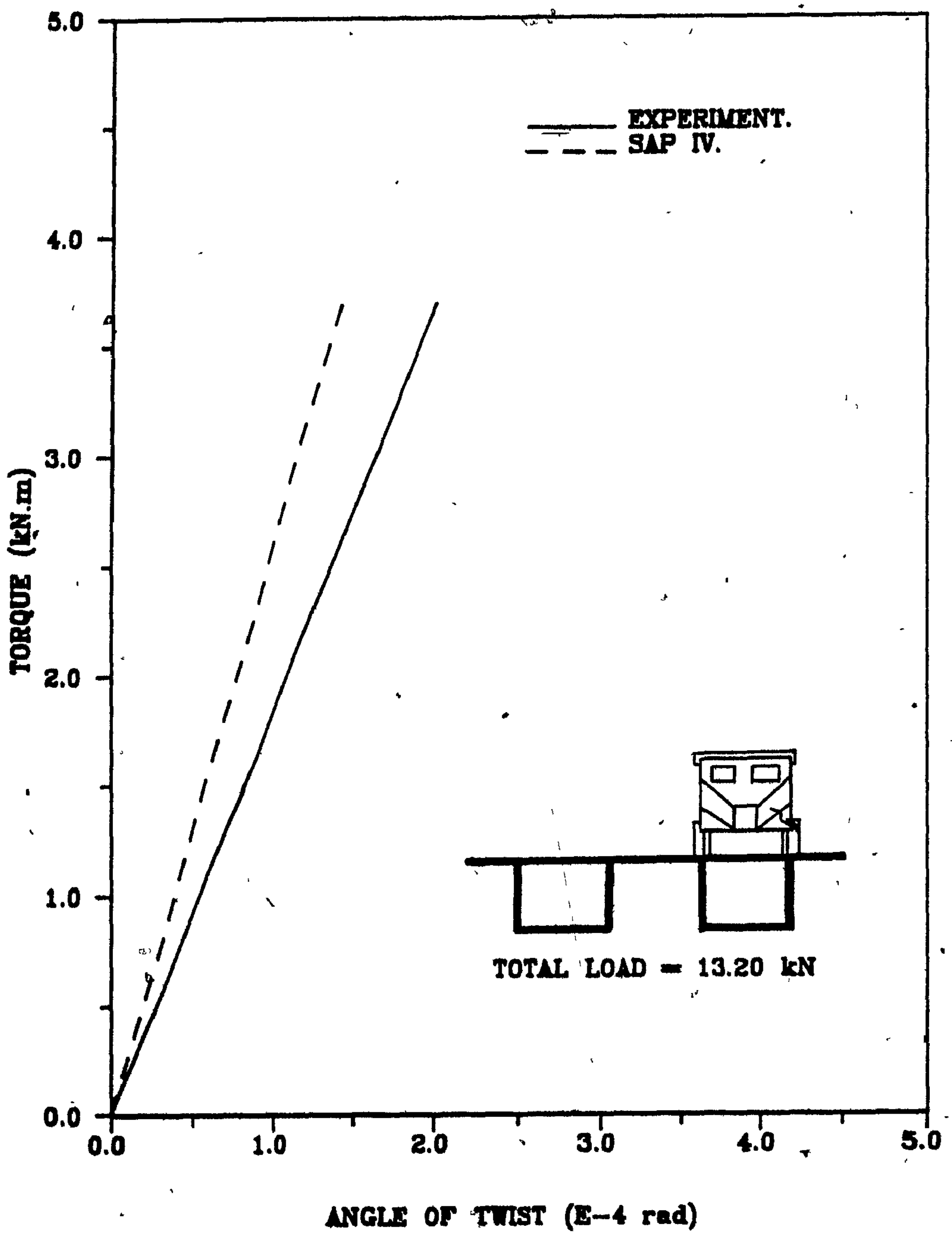

Figure 5.17 Torque–Midspan Twist Under Eccentric Truck Load (After 4 Truck Loads).

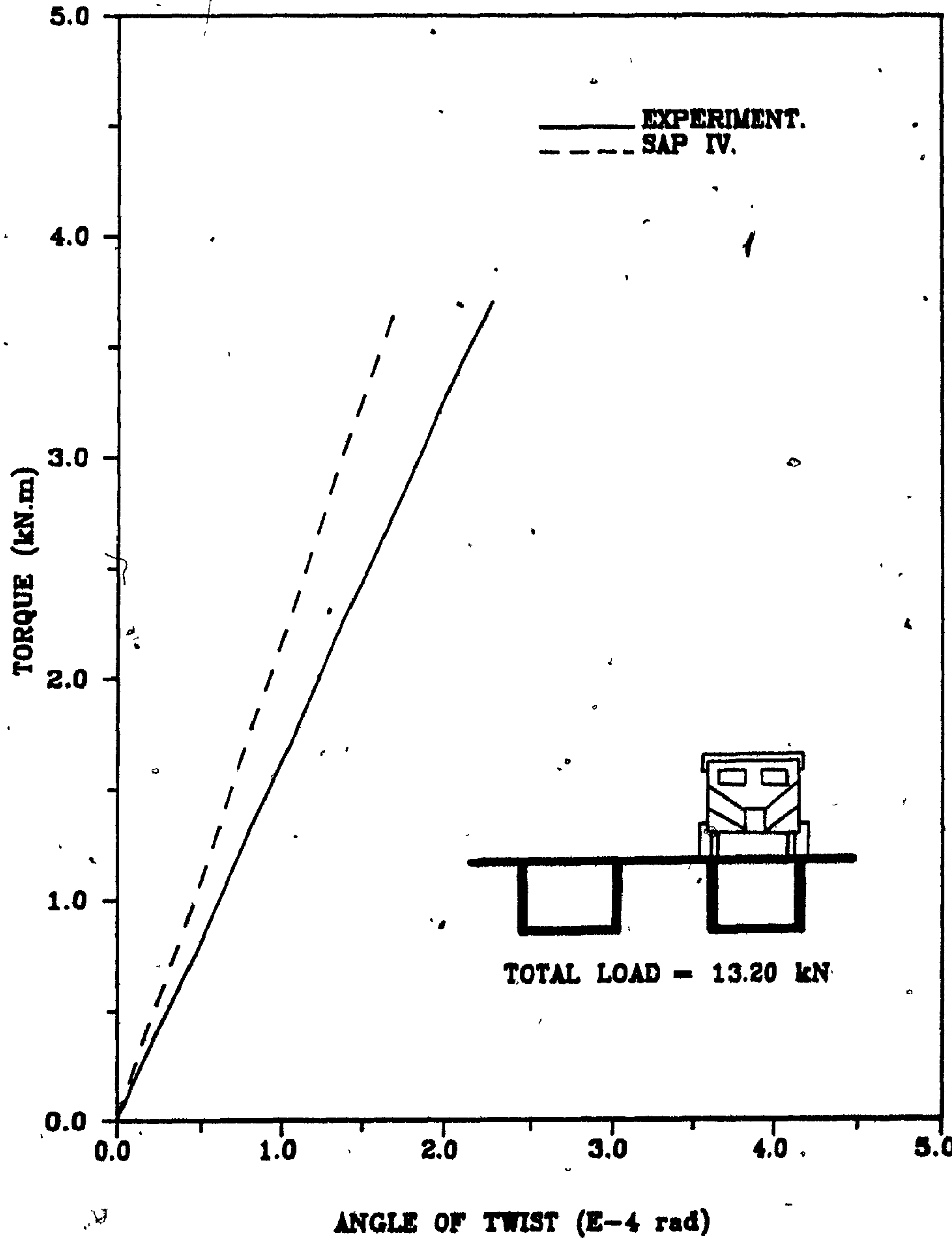

Figure 5.18 Torque–Midspan Twist Under Eccentric Truck Load (After 6 Truck Loads).

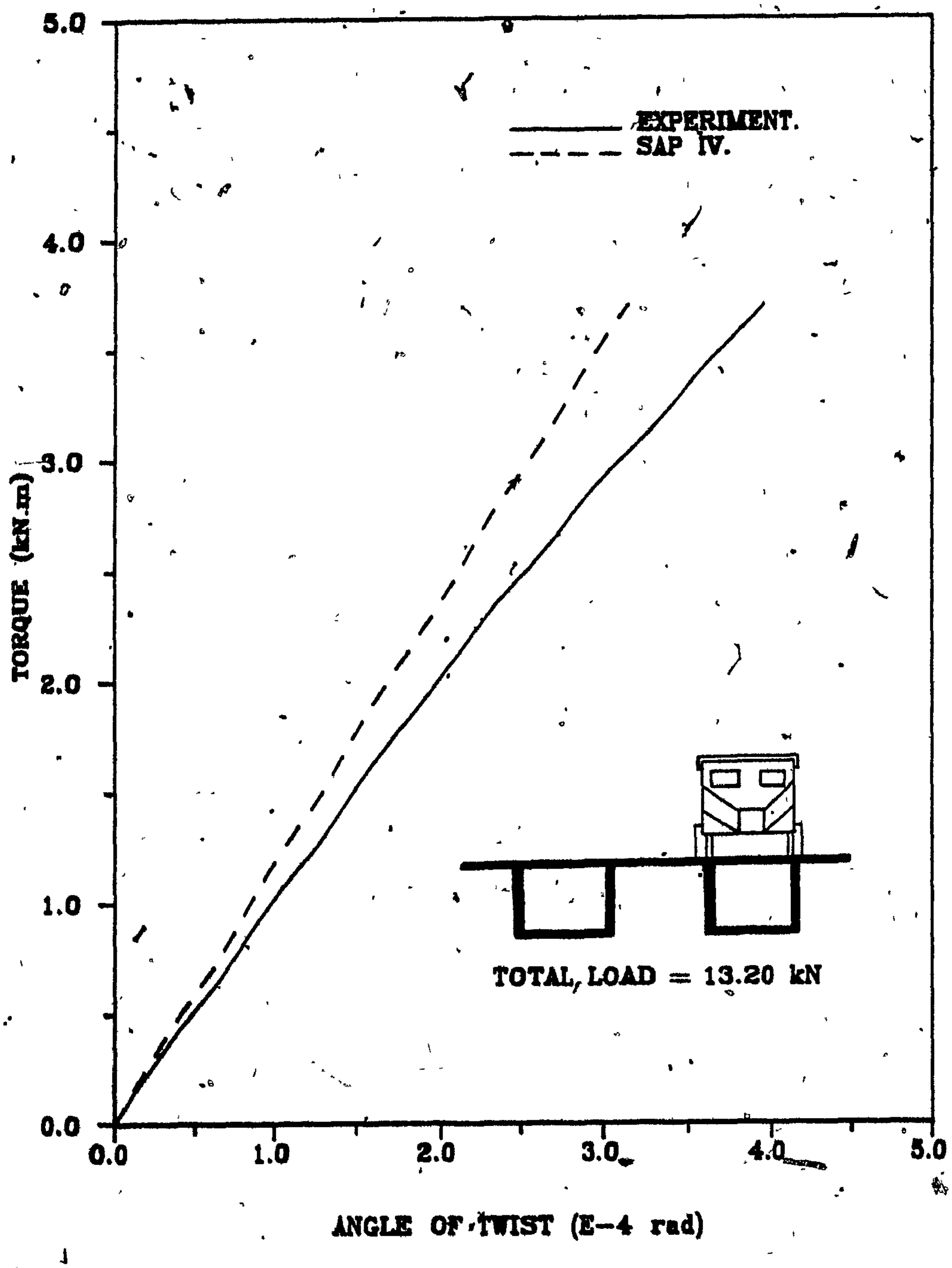

Figure 5.19 Torque–Midspan Twist Under Eccentric Truck Load (After 8 Truck Loads).

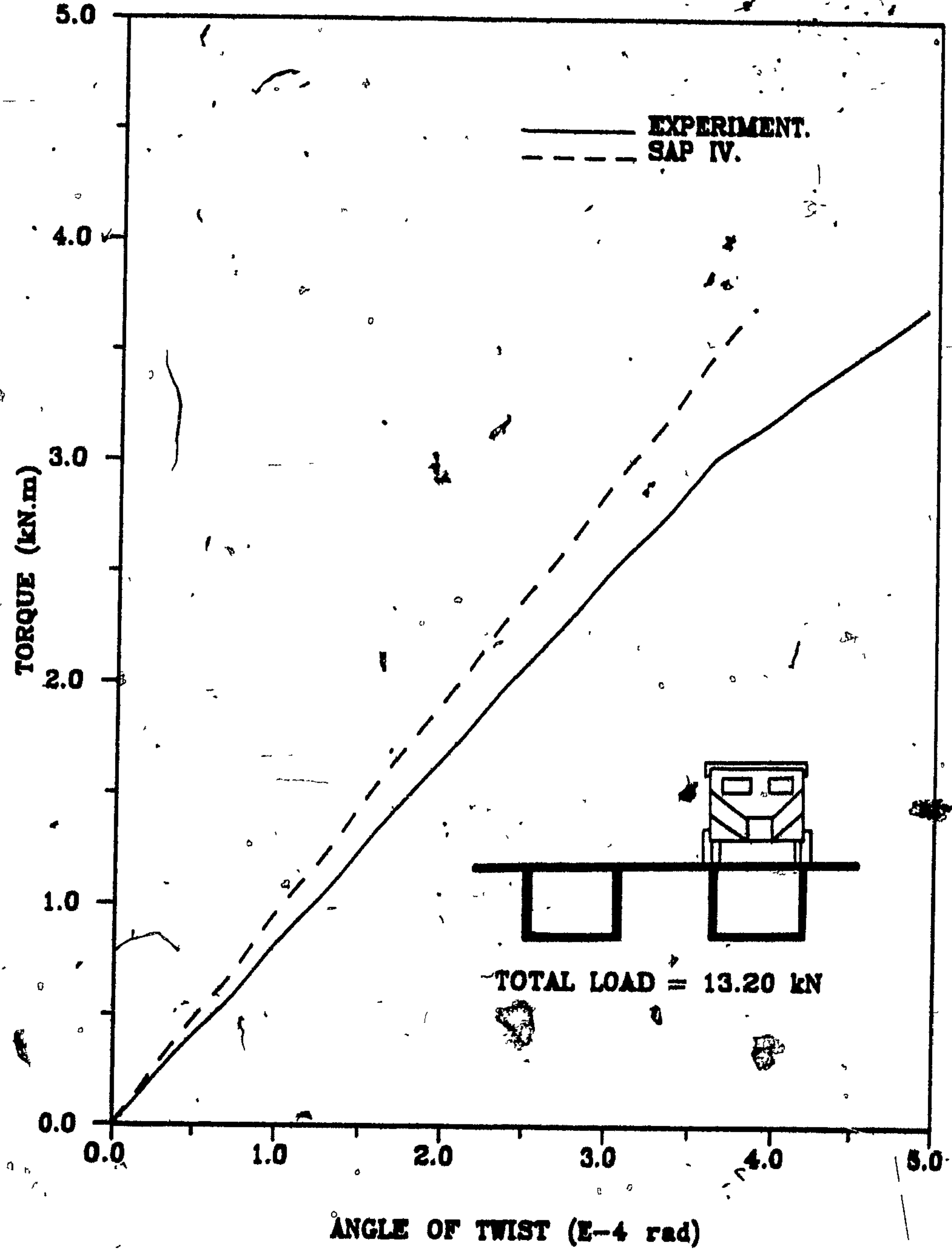

Figure 5.20 Torque–Midspan Twist Under Eccentric Truck Load (After 10 Truck Loads).

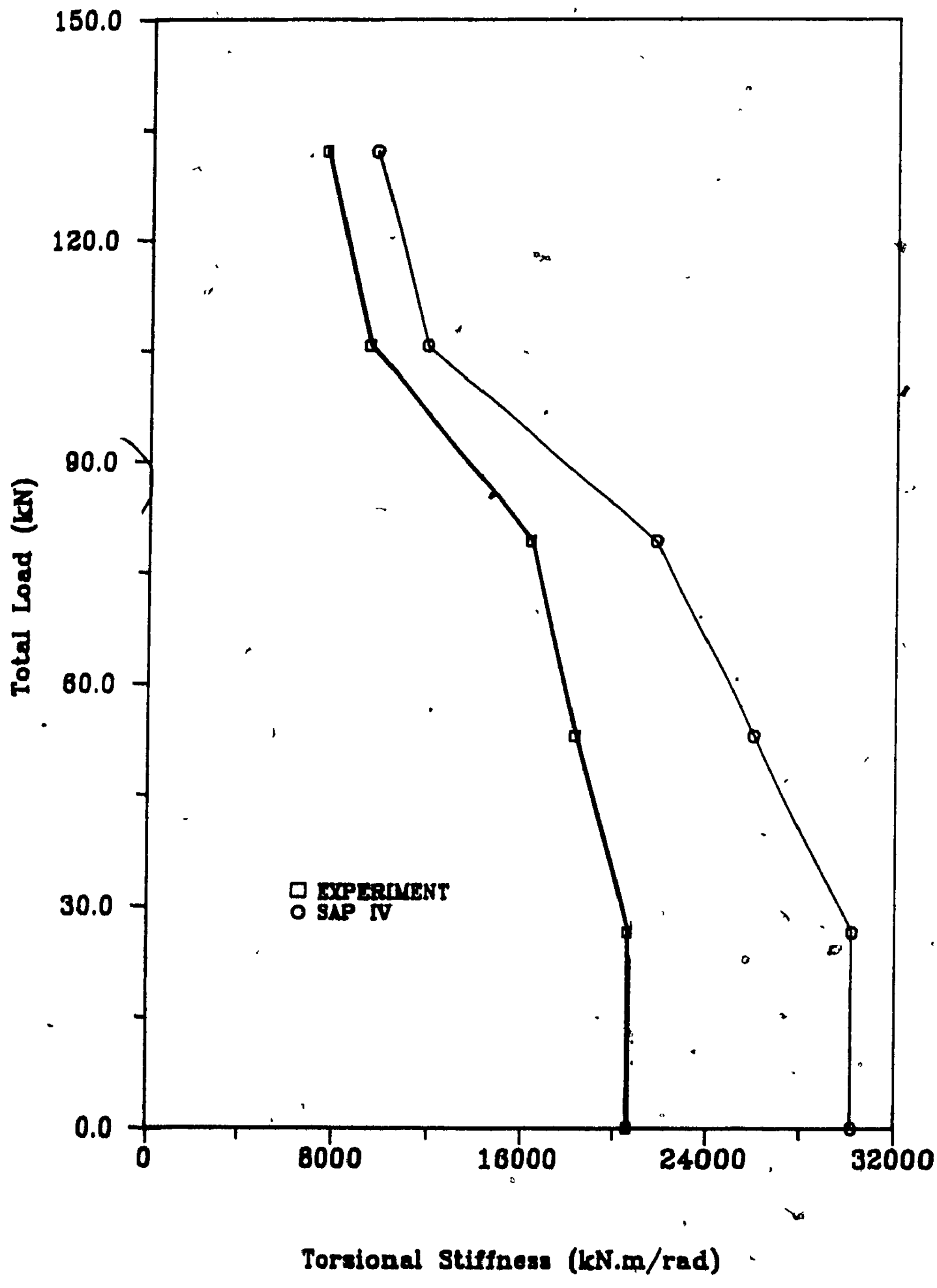

Figure 5.21 Variation of Torsional Stiffness with Load Level.

a load of 52.80 kN (4 trucks), the torsional stiffness of the bridge decreased by 11%. After a load of 105.60 kN (8 trucks), when the cracks opened and increased in number, the torsional stiffness decreased to about half its initial value (Fig. 5.19). At the ultimate load level the bridge was severely damaged and its torsional stiffness dropped to 7505 $kN.m/rad$.

Table 5.3 Torsional Stiffness of the Bridge.

	Torsional Stiffness(kN.m/rad)	
Number of Trucks	Experiment	SAP IV
2	20,555	30,081
4	18,317	25,874
6	16,300	21,765
8	9,367	11,821
10	7,505	9,610

5.3.3 Stresses in Concrete

The values of the stresses in the concrete were obtained by converting the experimental strain reading from the electrical resistance strain gauges to stresses using the stress–strain curve for concrete (Fig. 3.1). The average longitudinal stresses in the top slab, at midspan and at quarterspan, obtained experimentally and the finite element analyses, are compared in Figures 5.22 and 5.23, respectively. Tables 5.4 and 5.5 summarize the values of stresses in the concrete slab at midspan and at quarterspan.

Figure 5.22 shows excellent correlation between the experimental stresses and the NONLACS finite element results. Up to a load of 105.60 kN corresponding to 8 truck loads, the diffrence between NONLACS and experimental stress values did not exceed 5%. At eight truck loads the NONLACS program gave a stress of 10.57 MPa at midspan, while the corresponding experimental value was 10.16 MPa (Table 5.4). As

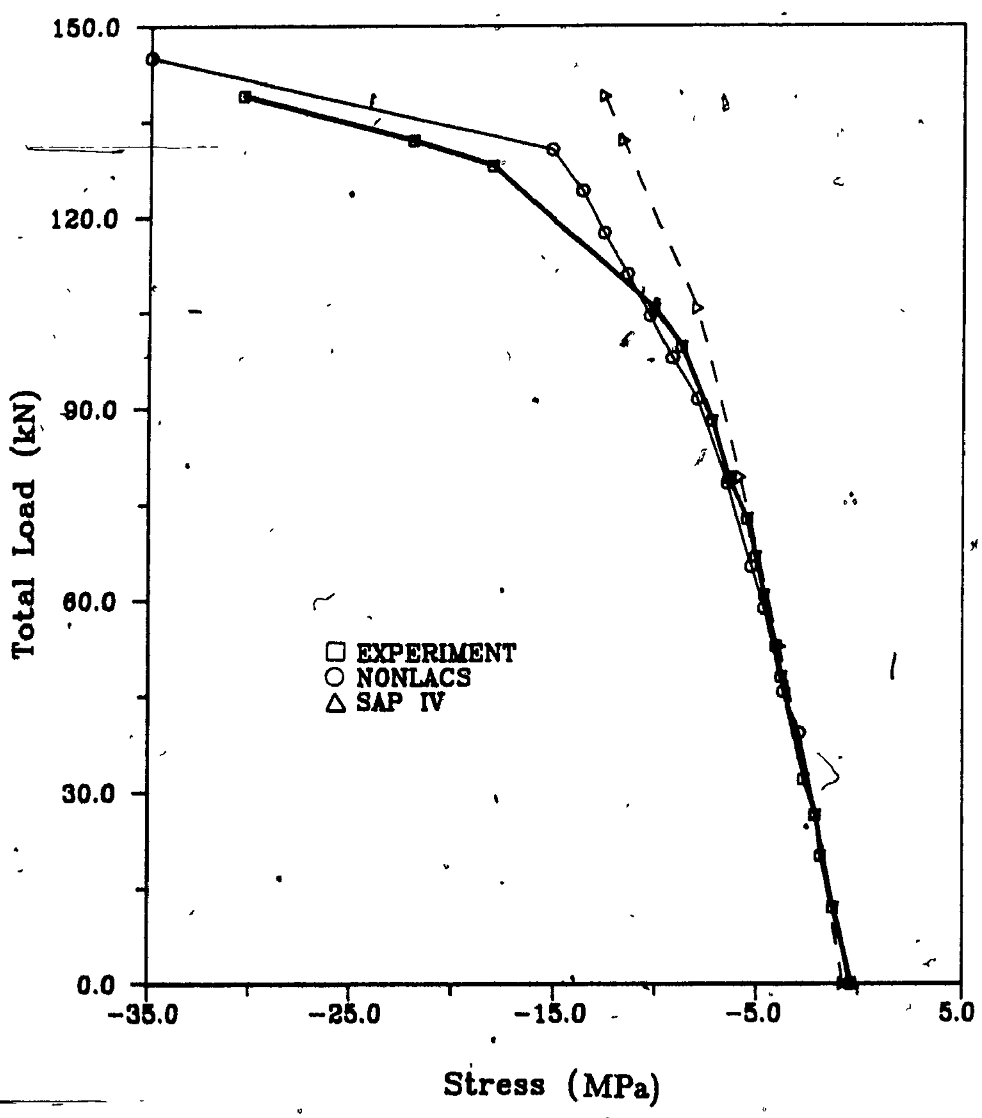

Figure 5.22 Longitudinal Stress Variation at Midspan in the Top Slab.

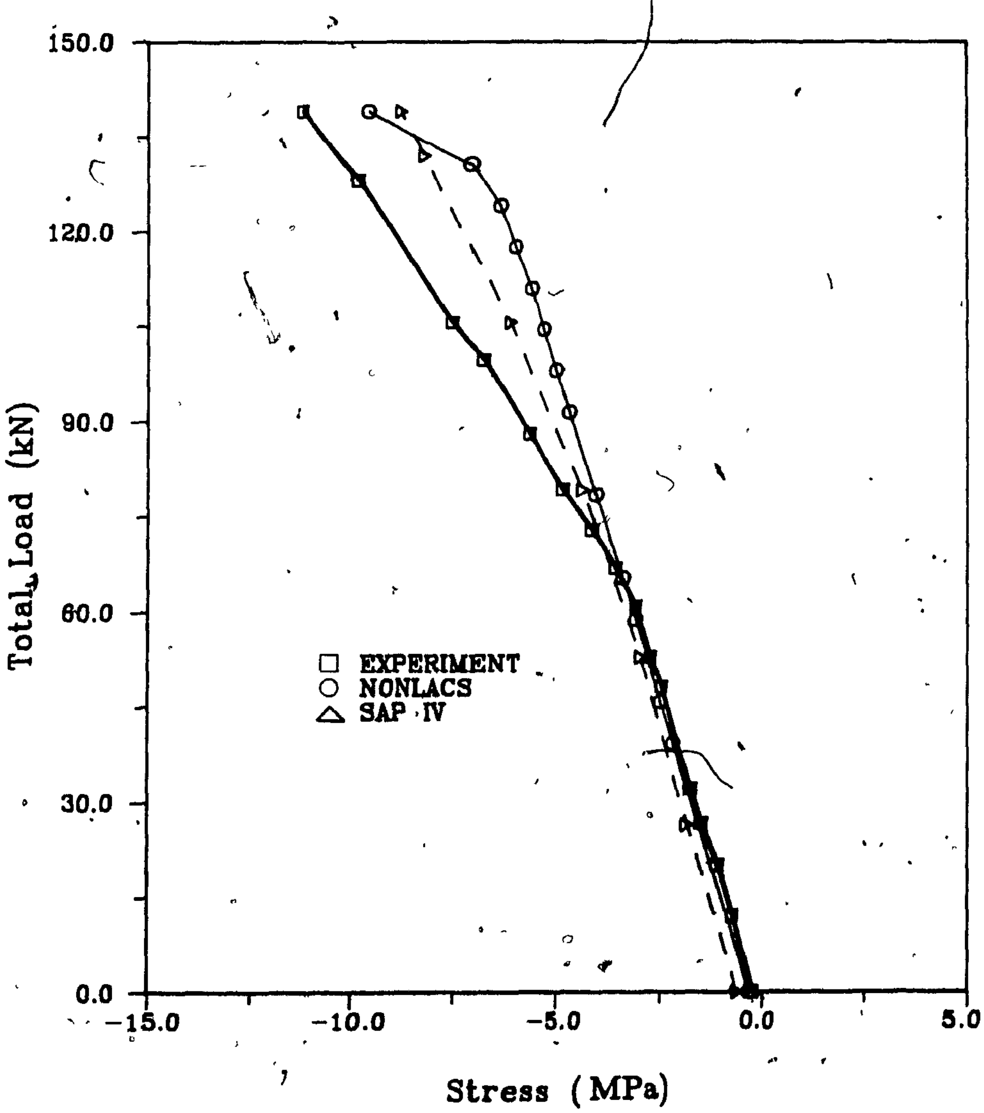

Figure 5.23 Longitudinal Stress Variation at Quarterspan in the Top Slab.

the applied load approached the ultimate load, the difference increased and was about 30% at a load level equivalent to ten trucks.

Table 5.4 Stresses in the Concrete Slab at Midspan.

	Stress (MPa)		
Total Load (kN)	Experiment	NONLACS	SAP IV
0	-0.39	-0.47	-0.80
26.40	-2.20	-2.17	-2.23
52.80	-4.10	-4.24	-3.92
79.20	-6.50	-6.68	-5.88
105.60	-10.16	-10.57	-8.10
132.00	-22.00	-15.21	-11.73

Table 5.5 Stresses in the Concrete Slab at Quarterspan.

	Stress (MPa)		
Total Load (kN)	Experiment	NONLACS	SAP IV
0	-0.26	-0.36	-0.67
26.40	-1.50	-1.60	-1.82
52.80	-2.75	-2.80	-3.00
79.20	-4.85	-4.09	-4.36
105.60	-7.54	-5.32	-6.19
132.00	-10.36	-7.52	-8.22

Until a load of 79.20 kN, the SAP IV quasi–nonlinear analysis yielded results close to the test values with the largest error being 10% at the total load value of 79.20 kN (Table 5.4). However, as the cracks propagated and the structural response became nonlinear, SAP IV results continued to increase linearly showing higher stiffness while

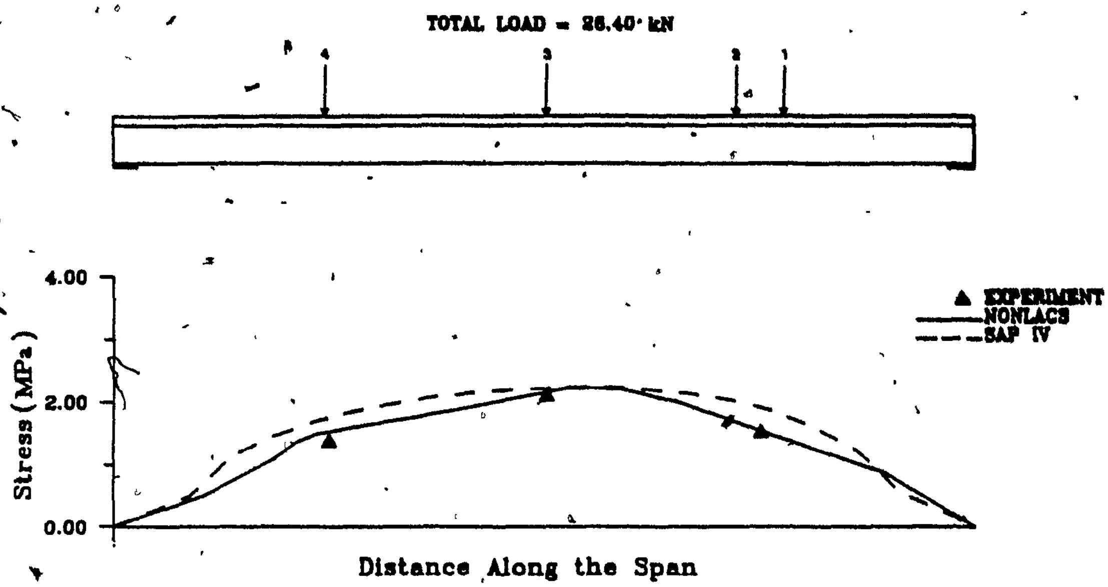

Figure 5.24 Stress Distribution Along the Span in the Concrete Slab Under Two Truck Loads.

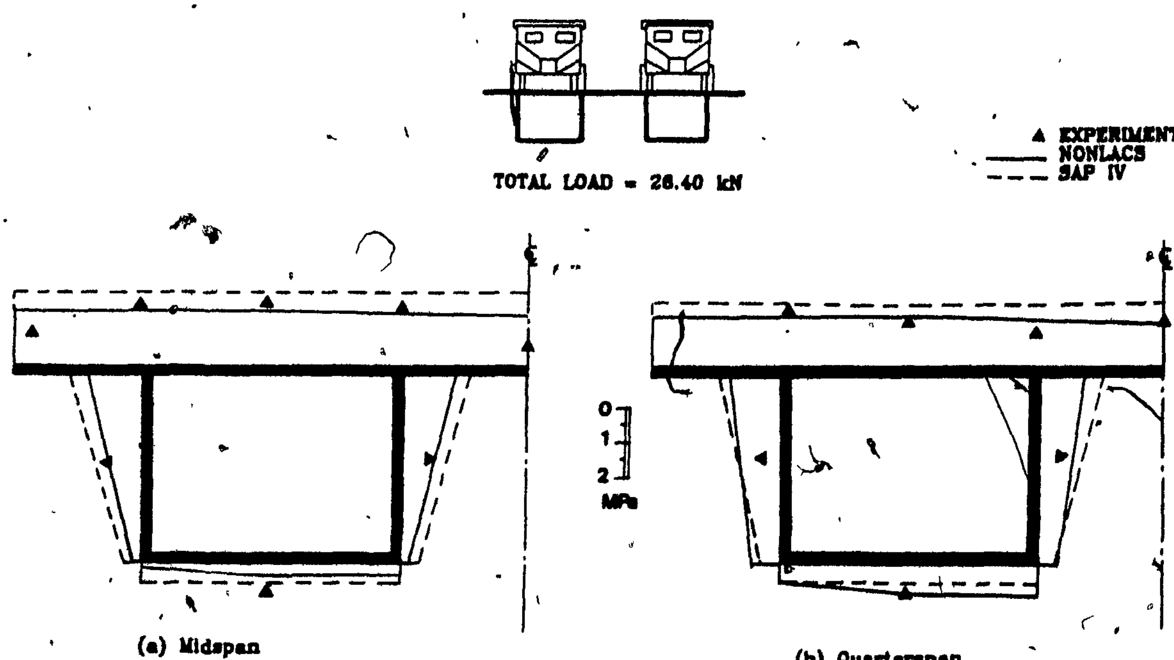

Figure 5.25 State of Stresses Under Two Truck Loads.

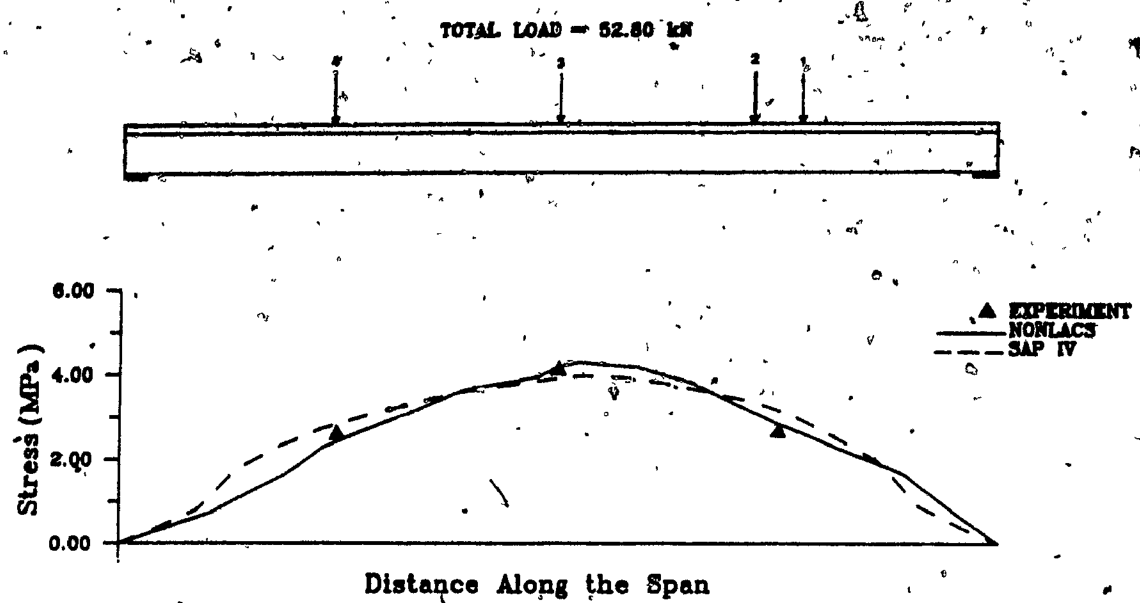

Figure 5.26 Stress Distribution Along the Span in the Concrete Slab Under Four Truck Loads.

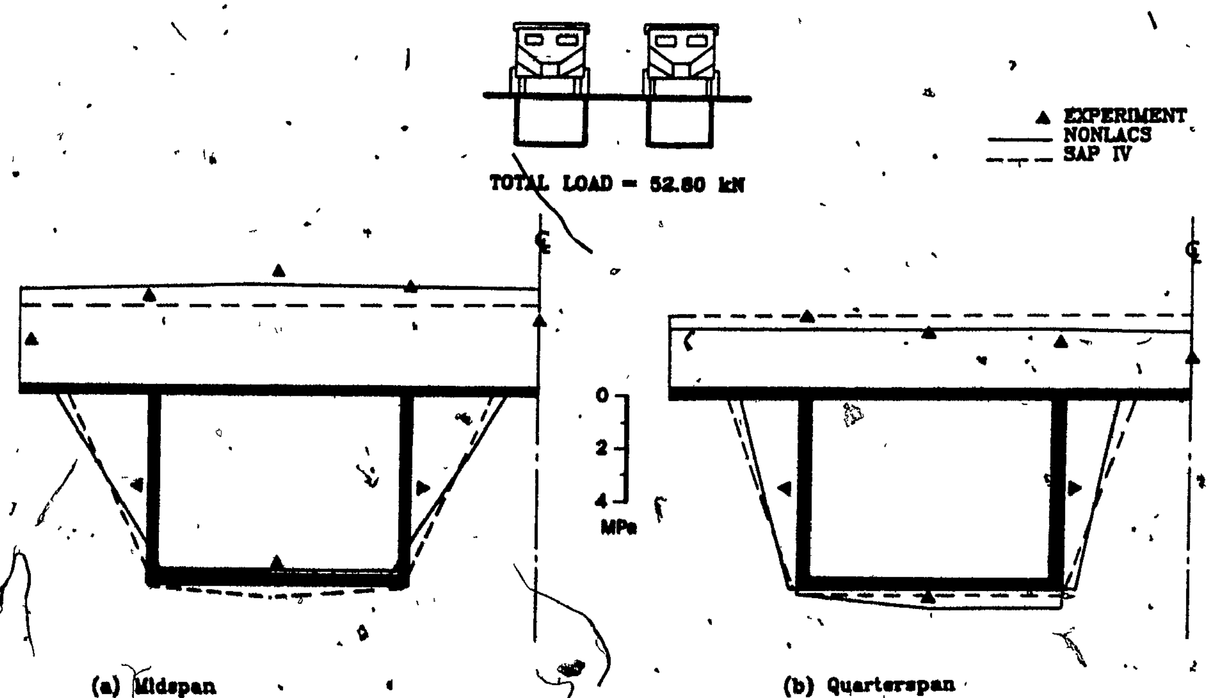

Figure 5.27 State of Stresses Under Four Truck Loads.

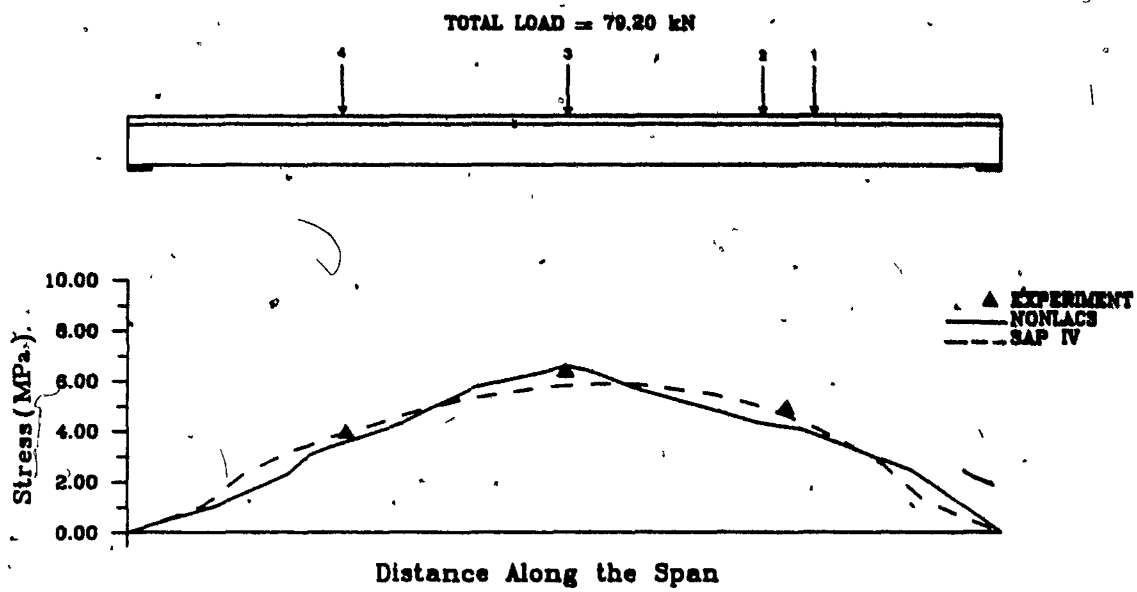

Figure 5.28 Stress Distribution Along the Span in the Concrete Slab Under Six Truck Loads.

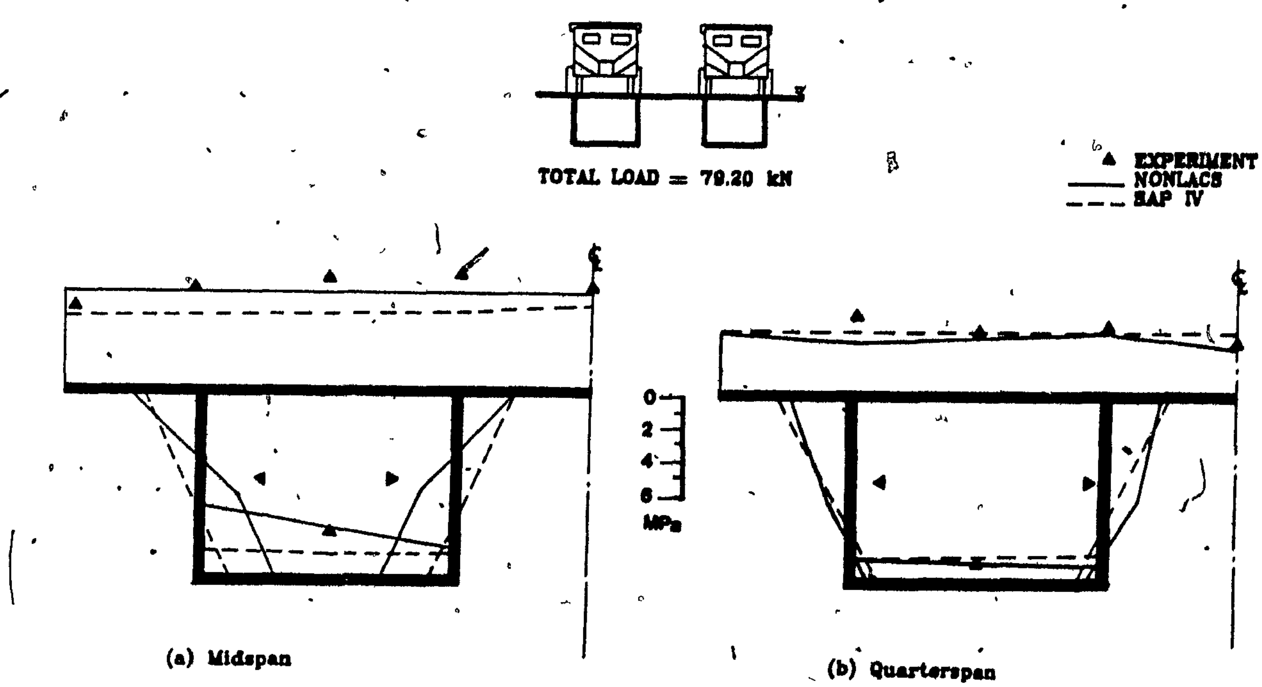

Figure 5.29 State of Stresses Under Six Truck Loads.

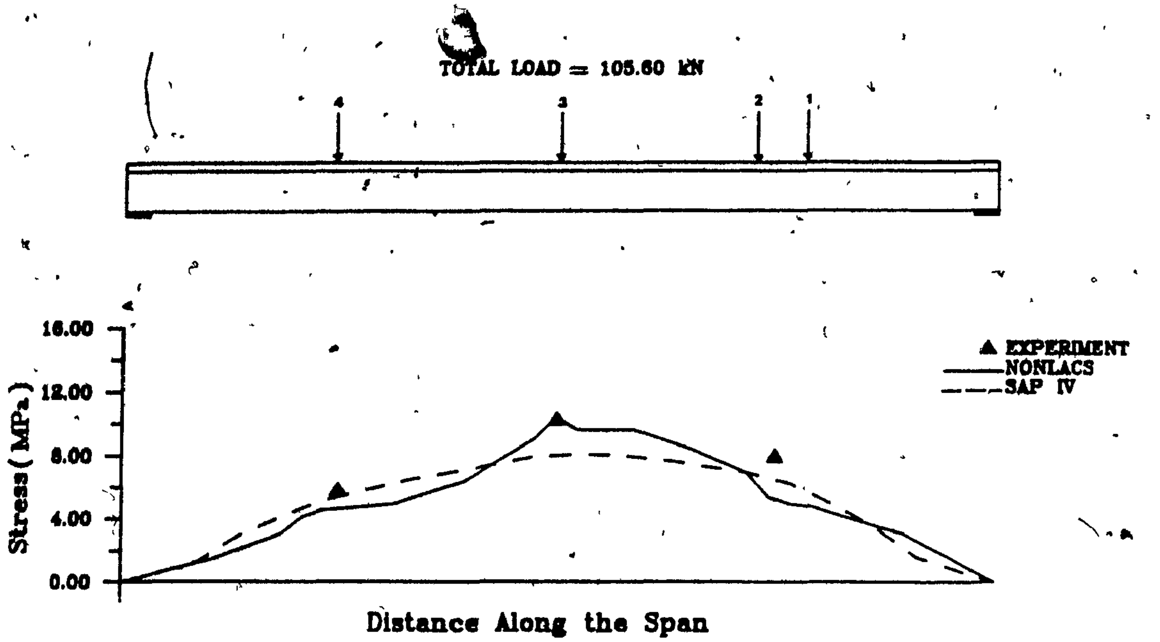

Figure 5.30 Stress Distribution Along the Span in the Concrete Slab Under Eight Truck Loads.

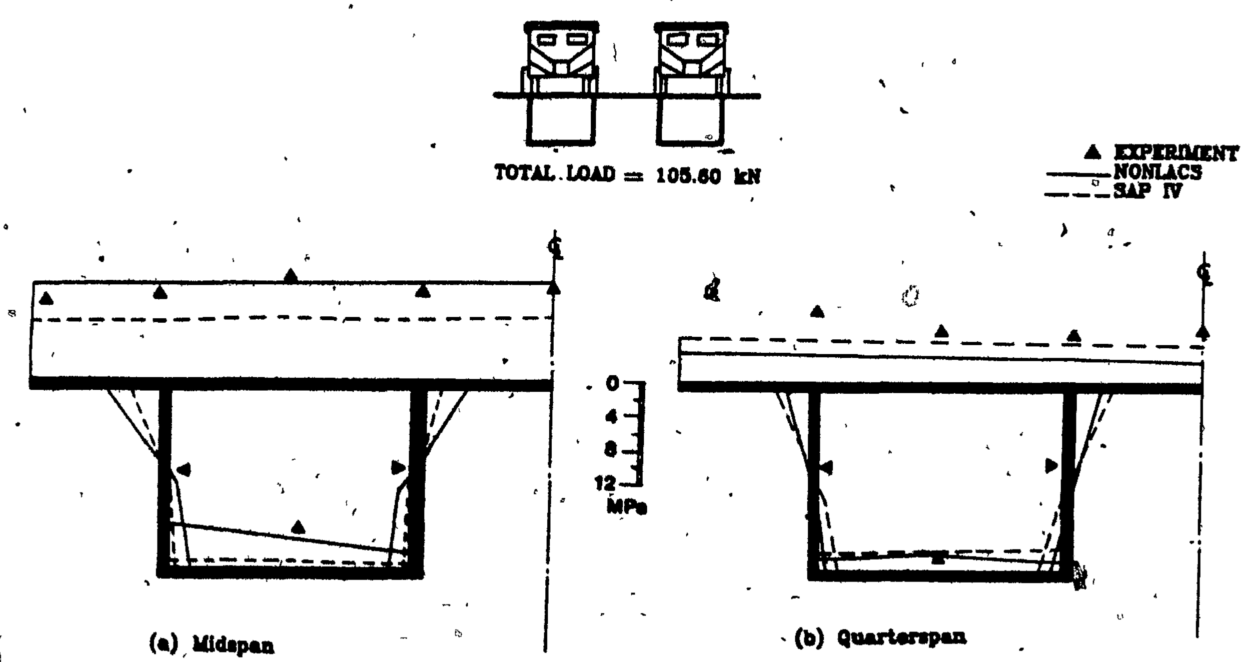

Figure 5.31 State of Stresses Under Eight Truck Loads.

the experimental model showed a considerable loss of stiffness. At a load of 132 kN, SAP IV gave a stress of 11.73 MPa at midspan while the corresponding test value was 22 MPa, which represents a difference of 47%.

The state of stress at midspan and at quarterspan as well as the stress distribution along the span in the top slab at different loading stages are shown in Figures 5.24 through 5.31. Under two truck loads the structure was entirely in compression as shown in Fig. 5.25. At a total load of 52.80 kN, the NONLACS model and the experimental model started to show tensile stresses in the bottom of the webs and in the bottom slab, while the SAP IV model was still showing the section to be in compression (Fig. 5.27). At a load of 79.20 kN, equivalent to six truck loads, the test value of the tensile stress in the bottom slab was 2.75 MPa while the NONLACS value was 3.10 MPa and the SAP IV value was only 1.5 MPa as shown in Fig. 5.29. At a load equivalent to eight trucks, the webs and the bottom slabs were almost entirely cracked (Fig. 5.31).

The longitudinal stress distribution was almost uniform across the width of the bridge showing the ability of the slab to distribute the load uniformly. This confirms the excellent load distribution characteristics of the box girder bridge.

5.3.4 Strains in the Prestressing Wires

The locations of the strain gauges on the prestressing wires are shown in Fig. 5.32. The variation of strain in wires 1, 2, 3 and 4 measured experimentally and calculated using the NONLACS and the SAP IV analyses are plotted in Figures 5.33 through 5.36.

The prestressing wires behaved linearly up to a load of about 60 kN. When the load exceeded 60 kN, the load–strain curves departed somewhat from their initial linear slope indicating that at this load level more load was transferred to the prestressing wires. These figures also show that all the prestressing wires started yielding at a load of about 120 kN which is about 86% of the failure load.

As can be seen from Figures 5.33 through 5.36, the NONLACS model was able to simulate the true behaviour of the prestressing wires all the away up to the failure load. The SAP IV model yielded acceptable results, compared with the experimental ones, in the linear range. However, when cracking appeared the difference between the two anlyses became very large. Although the SAP IV model did not simulate the true behaviour of the prestressing wires with good accuracy in the nonlinear range, it predicted the general shape of the load–strain curve.

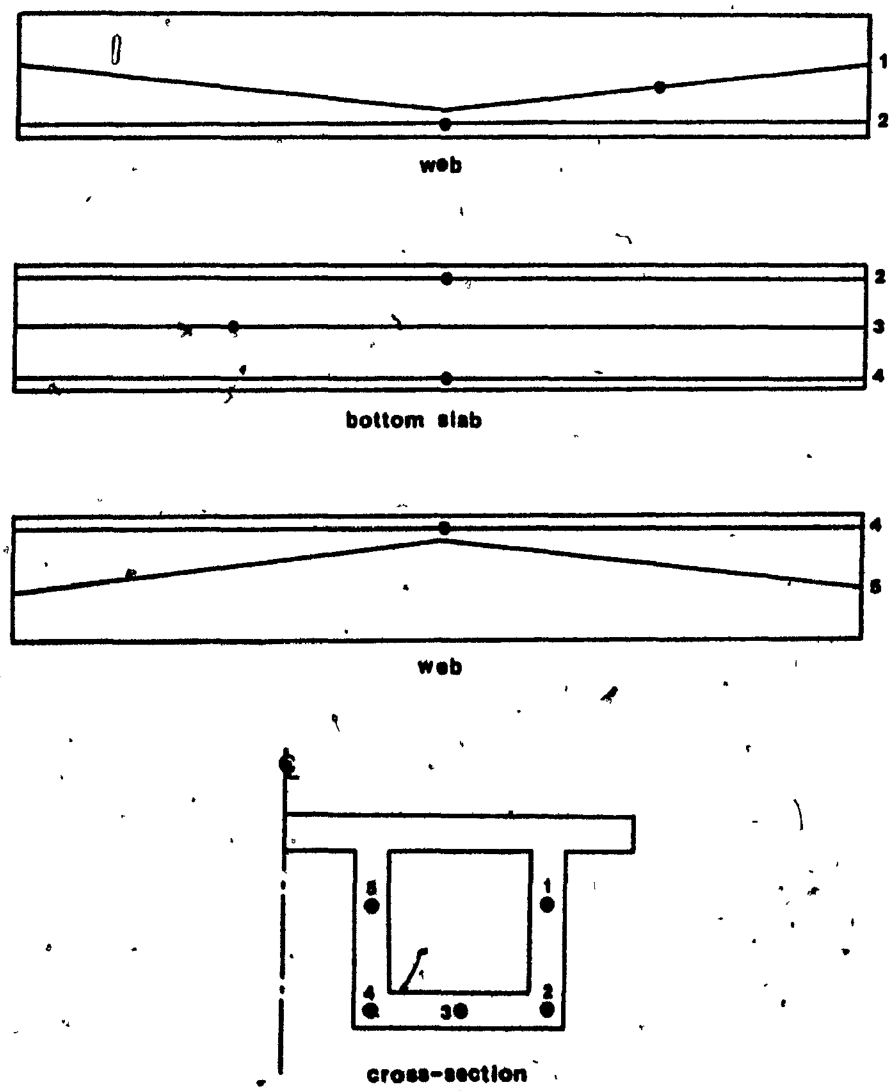

Figure 5.22 **Location of the Strain Gauges on the Prestressing Wires.**

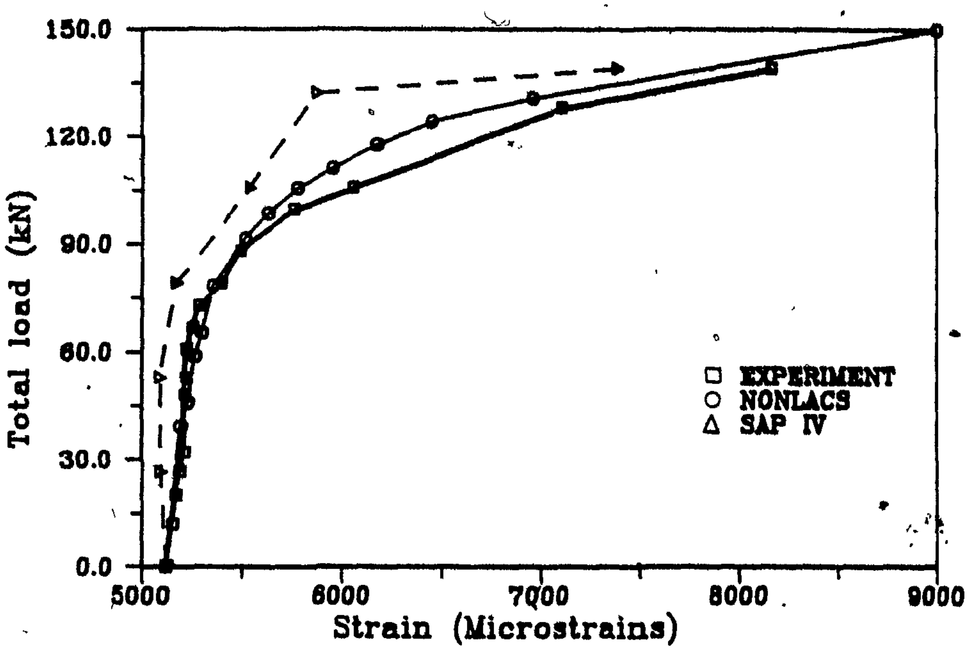

Figure 5.33 Strain Variation in Wire 1.

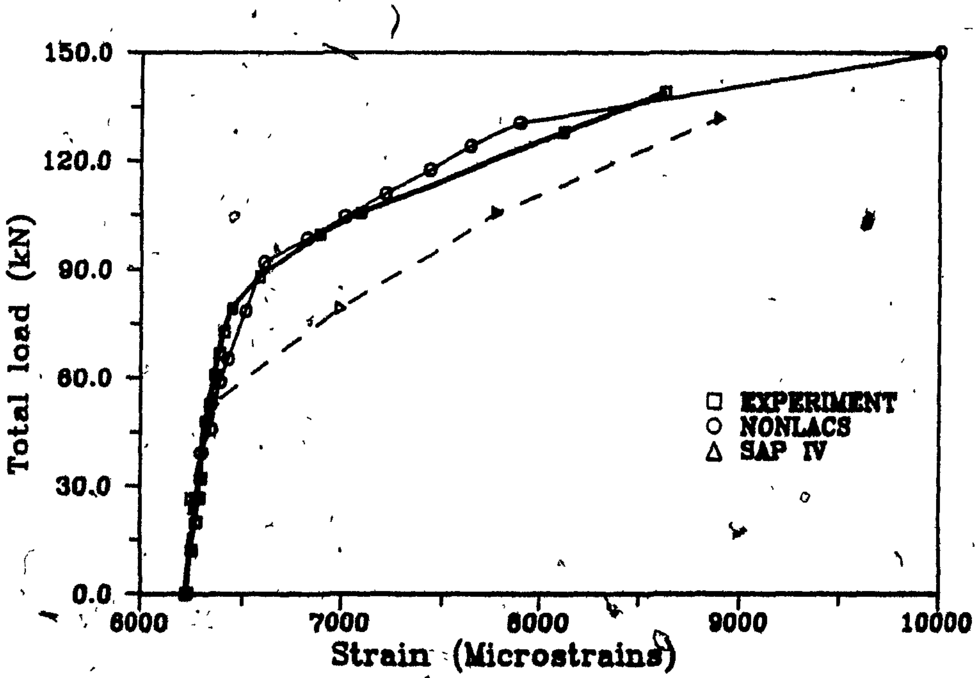

Figure 5.34 Strain Variation in Wire 2.

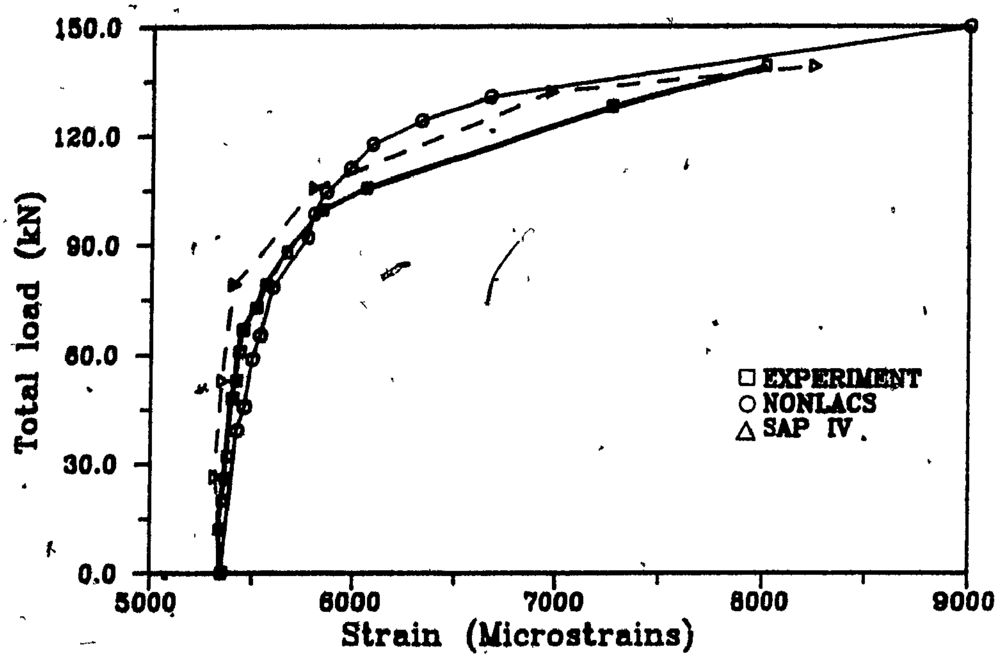

Figure 5.35 Strain Variation in Wire 3.

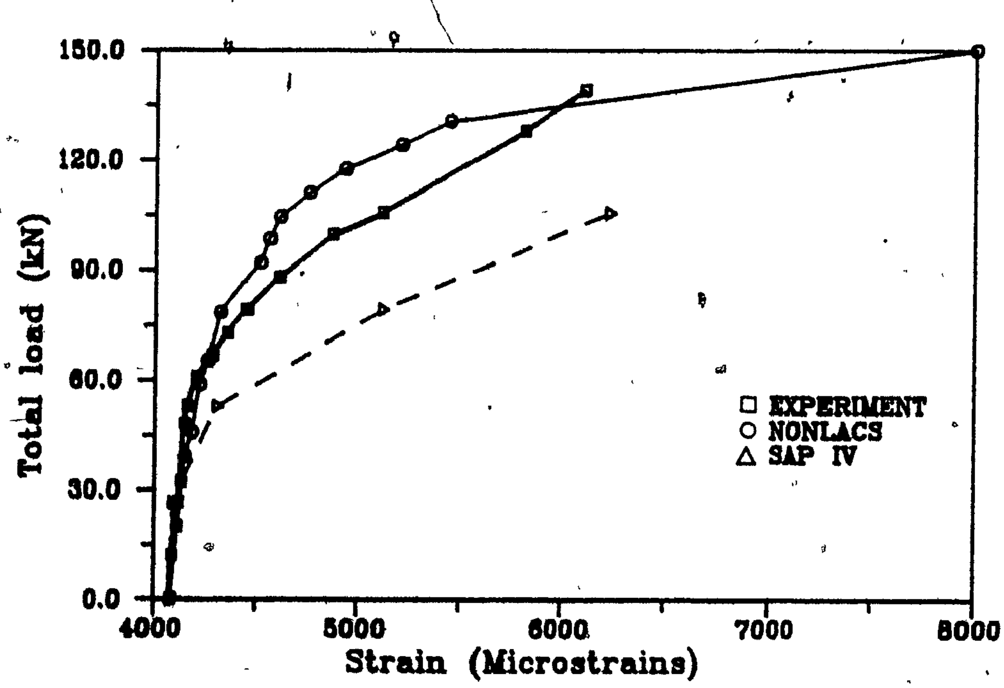

Figure 5.36 Strain Variation in Wire 4.

Tables 5.6 through 5.9 summarise the variation of the strain in the prestressing wires obtained experimentally and from the finite element analyses.

Table 5.6 Strain Variation in Wire 1.

	Strain (Microstrains)		
Total Load (kN)	Experiment	NONLACS	SAP IV
0	5121	5121	5120
26.40	5181	5164	5131
52.80	5211	5236	5406
79.20	5391	5352	6160
105.60	6053	5768	7836
132.00	7488	6955	8875

Table 5.7 Strain Variation in Wire 2.

	Strain (Microstrains)		
Total Load (kN)	Experiment	NONLACS	SAP IV
0	6229	6229	6229
26.40	6286	6273	6252
52.80	6337	6360	6646
79.20	6442	6520	7496
105.60	7095	7011	9000
132.00	8289	7895	—

Table 5.8 Strain Variation in Wire 3.

	Strain (Microstrains)		
Total Load (kN)	Experiment	NONLACS	SAP IV
0	5358	5358	5358
26.40	5376	5403	5324
52.80	5421	5479	5358
79.20	5556	5603	5409
105.60	6053	5861	5800
132.00	7529	6754	6964

Table 5.9 Strain Variation in Wire 4.

	Strain (Microstrains)		
Total Load (kN)	Experiment	NONLACS	SAP IV
0	4084	4084	4083
26.40	4120	4131	4095
52.80	4165	4210	4313
79.20	4451	4341	5119
105.60	5113	4603	6227
132.00	6105	5444	—

5.4 Cracking and Failure of the Bridge

On the first day of testing, up to a load of 26.40 kN (2 trucks), there were no visible cracks. On the second day of testing, at a load of 48 kN (3.64 trucks), cracks were observed at the bottom surface of the webs and the bottom slabs under the load axle No.3 (midspan region). As the load was increased, cracks in the webs increased in number and extended towards the compression zone. However, they remained closed

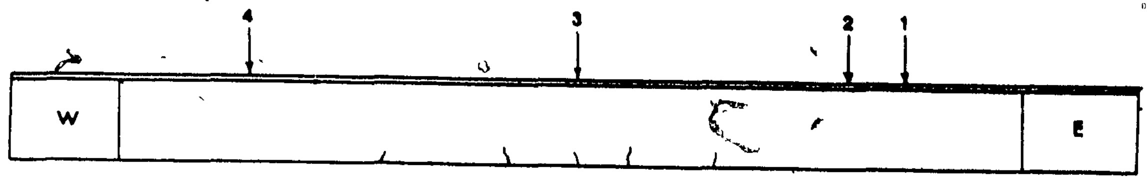

(a) 4 Trucks

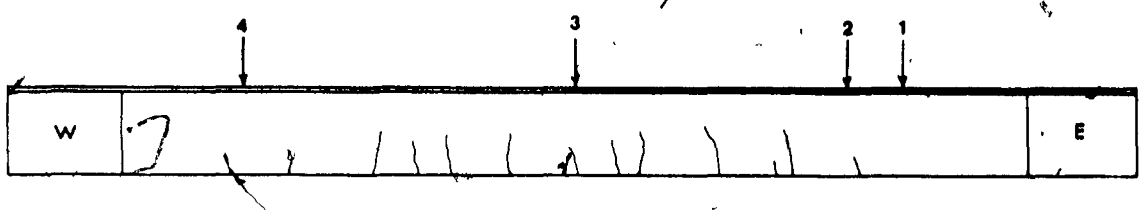

(b) 6 Trucks

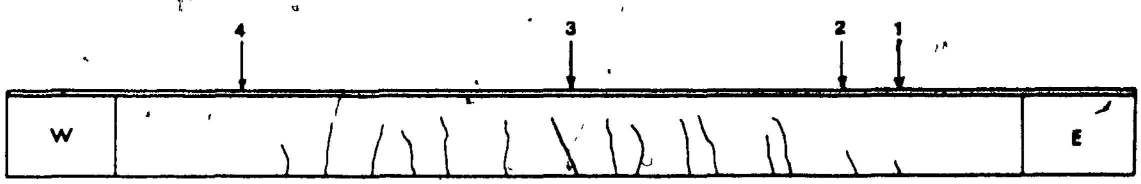

(c) 8 Trucks

Figure 5.37 **Cracking Patterns.**

and did not extend beyond half the height of the webs. At a load of 105.60 kN (8 trucks), cracks increased in number, and those near the midspan region widened and extended further up into the compression zone. Some shear cracks also appeared near support region but they remained closed. The cracks were distributed at more or less equal spacings indicating good flexural bond characteristics. At this stage, the largest crack observed was located right at midspan under the third axle (section of the maximum bending moment). Nothing unusual was noticed, until the fifth day of testing at a load of 132 kN (10 trucks), when a loud noise was heard and the dial gauge readings dropped slightly. This sound was due to the fracture of one of the prestressing wires. At this load level, the cracks at midspan opened considerably and extended upward towards the top slab. The width of the largest crack was about 0.80 mm. The cracking patterns under 4, 6 and 8 truck loads are shown in Fig. 5.37

The ultimate load of the structure was very close to 139 kN (11 trucks). There were some indications that failure was imminent on the previous day of testing. More noise from fractured wires was heard and the deflections continued to increase extremely rapidly. On the last day of testing, after a load of 132 kN, the load was increased very slowly and extreme care was taken to avoid any accident. As the load increased, more noises similar to the one which occurred at a load of 132 kN were heard and again deflections kept increasing rapidly. As the load was increased slightly, the crack at midspan opened widely, and moments later, the bridge collapsed. The mode of failure of the bridge is shown in Fig. 5.39. Upon inspection of the midspan section, it was found that all of the wires were broken (Fig. 5.40).

As mentioned in the previous chapter, the NONLACS output includes the principal stresses and the principal directions. Therefore, it is possible to trace the cracking patterns from the results of the NONLACS analysis. The cracking pattern under ten truck load obtained experimentally and by the NONLACS are presented in Fig. 5.38 for comparison. It is noted that the NONLACS model started showing cracks at a

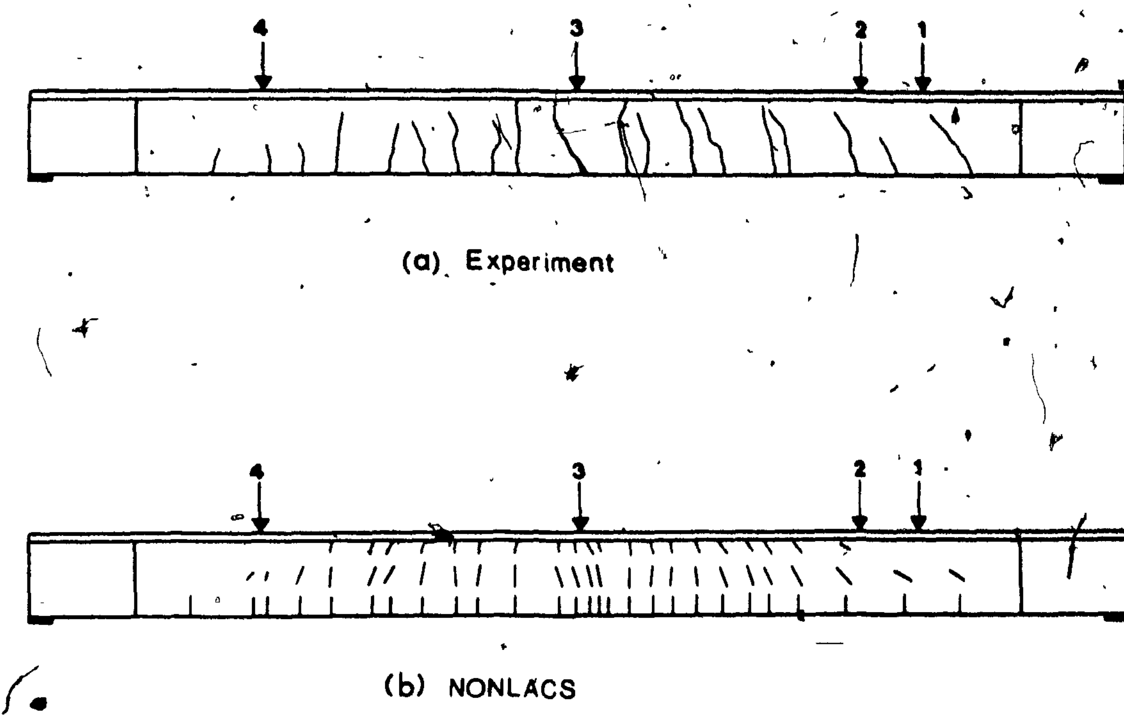

Figure 5.38 Cracking Pattern Under Ten Truck Loads.

load of about 60 kN (4.55 trucks) while the bridge model started cracking at a load of 48 kN (3.64 trucks). An examination of Fig. 5.38 shows that at a load of ten trucks, the experimental cracking patterns was simulated quite closely, by the NONLACS program.

5.5 Dynamic Analysis

The dynamic analysis consisted of studying the free–vibration response of the bridge model. The main objective of this part of the study was to evaluate the dynamic characteristics of the structure and to examine the influence of cracking of the concrete on these parameters. An experimental study and a quasi–nonlinear finite element analysis using the SAP-IV program were performed. The bridge was excited by a mass of 250 kN suspended at midspan as explained in Chapter 3. The time-dependent deflections at each level of damage of the bridge were obtained and are shown in Figures 5.41 through 5.43. The dynamic properties such as the frequencies of

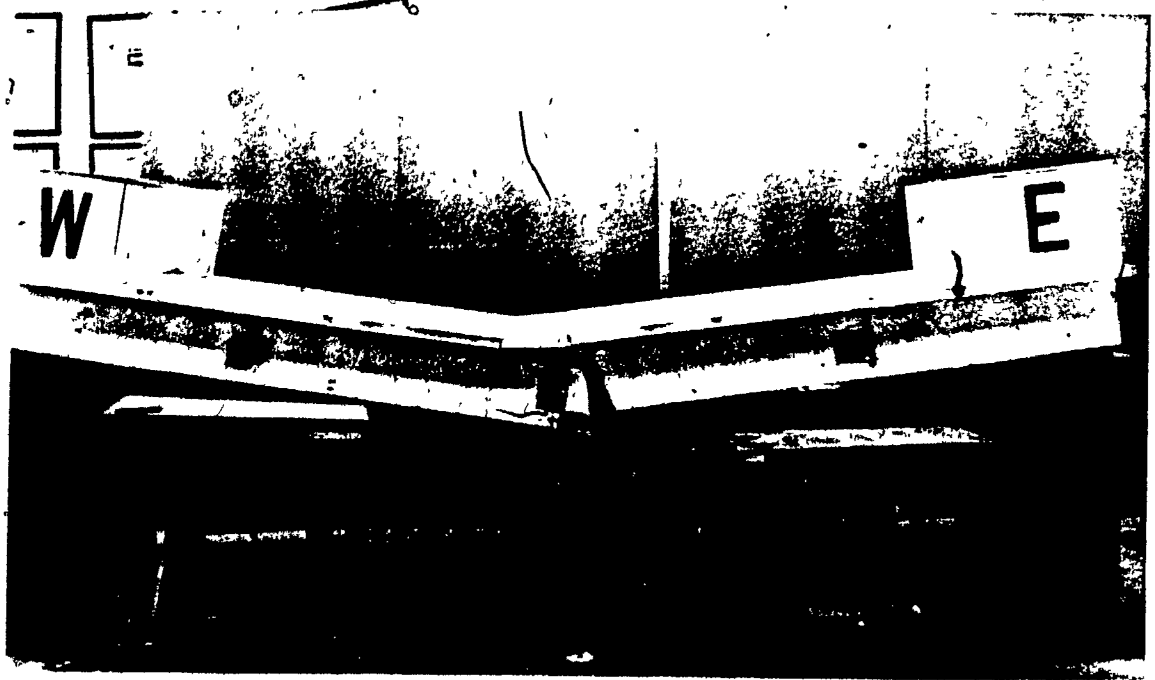

(a) Elevation View

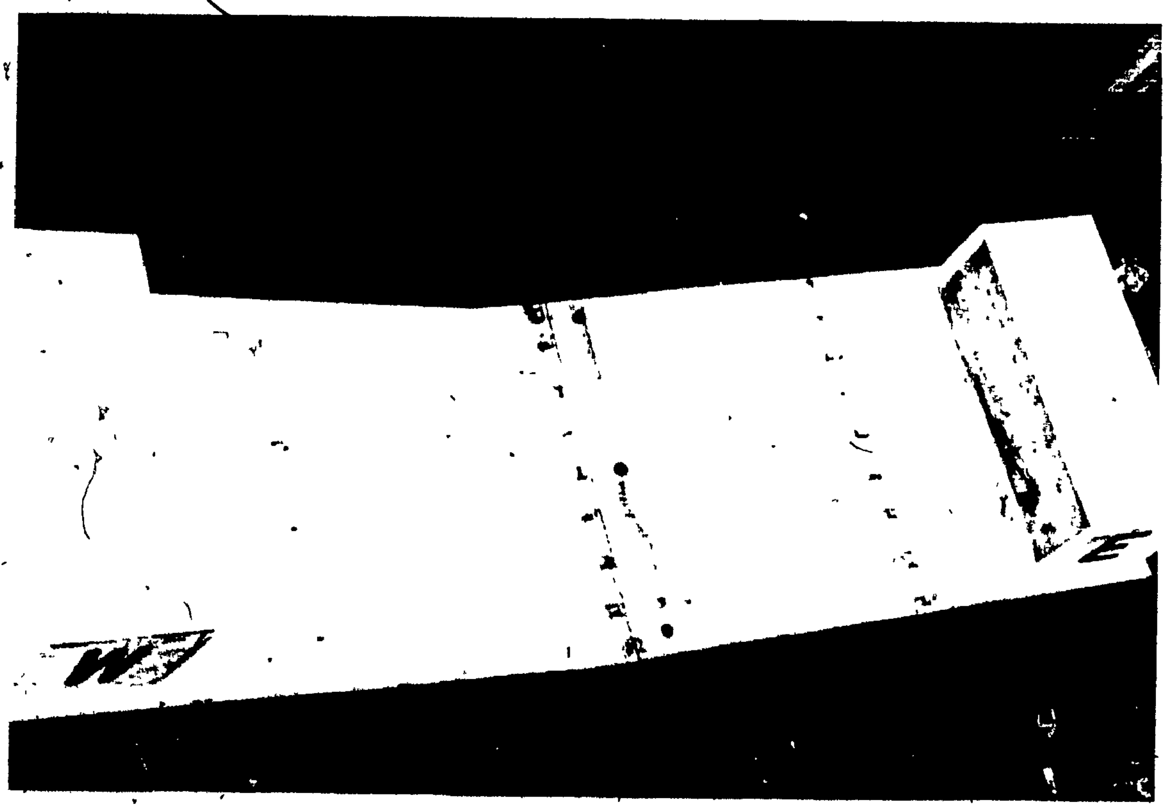

(b) Top View

Figure 5.39 Failure Mode of the Bridge Model.

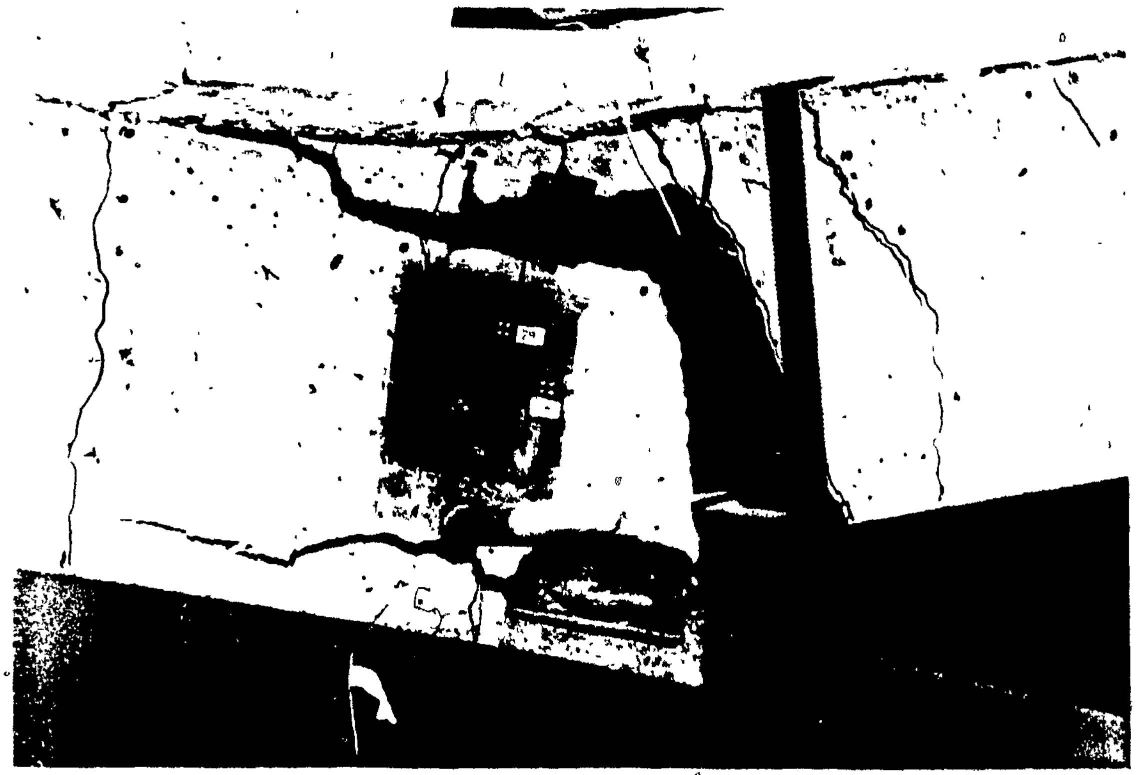

Figure 5.40 Close Up View of the Midspan Region.

vibrations and the damping coefficients were obtained graphically from these curves. In the SAP IV quasi-nonlinear dynamic analysis, the elasticity matrix was modified at each load level depending on the crack pattern observed in the experiment. The frequency of vibration of the bridge was also calculated assuming the bridge to vibrate as a simple beam, using Eq. 5.1 for the simplified straight beam with a uniformly distributed mass along the length and the flexural rigidity obtained from the experimental deflection curves at each cracking stage.

$$\omega = \pi^2 \left(\frac{EI}{ml^4}\right)^{1/2} \tag{5.1}$$

where m is the mass per unit length of the structure and EI is the flexural rigidity. The variation of the natural frequency with load level is presented in Fig. 5.44.

Before applying any live load, the natural frequency of vibration of the bridge was 98.11*rad/sec.* After two truck loads, the natural frequency of vibration of the bridge remained unchanged. This shows that after two truck loads, the bridge did not suffer any cracking damage. After the first cracks appeared (after 4 trucks), the value of the natural frequency of vibration decreased slightly by 7%. However, with the propagation of cracks and when the structure became severely damaged (after 10 trucks) the natural frequency of vibration decreased by 23%. The quasi–nonlinear analysis yielded similar results as the test results, with the difference being less than 11% except after ten trucks where the difference increased to about 19%. Figure 5.44 shows that the quasi–nonlinear analysis is able to predict the dynamic behaviour of the structure, if the experimental data for cracking patterns is introduced appropriately. The figure shows also that the beam theory overestimates the natural frequency of vibration of the bridge. A summary of the natural frequencies of vibration of the bridge is presented in Table 5.10.

Table 5.10 Natural Frequency of Vibration of the Bridge at Each Cracking Stage.

	Natural Frequency of Vibration (rad/sec)		
Total Load (kN)	Experimental	SAP IV	Simple Beam Analysis
0	98.11	97.33	118.92
26.40	98.11	97.33	113.23
52.80	91.10	93.29	103.79
79.20	85.03	80.51	96.36
105.60	79.72	71.01	90.15
132.00	75.07	60.86	68.15

The flexural rigidity of the bridge at each load level was calculated by substituting the values of the natural frequencies of vibration in Eq. 5.1. The values obtained are compared with the test values and are presented in Figure 5.45. Table 5.11 summarizes the variation of the flexural rigidity and Table 5.12 presents the first six natural frequencies of vibration obtained using the SAP IV quasi–nonlinear analysis.

The damping ratio of the bridge model at different levels of damage was evaluated directly using the experimental results for the decay of free vibrations. When a system has been set into free vibrations, the damping ratio can be determined from the ratio of two displacement amplitudes measured at an interval of m cycles. Thus, if v_n is the experimental amplitude of vibration at any time and v_{n+m} is the experimental amplitude m cycles later, the damping ratio is given by:

$$\xi = \frac{\delta_m}{2\pi m(\omega/\omega_D)} \tag{5.2}$$

where $\delta_m = ln(v_n/v_{m+m})$ represents the logarithmic decrement and ω and ω_D are the undamped and damped frequencies, respectively. In most practical structures, the damping ratio is less than 20% and therefore, the change of frequency due to damping is neglected (i.e. $\omega = \omega_D$). Thus Eq. 5.2 can be approximated by:

$$\xi \simeq \frac{\delta_m}{2\pi m} \tag{5.3}$$

Figures 5.41 through 5.43 show that the vibration gets considerably damped after one second. The damping ratio of the uncracked structure was evaluated at 2.20% Prior to failure, this value increased to about 7.64%, which represents an increase of about 250%. The variation of the damping ratio is presented in Figure 5.46. The values of the damping ratio at each level of damage of the bridge are summarized in Table 5.13

Newmark and Hall[22] recommended damping values for prestressed concrete structures depending on the level of deformation or strain in a structure. They suggested a value of 2 to 3% for working stress levels or stress levels no more than one–half the yield point and a value of 5 to 10% for levels of deformation corresponding to stresses at or just below yield levels. These values are compared with the experimental values of the damping ratio and are presented in Table 5.14. As can be seen, the values of the damping ratio of the bridge model are in good agreement with the values proposed by Newmark and Hall.

Table 5.11 Variation of The Flexural rigidity of the Bridge.

Number of Trucks	Natural Frequancy (rad/sec)	Computed Flexural Rigidity	Experimental Flexural Rigidity
0	98.11	EI	EI
2	98.11	EI	0.90 EI
4	91.10	0.86 EI	0.76 EI
6	85.03	0.75 EI	0.65 EI
8	79.72	0.66 EI	0.57 EI
10	75.07	0.59 EI	0.33 EI

Table 5.12 First Six Natural Frequencies of the Bridge at Each Cracking Stage.

	Total Load (kN)				
Mode	0.00	52.80	79.20	105.60	132.00
1	97.33	93.29	80.51	71.01	60.86
2	249.70	248.00	242.90	238.00	231.60
3	336.90	332.30	306.60	275.00	239.00
4	371.10	367.20	346.60	336.10	320.30
5	505.00	499.70	475.60	453.00	418.20
6	510.70	507.70	480.80	459.60	430.30

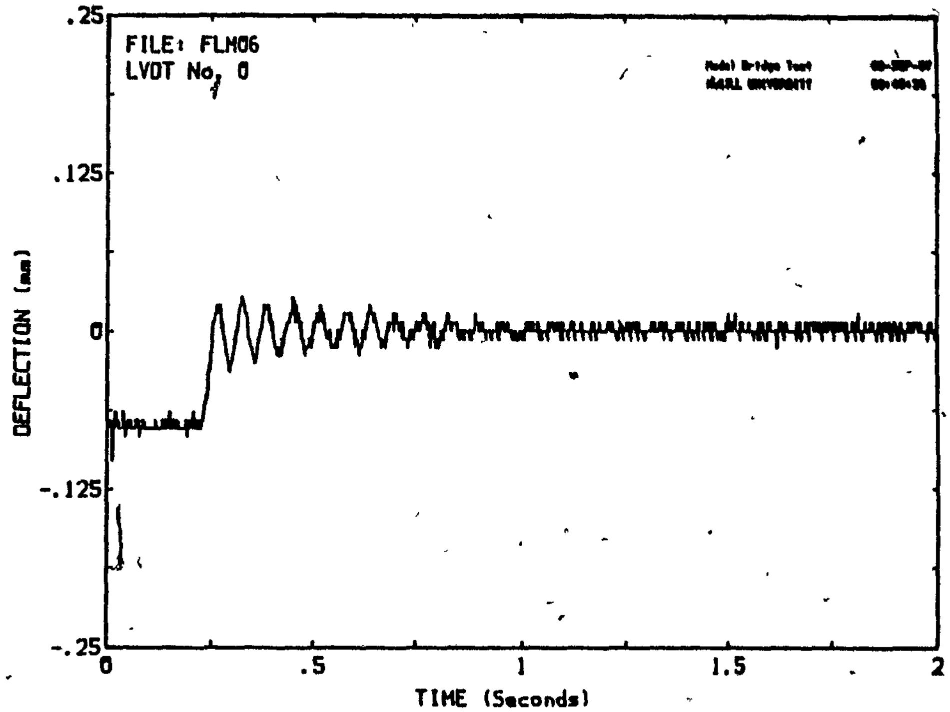

(a) At Zero Load

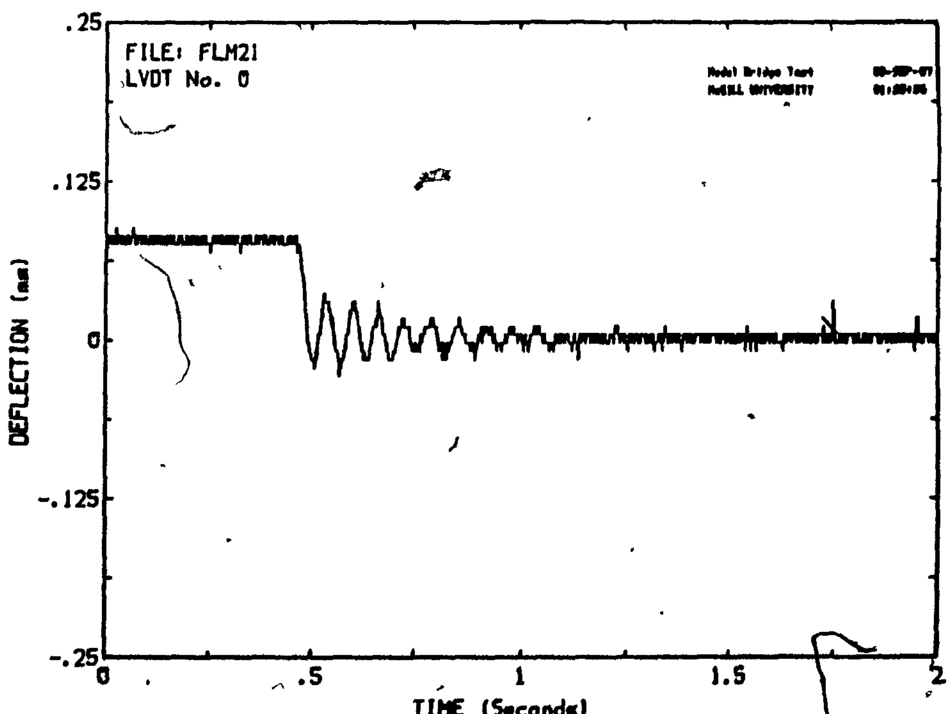

(b) After the Static Test with Two Truck Loads

Figure 5.41 Midspan Time–Dependent Deflections in the Uncracked Stage.

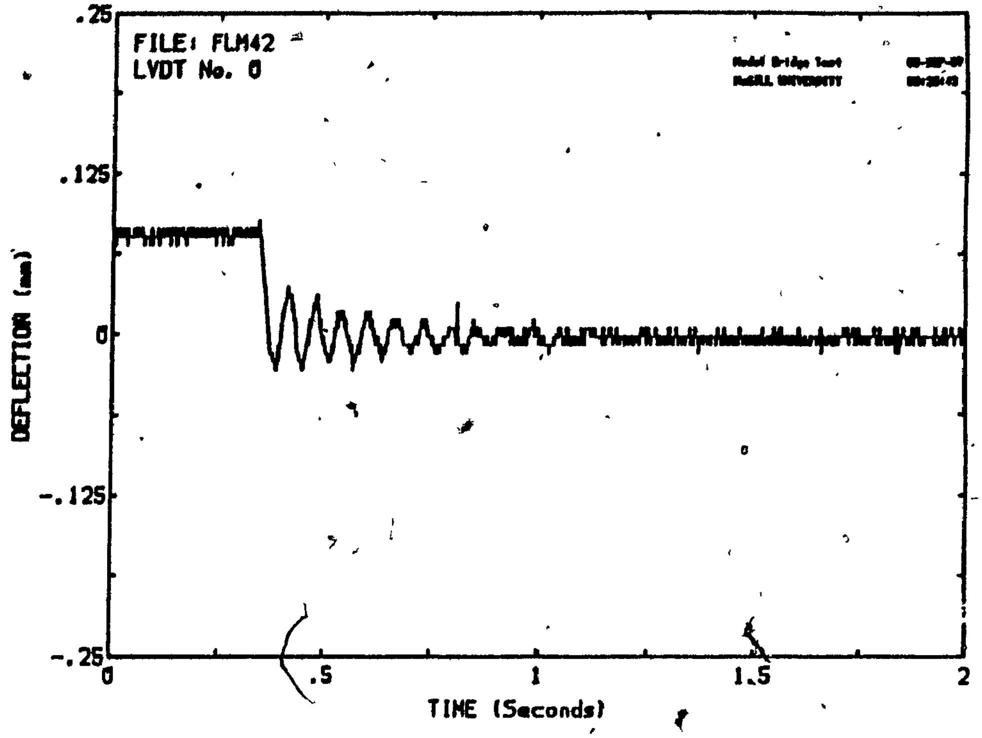

(a) After the Static Test with Four Truck Loads

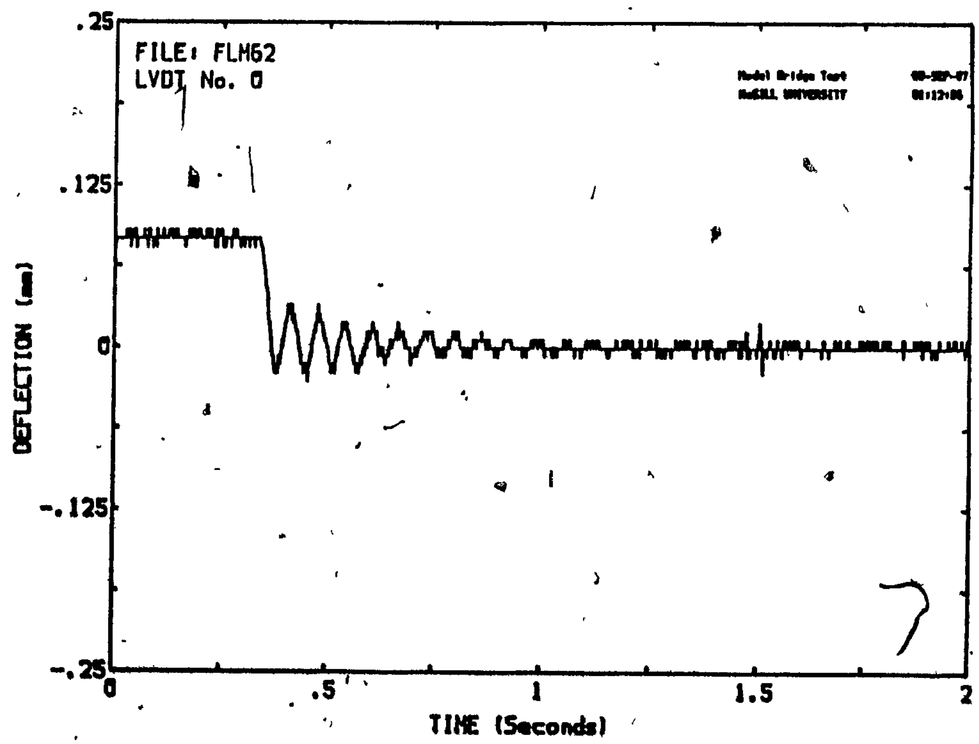

(b) After the Static Test with Six Truck Loads

Figure 5.42 Midspan Time–Dependent Deflections in the Overload Stage.

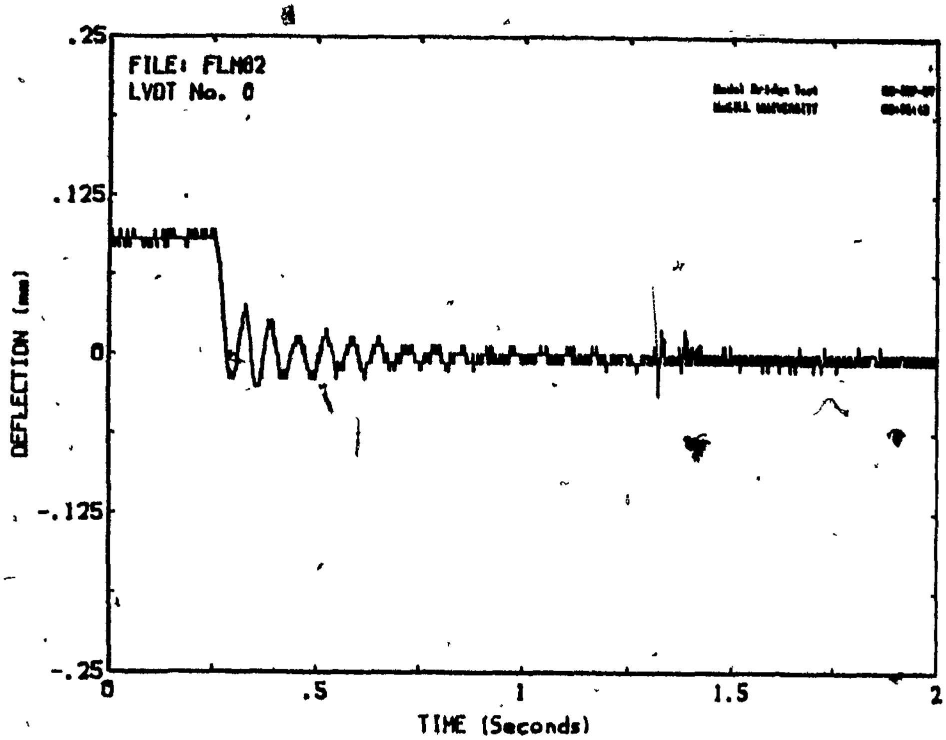

(a) After the Static Test with Eight Truck Loads

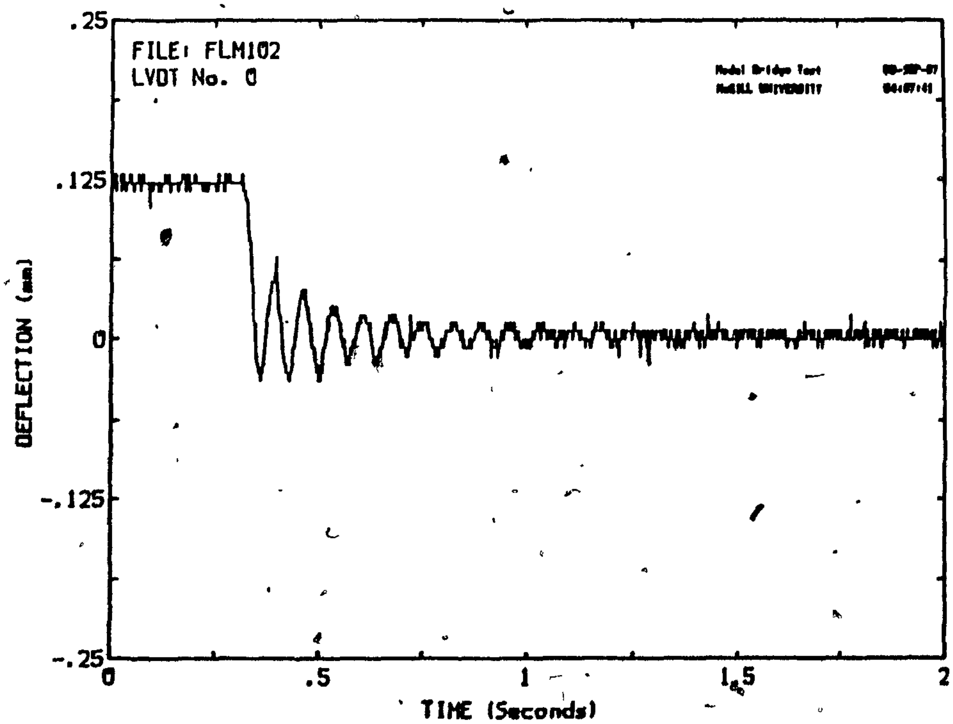

(b) After The Static Test with Ten Truck Loads

Figure 5.43 Midspan Time-Dependent Deflections Prior to Failure.

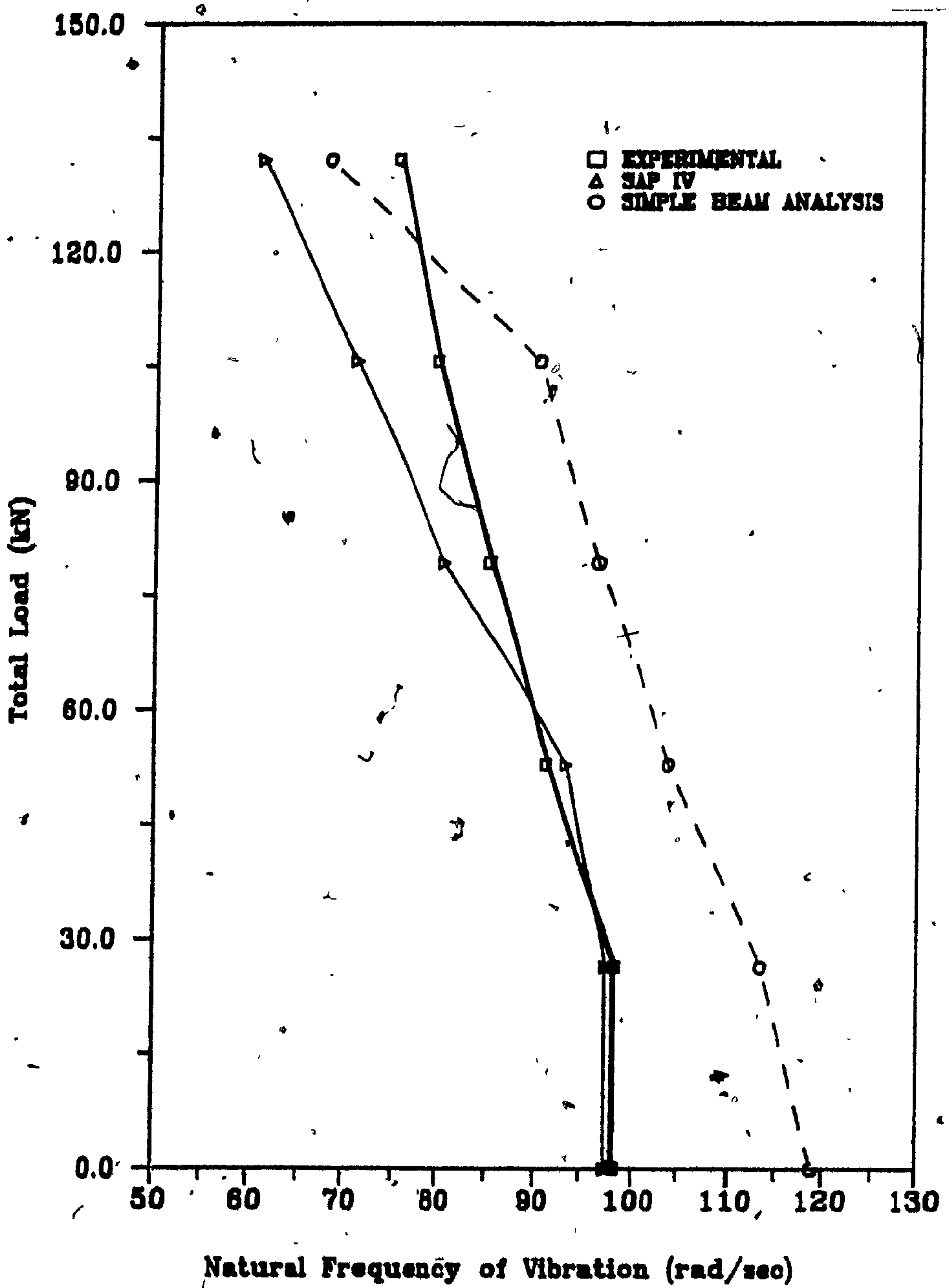

Figure 5.44 Variation of Natural Frequency of Vibration with Load Level.

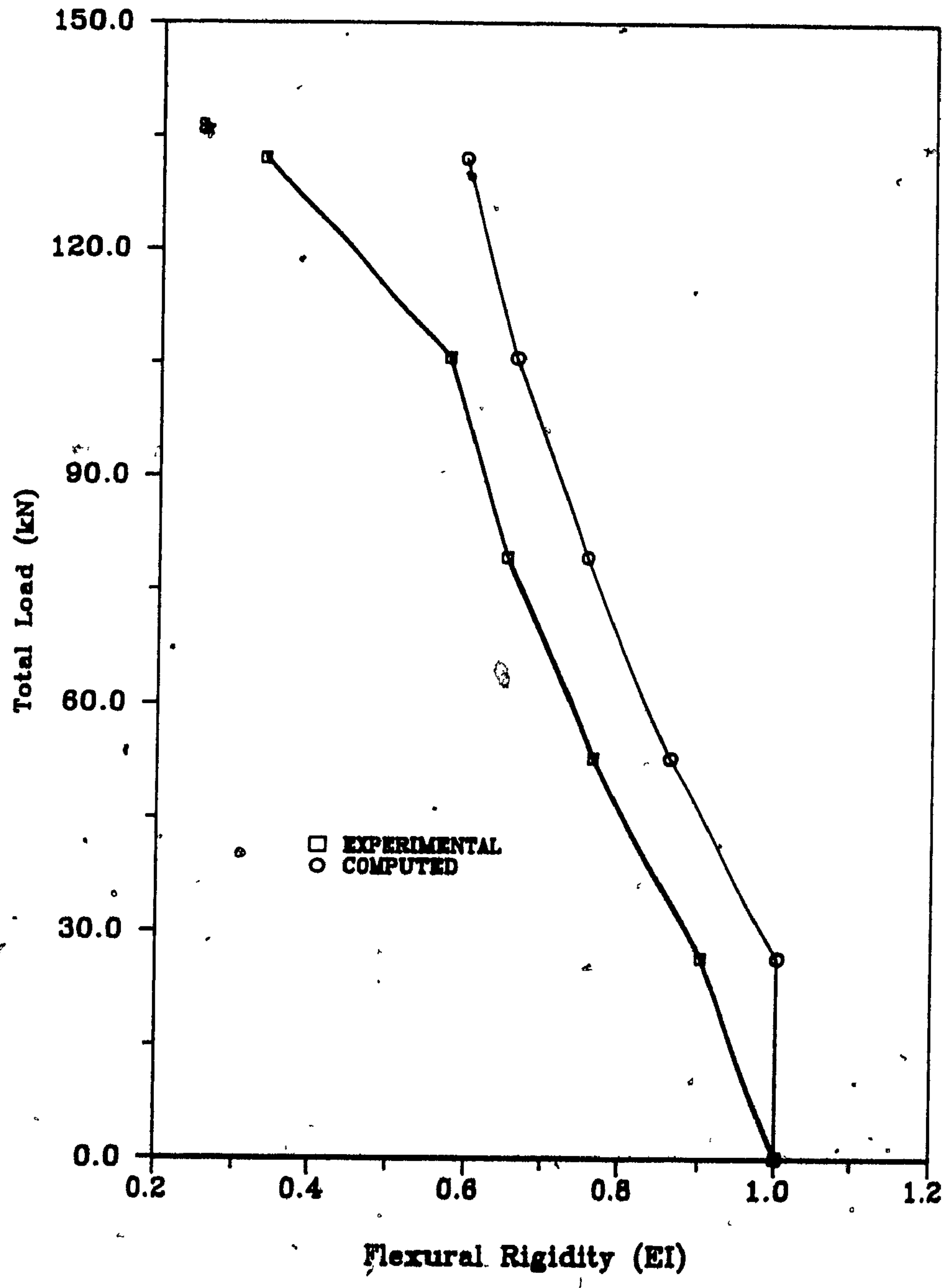

Figure 5.45 Variation of Flexural Rigidity EI with Load level.

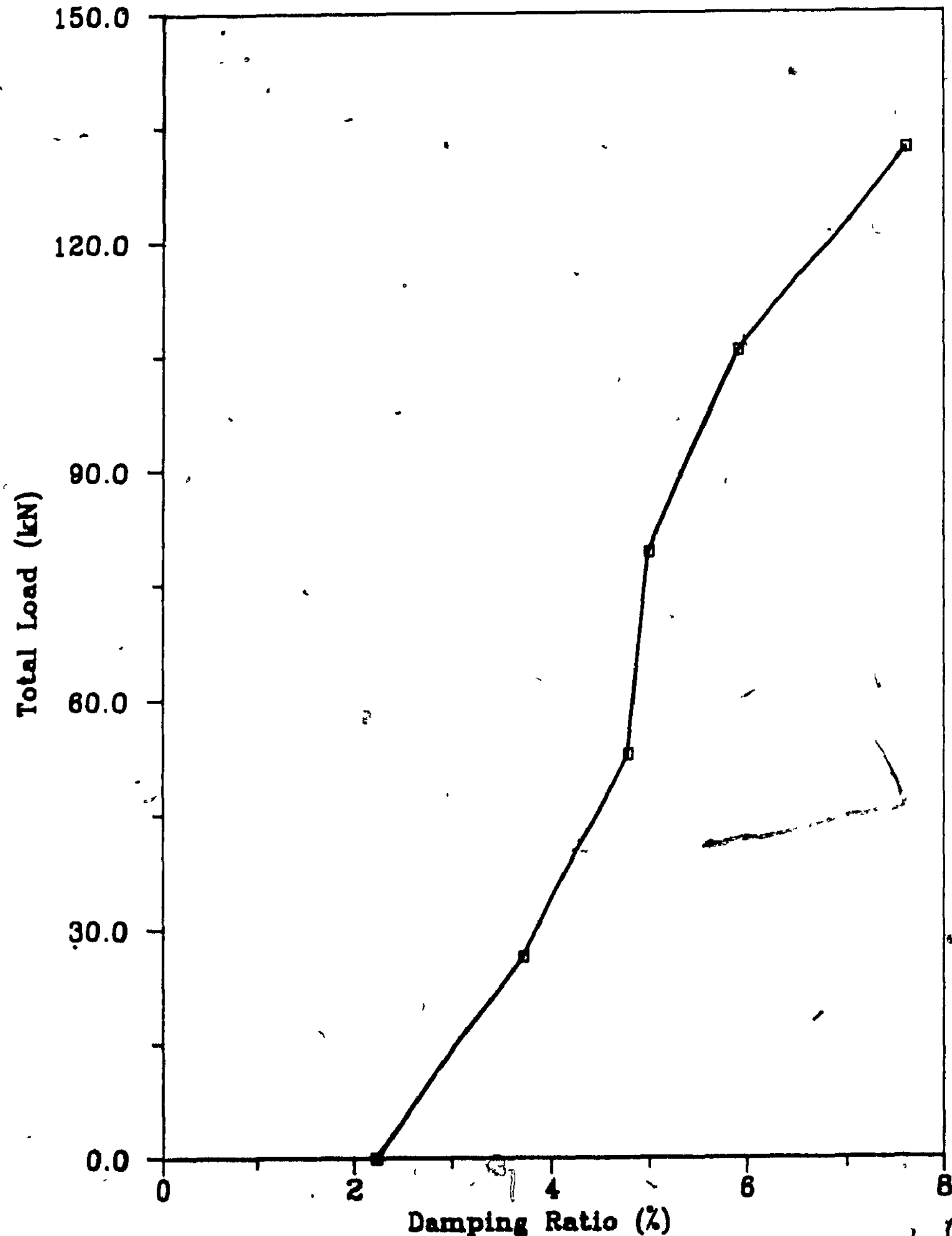

Figure 5.46 Variation of Damping Ratio with Load Level.

Table 5.13 Damping Ratio at Each Cracking stage.

Cracking Stage	Damping Ratio (%)
Uncracked	2.20
After 2 Truck Loads	3.70
After 4 Truck Loads	4.77
After 6 Truck Loads	5.00
After 8 Truck Loads	5.91
After 10 Truck Loads	7.64

Table 5.14 Recommended Damping Values.

	Damping Values (%)	
Stress Level	Newmark and Hall[22]	Experimental
Working stress, no more than about $\frac{1}{2}$ yield point	2 to 3	3.70
At or just below yield point:		
• Without complete loss in prestress	5 to 7	5.91
• With no prestress left	7 to 10	7.64

CHAPTER 6

CONCLUSIONS

6.1 Summary and Conclusions

The results of this investigation can be summarised and conclusions drawn as follows:

1. Two finite element programs were used to analyse the bridge model: a quasi–nonlinear program and a nonlinear program. The quasi–nonlinear program using SAP IV was shown to predict the behaviour of the bridge with acceptable accuracy. The cracking pattern was found to be an important parameter for the quasi–nonlinear analysis and therefore, accurate information about the cracking pattern should be available for the program to simulate the behaviour of a structure with good accuracy.

2. For a more sophisticated analytical investigation on the behaviour of a structure such as the box girder bridge, the NONLACS nonlinear finite element program is recommended. The NONLACS program can predict the complete nonlinear response up to failure of the box girder bridge with good accuracy. It promises to be a good alternative to model testing for the analysis of complex structures.

3. The bridge behaved linearly up to approximately 2 times the service load and showed no signs of cracking. The midspan deflections were very small. At service

load, the deflection was of the order of $\frac{1}{4400}$ of the span length at midspan.

4. The load capacity well in excess of that predicted by conventional ultimate strength theory was observed; this indicates a substantial degree of conservatism in the bridge design procedures. The bridge model resisted an ultimate load equal to 3.5 times the ultimate load calculated using the Ontario Highway Bridge Design Code. The mode of failure of the bridge was flexural as expected.
5. The torsional stiffness of the bridge model decreased with the appearance and the propagation of cracking. With the opening of the cracks at midspan, the prestressing steel was highly stressed and the structure lost about half of its torsional stiffness.
6. There was reasonable agreement between the computed first natural frequencies of vibration and those observed in the physical model at different levels of damage of the structure. The natural frequency of vibration of the bridge decreased slightly as the first cracks appeared. However, as the bridge approached failure, the natural frequency of vibration of the structure decreased by only 23%.
7. The damping ratio was found equal to 2.20% for the uncracked prestressed concrete box girder bridge; when the structure was severely damaged, the damping ratio increased to 7.64%. The damping ratios of the structure were found in good agreement with the values proposed by Newmark and Hall[22].

6.2 Suggestions for Further Reaserch

The results of the present experimental–analytical investigation using a $\frac{1}{7.00}$–scale direct model and finite element programs gave valuable insight into the linear and nonlinear static and dynamic response of a two–cell, prestressed concrete box girder bridge. These data combined with the available data from the previous work of Ferdjani and Hadj–Arab on a one–cell, prestressed concrete box girder bridge should help the design engineer to understand the basic static and dynamic response of prestressed concrete box girder bridges. However, it is strongly recommended that serious consideration be given to further experimental–analytical studies on direct physical models of single–cell and multi–cell concrete box girder bridges to fully understand the static and dynamic behaviour of such complex structures, especially in the nonlinear range.

More study on the effect of cracking on the dynamic characteristics of box girder bridges is needed. An alternative to an experimental research using direct models is to implement the nonlinear program NONLACS so that it can perform dynamic analyses. A parametric study of the effect of cracking on the dynamic characteristics such as the damping coefficient and the frequency of vibration can be very useful and inexpensive, compared with an expensive experimental program, in generating these useful data.

Extensive experimental and analytical studies are needed to investigate more deeply the value of the modulus of elasticity of concrete perpendicular to cracks (E_P) and the reduction factor β for the shear modulus. These two parameters are important for the accuracy of a quasi–nonlinear analysis and therefore need to be examined further.

REFERENCES

1. Freyssinet, E., "A Revolution in the Technique of the Utilisation of Concrete", A Paper Read at a Joint Meeting of the British Section of the Societé des Ingénieurs Civils de France and the Institution of Structural Engineers, London, March 19, 1936, 23 pp.

2. Scordelis, A.C., "Analysis of Simply Supported Box Girder Bridges", Structural Engineering and Structural Mechanics, Report No. SESM-66-17, University of California, Berkely, October 1966.

3. Cordoba, R.A, "Behaviour of Open Web Precast Bridge Girder–Experimental Study", M.Eng. Thesis, Department of Civil Engineering and Applied Mechanics, McGill University, Montreal, August 1974.

4. Tschanz, T., "Behaviour of Open Web Precast Bridge Girder–Analytical Study", M.Eng. Thesis, Department of Civil Engineering and Applied Mechanics, McGill University, Montreal, August 1974.

5. Leonhardt, F. and Walter, R., "*Torsion-und Schubversuche an Vorge–Spanten Hohlkastentragen 1963–64*", (Torsion and Shear Tests on Prestressed box Girders, 1963–64), *Beton-und Monierban A.G., Stuttgart, 1965*, Translation made by C.V. Amerongen, Cement and Concrete Association, London 1968, pp 41.

6. Scordelis, A.C., Bouwkamp, J.G. and Wasti, S.T., "Study of AASHTO Loadings on a Concrete Box Girder Bridge model", Highway Research Record, No. 428, July 1973, pp. 22-31.

7. Swamy, N., "Prestressed Concrete Hollow Beams Under Combined Bending and Torsion", *Journal of the Prestressed Concrete Istitute*, Vol. 10, No. 2, April 1965, pp. 48-61.

8. Soliman, M.I., "Behaviour and Analysis of Reinforced Concrete Box Girder Bridge", Ph.D. Thesis, Department of Civil Engineering and Applied Mechanics, McGill University, Montreal, March 1979.

9. Razaqpur, A.G. and Mazikins, P., "Nonlinear Finite Element Analysis of Reinforced Concrete Structures", Carleton University, Ottawa, Ontario, 1986.

10. Campbell, T.I., Batchelor, B. de V., "Load Testing of a Model Two-Span Continuous Prestressed Concrete Trapezoidal Bridge Girder", *Journal of Prestressed Concrete Institute*, Vol. 22, November-December 1977, pp. 62-79.

11. Swann, R.A., "Tests on a Prestressed Micro-Concrete Model of Three Cell Box Beam Bridge", Models for Concrete Structures, *ACI Publication* No. 24, SP24, *American Concrete Institute*, Detroit, Michigan 1970.

12. Spiller, R.M., Kromolicki, R.E. and Danglidis, M.I., "Lateral Forces due to Longitudinal Prestressing of Concrete Box Spine-Beam Bridges with Inclined Webs", *The Structural Engineer*, London, Vol. 63A, No. 2, February 1985, pp. 54-57.

13. Seible, F. and Scordelis, A.C.,"Non-Linear Behaviour and Failure Analysis of Multi-Cell RC Box Girder Bridges", *Proceeding of the International Conference on Short and Medium Span Bridges*, Toronto, August 1982, pp. 391-405.

14. West, H.H. and McClure, R.M.,"Full Scale Testing of a Prestressed Concrete Concrete Segmental Bridge", *Proceedings of the International Conference on Short and Medium Span Bridges*, Toronto, August 1982, pp. 375-389.

15. Kostovos, M.D. and Newman, J.B., "Generalized Stress-Strain Relations for Concrete", *Journal of the Engineering Mechanics Divison, American Society of Civil Engineers*, Vol. 104, No. EM4, pp. 845-856, August 1978.

16. Huang, T.,"Vibration of Bridges", *Shock and Vibration Digest*, Vol. 8, No. 3, Abstracts 1-948, March 1976, pp. 61-76.

17. Mirza, M.S., et al.,"An Analytical–Experimental Study of the Behaviour of a Composite Concrete Deck–Steel Box Girder Bridge", Report prepared for Public Works Canada, Department of Civil Engineering and Applied Mechanics, McGill University, Montreal, March 1985.

18. Conrad, P.H. and Sahin, M.A.,"Natural Frequency of Curved Box Girder Bridges", *ASCE, Journal of the Structural Division*, Vol. 105, ST 7-12, December 1979, pp. 2591-2600.

19. Tabba, M.M., "Free Vibrations of Curved Box Girder Bridges", M.Eng. Thesis, Department of Civil Engineering and Applied Mechanics, McGill University, Montreal, Jully 1972.

20. Hadj-Arab, A., "Behaviour of One Cell Prestressed Box Girder Bridge–Experimental Study", M.Eng. Thesis, Department of Civil Engineering and Applied Mechanics, McGill University, Montreal, February 1987.

21. Ferdjani, O., "Behaviour of One Cell Prestressed Box Girder Bridge–Analytical Study", M.Eng. Thesis, Department of Civil Engineering and Applied Mechanics, McGill University, Montreal, March 1987.

22. Newmark, N.M. and Hall, W.J., "Earthquake Spectra and Design", *Earthquake Engineering Research Institute*, Pasadena, California, March 1967.

23. National Research Council of Canada, "National Building Code of Canada", Ottawa, Ontario 1980.

24. Ontario Ministry of Transportation, "Ontario Highway Bridge Design Code", Toronto, Ontario 1978.

25. Maisel, B.I., Rowe, R.E. and Swann, R.A, "Concrete Box Girder Bridges", *The Structural Engineer*, London, Vol. 51, No. 10, October 1973.

26. Mirza, M.S., "Bond in Reinforced Concrete Models", Reinforced and Prestressed Microconcrete Models, *The Construction Press*, London, pp.85–101.

27. Mirza, M.S., "Structural Concrete Models: *A State-of-the-Art Report*", McGill University, Montreal, Quebec, October 1972.

28. Mirza, M.S., "Heat Treatement of Deformed Steel Wires for Model Reinforcement", *Structural Concrete Series*, No. 72-4, McGill University, March 1982.

29. Sabnis, G.M. et al., "Structural Models and Experimental Techniques", Prentice Hall inc., Englewood Cliffs, New Jersey 1983.

30. Cook, R.D., "Concepts and Applications of The Finite Element Analysis", University of Wisconsin, Madison, Wisconsin 1981.

31. Ngo, D. and Scordelis, A.C., "Finite Element Analysis of Reinforced Beams", *ACI Journal*, Proceedings, Vol. 64, No. 3, March 1967.

32. Ghoneim, G.A.M. and Ghali, A., "Nonlinear Analysis of Concrete Structures", *Canadian Journal of Civil Engineering*, Vol. 9, No. 3, September 1982.

33. Wilson, E.L., "SAP - A General Structural Analysis Program", Structural Engineering Laboratory Report No. UC SESM 70-20, University of California, Berkeley, California, September 1970.

34. Saenz, L.P., "Equation for the Stress-Strain Curve of Concrete", Discussion of Paper by Desayi and Krishnan, *Journal of the American concrete Institute*, Vol. 61, pp. 1229–1235, 1974.

35. Smith, G.M. and Young, L.E., "Ultimate Theory in Flexure by Exponential Function", *Journal of the American Concrete Institute*, Vol. 52, pp. 349–359, 1955.

36. Razaqpur, A.G., "FELARC Users Manual", Departement of Civil Engineering, Carleton University, Ottawa, Ontario 1986.

37. Bathe, K.J., Wilson, E.L. and Peterson, F.E., "SAP IV - A Structural Analysis Program for Static and Dynamic Response of Linear Systems", Earthquake Engineering Research Center Report No. EERC 73-11, University of California, Berkeley, California, June 1973, Revised April 1974.

38. Chen, W.F., "Plasticity in Reinforced Concrete", MacGraw Hill, 1982.

39. Berg, S., "Nonlinear Finite Element Analysis of Concrete Plates", *Division of Structural Mechanics, The Norwegian Institute of Technology*, Trondheim, Norway, February 1973.

40. Houde, J. and Mirza, M.S., "A Finite Element Analysis of Shear Strength of Reinforced Concrete Beams", Shear in Reinforced Concrete, Vol. 1, *ACI Special Publication SP–42, American Concrete Institute*, Detroit, Michigan 1974.

41. Hanna, Y.G., "Finite Element Modeling of Reinforced Concrete Structures", Ph.D. Thesis, Department of Civil Engineering and Applied Mechanics, McGill University, Montreal, February 1983.

42. Joucdar, K., "Behaviour of a Two–Cell Prestressed Concrete Box Girder Bridge–Experimental Study", M.Eng. Thesis, McGill University, Montreal, Quebec, January 1988.

43. Nofal, M., "Load Distribution in Slab Girder Bridge at Ultimate Load", M.Eng. Thesis being finalized at the Department of Civil Engineering at Carleton University, Ottawa, Ontario.

44. Razaqpur, A.G. and Nofal, M., "Performance of a New Quadrilateral Finite Element With Rotational Degrees of Freedom", A Paper Presented at the Finite Element Method Congress at Salzburg, 1987.

APPENDIX

EXEMPLE OF THE NONLACS APPLICATION

```
******************************************************************
*
*     MCGILL UNIVERSITY PRESTRESSED BOX-GIRDER BRIDGE TEST       *
*                                                                *
*
*                                                                *
******************************************************************

NUMBER OF JOINTS IN SYSTEM.....................   168
NUMBER OF TYPES OF ELEMENTS....................     1
NUMBER OF TIME STEPS...........................     1
CREEP ANALYSIS INDICATOR.......................     0
SHRINKAGE ANALYSIS INDICATOR...................     0
TEMPERATURE ANALYSIS INDICATOR.................     0
     0 = ANALYSIS NOT REQUIRED
     1 = ANALYSIS REQUIRED

CONVERGENCE NORM INDICATOR.....................     1

     0 = FORCE NORM USED
     1 = DISPLACEMENT NORM USED

CONVERGENCE DATA INDICATOR.....................     1

     0 = USE FRACTION OF INPUT LOAD OR DISPL.
     1 = READ IN VALUES

ULTIMATE ANALYSIS INDICATOR....................     1

     0 = ULT. ANALYSIS AT ONE TIME STEP NOT REQD.
     1 = ULT. ANALYSIS AT ONE TIME STEP REQD.

ORDER OF INTEGRATION...........................     3

 OUTPUT CONTROL CODES.
 =====================

CODE FOR ITERATIONS............................     0
CODE FOR NODAL DISPL. IN LOCAL COORDS. .....        0
CODE FOR CURVATURES............................     0
CODE FOR STRAINS...............................     1
CODE FOR DISPL. UNBAL. FORCES..................     0

     0 = NO OUTPUT
     1 = OUTPUT

 TOLERANCES
 ==========

   0.00010   0.00010   0.00010   0.00050   0.00050   0.00050
 MAXIMUM ALLOWABLE VALUES
 ========================

 10.00000 100.00000  10.00000   0.50000   0.50000   0.50000
 ANALYSIS REQD. AT FOLLOWING DAYS AFTER CASTING
 ==============================================

    28.000
```

NODAL POINT DATA AS INPUT

NODE NUMBER	BOUNDARY CONDITION CODES X	Y	Z	XX	YY	ZZ	NODAL POINT COORDINATES X	Y	Z	
1	1	1	0	0	0	0	0.000	0.000	139.500	0
9	0	0	0	0	0	0	85.500	0.000	139.500	0
25	0	0	0	0	0	0	654.000	0.000	139.500	8
41	0	0	0	0	0	0	825.000	0.000	139.500	8

COMPLETE NODAL POINT DATA

NODE NUMBER	BOUNDARY CONDITION CODES X	Y	Z	XX	YY	ZZ	NODAL POINT COORDINATES X	Y	Z
1	1	1	0	0	0	0	0.000	0.000	139.500
2	0	0	0	0	0	0	0.000	225.000	139.500
3	0	0	1	1	1	0	0.000	225.000	0.000

CONCRETE MATERIAL PROPERTIES

TYPE NO.	1
MATERIAL DATA INPUT INDICATOR..............	1
CREEP DATA INDICATOR.......................	0
SHRINKAGE DATA INDICATOR...................	0
COMPRESSIVE STRENGTH AT 28 DAYS............	0.37000+002
POISSONS RATIO.............................	0.18000+000
WEIGHT PER UNIT VOLUME.....................	0.22500-004
COEFFICIENT OF THERMAL EXPANSION...........	0.00000+000

CREEP SHRINKAGE INDICATOR = 1 READ IN VALUES
2 USE ACI.DATA

DAYS AFTER CASTING.........................	0.28000+002
COMPRESSIVE STRENGTH.......................	0.37000+002
TENSILE STRENGTH...........................	0.22000+001
MODULUS OF ELASTICITY......................	0.28663+005
STRAIN AT COMPRESSIVE STRENGTH.............	0.18000-002
ULTIMATE STRAIN IN COMPRESSION.............	0.45000-002
ULTIMATE STRAIN IN TENSION.................	0.80000+000
CRACKED SHEAR CONSTANT.....................	0.50000-001

STEEL MATERIAL PROPERTIES

TYPE	MODULUS	YIELD STRENGTH	BI-MODULUS	ULT. STRAIN
1	0.20000+006	0.29800+003	0.00000+000	0.18000-001

MATERIAL PROPERTIES OF PRESTRESSING STEEL

TYPE NO.	E-MODULUS	YIELD STRESS	E-STAR	ULT.STRAIN
1	0.17500+006	0.13500+004	0.00000+000	0.35000-001

CONCRETE LAYER SYSTEMS

TYPE NO. 1
Z-COORDINATES =
-16.00000000 -8.00000000 0.00000000 8.00000000 16.00000000

TYPE NO. 2
Z-COORDINATES =
-22.00000000 -11.00000000 0.00000000 11.00000000 22.00000000

TYPE NO. 3
Z-COORDINATES =
-69.80000000 -34.90000000 0.00000000 34.90000000 69.80000000

GRAVITY LOAD MULTIPLIERS

X	Y	Z
0.00000	-1.00000	0.00000

INPUT SHELL ELEMENT DATA

ELEMENT	NODES I	J	K	L	CONCRETE TYPE	LAYER	ST.LAY.	GENER. KN
1	4	12	9	1	1	1	0	0
2	12	20	17	9	1	1	0	0
3	20	28	25	17	1	1	0	0

UNIFORMLY DISTRIBUTED LOADS

LATERAL	X	Y	Z
0.00000	0.00000	-0.01400	0.00000
0.00000	0.00000	-0.01400	0.00000
0.00000	0.00000	-0.00700	0.00000

LOAD CONTROL DATA

NUMBER OF LOAD STEPS........................ 20
NUMBER OF ITERATIONS PERMITTED.............. 10
NUMBER OF LOADED JOINTS..................... 8
FRACTION OF DEAD LOAD....................... 1.0000
FRACTION OF SURFACE LOAD.................... 1.0000
FRACTION OF SPRING LOAD..................... 0.0000
FRACTION OF BAR LOAD........................ 1.0000
NUMBER OF LOAD STEPS FOR CREEP.............. 0
NUMBER OF ITERATIONS FOR CREEP.............. 0
TEMPERATURE OR SHRINKAGE INDICATOR.......... 0

INPUT CONCENTRATED JOINT LOADS

NODE	PX	PY	PZ
34	0.0000+000	-0.2497+000	0.0000+000
39	0.0000+000	-0.2497+000	0.0000+000
74	0.0000+000	-0.3124+000	0.0000+000
79	0.0000+000	-0.3124+000	0.0000+000
114	0.0000+000	-0.2189+000	0.0000+000
119	0.0000+000	-0.2189+000	0.0000+000
130	0.0000+000	-0.2189+000	0.0000+000
135	0.0000+000	-0.2189+000	0.0000+000

MX	MY	MZ
0.0000+000	0.0000+000	0.0000+000
0.0000+000	0.0000+000	0.0000+000
0.0000+000	0.0000+000	0.0000+000
0.0000+000	0.0000+000	0.0000+000
0.0000+000	0.0000+000	0.0000+000
0.0000+000	0.0000+000	0.0000+000
0.0000+000	0.0000+000	0.0000+000
0.0000+000	0.0000+000	0.0000+000

****
RESULTS
TIME STEP NUMBER 1
****

LOAD STEP NUMBER.............................. 1
ITERATION NUMBER.............................. 3

TOTAL EXTERNAL NODAL FORCES

NODE	PX	PY	PZ
1	0.00000+000	0.00000+000	0.00000+000
2	0.10438+005	-0.65119+003	0.00000+000
3	0.00000+000	-0.37929+002	0.00000+000

MX	MY	MZ
0.10205+004	0.00000+000	-0.84073+003
-0.16639+004	0.00000+000	-0.27645+003
0.00000+000	0.00000+000	-0.54048+003

UNBALANCED NODAL FORCES

NODE	PX	PY	PZ
1	0.00000+000	0.00000+000	0.71199-001
2	0.37669-002	0.14197-002	0.13803-001
3	0.20747-004	0.16946-004	0.00000+000

MX	MY	MZ
0.32915+000	0.17569+001	0.32694+001
-0.14827+000	-0.63874+000	0.75167+000
0.00000+000	0.00000+000	0.33247-003

JOINT DISPLACEMENTS

NODE	DISPL-X	DISPL-Y	DISPL-Z
1	0.00000+000	0.00000+000	0.21759-001
2	-0.19381+000	0.85835-002	-0.94426-003
3	-0.19926+000	-0.61087-003	0.00000+000

ROTAT-X	ROTAT-Y	ROTAT-Z
-0.10167-003	-0.27094-004	0.10577-002
-0.10067-003	-0.57440-006	0.65983-003
0.00000+000	0.00000+000	0.83887-003

STRESSES IN THE LAYER SYSTEMS

CONCRETE LAYERS

EL	IP	LN	STRESS-XX	STRESS-YY	STRESS-XY
1	1	1	-0.2368+001	0.2682+000	0.1038+000
1	1	2	-0.2714+001	0.2572+000	-0.7955-001
1	1	3	-0.3047+001	0.2462+000	-0.2632+000
1	1	4	-0.3380+001	0.2354+000	-0.4467+000

STRESS-11		STRESS-22	ANGLE	PROJ.		CODE 12		LR 12
0.2723+000	-0.2372+001	87.749	0.000	1	2	1	1	68.0000
0.2593+000	-0.2717+001	-88.468	0.000	1	2	1	1	68.0000
0.2671+000	-0.3068+001	-85.459	0.000	1	2	1	1	68.0000
0.2897+000	-0.3434+001	-83.059	0.000	1	2	1	1	68.0000

BAR STRESSES AND STRAINS

BAR NO.	LENGTH	KTB	MAT.NO.	STRESS	STRAIN	KCT	LR
1	0.85500+002	1	1	0.94476+003	0.53986-002	1	1
2	0.85500+002	1	1	0.71242+003	0.40710-002	1	1
3	0.85500+002	2	1	-0.25119+002	-0.12559-003	1	1
4	0.13950+003	2	1	0.44969+001	0.22485-004	1	1